PHOTOPRODUCTION OF THE $\psi(3095)$ AND $\psi'(3684)$ AT FNAL ENERGIES

BY

JOHN SEARLE SARRACINO

B.S., University of Chicago, 1966
M.S., University of Illinois, 1971

THESIS

Submitted in partial fulfillment of the requirements
for the degree of Doctor of Philosophy in Physics
in the Graduate College of the
University of Illinois at Urbana-Champaign, 1976

Urbana, Illinois

PHOTOPRODUCTION OF THE $\psi(3095)$ AND $\psi'(3684)$ AT FNAL ENERGIES

John Searle Sarracino, Ph.D.
Department of Physics
University of Illinois at Urbana-Champaign, 1976

In an experiment in the broad-band photon beam at FNAL, photoproduction of the $\psi(3095)$ was observed in the dimuon decay mode. The following cross sections for the interaction $\gamma + Be \to \psi + X$ are measured

$\hookrightarrow \mu^+\mu^-$

$$B\sigma = 23 \pm 2.7 \text{ nb} \qquad \text{per nucleus}$$

$$\left.\frac{d\sigma}{dt}\right|_{t=o} = 82 \pm 10 \text{ nb/(Gev/c)}^2 \qquad \text{per nucleon}$$

from which we obtain using vector meson dominance

$$\sigma_{tot}(\psi N) = 1.6 \pm 0.2 \text{ mb}$$

$$\sigma_{el}(\psi N) = 0.021 \pm 0.002 \text{ mb}$$

Distributions in $p_{\parallel}$ and $t_{\perp}$ for ψ photoproduction are also presented.

Based on limited statistics, an upper limit for the interaction $\gamma + Be \to \psi' + x$ is obtained. This limit at 90% confidence is

$\hookrightarrow \mu^+\mu^-$

$$B\sigma \leq 1.4 \text{ nb/nucleus (90\% confidence)} \quad .$$

ACKNOWLEDGMENTS

I wish to take this opportunity to express my gratitude to the many people without whose advice and assistance the work described in this thesis could not have been performed.

It is a pleasure to thank my advisor Dr. Tom O'Halloran for guidance and encouragement not only during the data taking and analysis portions of Ex 87A, but also over a period of six long years while I was his student. His unique way of getting to the heart of problems has been a continual source of inspiration to me.

I also wish to thank Dr. Albert Wattenberg for imparting to me what must be only a fraction of his expertise in the small details one needs to attend to in order to make a complex experiment run smoothly. His advice in the lab, on the floor, and in the Porta-Kamp has been invaluable.

My appreciation also extends to Dr. Wonyong Lee whose drive made our experiment possible and whose foresight in large part helped to make it the success it became.

It is also a pleasure to acknowledge the help and advice I received throughout my graduate career from Dr's Mike Gormley and Gary Gladding and also from Dr. Bob Messner during the latter stages of the experiment.

Thanks also go to John Peoples, Morris Binkley, Irwin Gaines, Bruce Knapp, Dave Yount, A. Lincoln Read, and Rich Orr for the many and varied contributions they made to the experiment.

For hard work and dedication I wish to thank my fellow graduate students Dean Wheeler, Larry Cormell, John Bronstein, Rick Coleman, Maury Goodman, Pat Leung, Dave Smith, Tony Wijangco, Dave Nease, and Jim Knauer.

For technical support throughout the experiment, I want to thank Leonard Seward, Ken Gray, Sal Marino, the U. of I. High Energy Physics Electronic Shop, and the FNAL Proton Lab.

For support in the use of computer facilities, I wish to thank the U. of I. High Energy Physics Group PDP-10 programming and software support staff as well as their counterparts at Fermi Lab.

For additional contributions during the experiment and data analysis, I wish to acknowledge J. J. Russell, Mark Flore, Bill Hagan, Jane Sekulski Chapin, Paul Nienaber, and Paul Avery.

Special thanks go to Lynell Cannell for her patience and understanding while the experiment and analysis were being done.

This thesis is dedicated to my parents whose love and support has sustained me throughout my career as a student.

This work was supported in part by the U. S. Energy Research and Development Agency under contract AT(11-1)-1195.

TABLE OF CONTENTS

I. INTRODUCTION

This thesis describes the analysis of a portion of the data collected by experiment 87A/358 during the end of 1975. The experiment was performed in the broad-band neutral beam in the Proton East area of the Fermi National Accelerator Laboratory (FNAL).[1] The data I will be concerned with are the dimuon photoproduction data taken under the standard running conditions in which a variety of leptonic and hadronic final states were observed.[2,3,4,5,6,7]

The first chapter of this thesis will present the theoretical framework in which the data will be analyzed with appropriate references to the experimental situation. The second and third chapters will describe the equipment and electronics used for data taking. The fourth chapter will describe the data reduction and analysis.

II. THEORY

A major part of the interpretation of the data will follow the ideas of vector meson dominence (VMD). This model assumes that the photon interacts with hadronic matter by first converting itself into a linear combination of spin one negative parity mesons, the so-called vector mesons, the rho (ρ), omega (ω), and phi (ϕ). Accordingly the photon amplitude may be expressed as a linear combination of the vector meson amplitudes. This interpretation of the photon-hadron interaction is summarized in the current-field identity:

$$j_\mu^{em}(\vec{x}) = - \sum_V \frac{m_V^2}{g_V^2} V_\mu(\vec{x}) \qquad (1)$$

where j_μ^{em} = hadronic part of the electromagnetic current

g_V = photon-vector meson coupling constant

V_μ = vector meson field

m_V = mass of vector meson

In particular, one can calculate the leptonic decay width of the vector mesons in terms of the coupling constants g_V. The Feynman graph for the process is shown in Fig. 1.

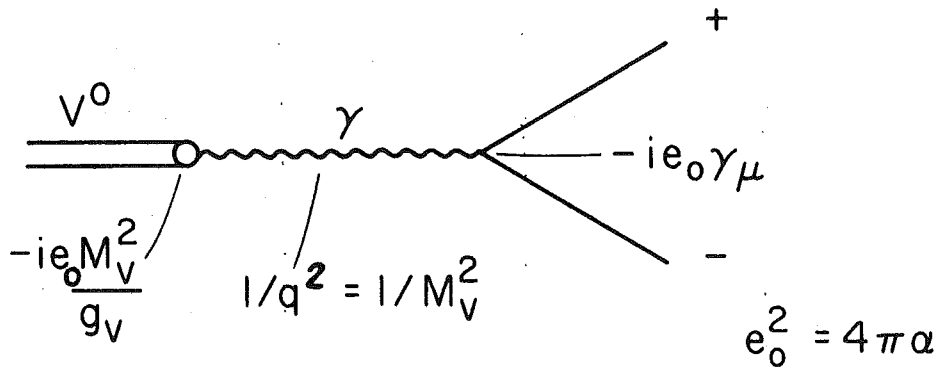

Fig. 1. Feynman diagram for the decay $V^o \rightarrow \ell^+\ell^-$.

A straight-forward calculation yields for the width:

$$\Gamma(V^o \to \ell^+\ell^-) = \frac{\alpha^2}{3}\frac{4}{g_V^2} M_V \left(1 - \frac{4m_\ell^2}{M_V^2}\right)^{1/2} \left(1 + \frac{2m_\ell^2}{M_V^2}\right) \qquad (2)$$

where α = fine structure constant

M_V = mass of vector meson

m_ℓ = mass of lepton

For $\psi \to \mu^+\mu^-$ decay this expression becomes:*

$$\Gamma(\psi \to \mu\mu) = \frac{\alpha^2}{3}\frac{4\pi}{g_V^2} M_\psi \qquad (3)$$

Vector dominence is used to relate the forward differential cross section for vector meson photoproduction to the total cross section for vector meson-nucleon scattering. Referring to Fig. 2, this relationship is:

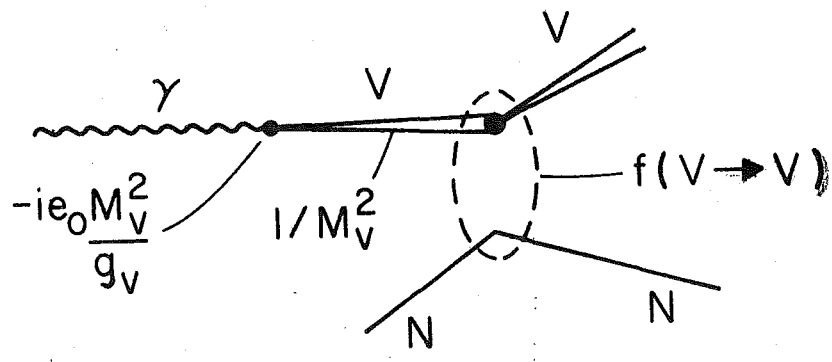

Fig. 2. Feynman diagram for vector meson photoproduction.

*See Appendix A for the derivation of this formula.

$$f(\gamma \to V) = -ie_o \frac{m_V^2}{g_V} \frac{1}{m_V^2} f(V \to V) \tag{4}$$

where $f(\gamma \to V)$ = amplitude for vector meson photoproduction

$-ie_o \frac{m_V^2}{g_V}$ = coupling at the photon-vector meson vertex

$e_o^2 = 4\pi\alpha$, α = fine structure constant

$\frac{1}{m_V^2}$ = vector meson propagator

$f(V \to V)$ = amplitude for V-N scattering

Squaring both sides and using the optical theorem,

$$\text{Im} \left.\frac{d\sigma}{d\theta}\right|_{\theta=0} = \frac{1}{16\pi} \sigma_{TOT} \tag{5}$$

one gets the VMD relation:

$$\left.\frac{d\sigma}{dt}(\gamma \to V)\right|_{t=0} = \frac{4\pi}{g_V^2} \frac{(1+R_V^2)}{16\pi} \alpha \sigma_T^2(V \to N) \tag{6}$$

where

$\frac{d\sigma}{dt}$ = differential cross section as a function of the invarient momentum transfer squared t (taken to be negative)

$\sigma_T(VN)$ = V-N total cross section

R_V = ratio of real to imaginary parts of $\frac{d\sigma}{d\theta}$

Furthermore, by assuming the same t-dependence for two different vector mesons, we can use the relation (4) with the optical theorem and equation (2) to derive the following result:

$$\frac{\sigma_{el}(\gamma \to V_1)}{\sigma_{el}(\gamma \to V_2)} = \frac{\Gamma_{V_1 \to \mu_\mu / m_{V_1}}}{\Gamma_{V_2 \to \mu_\mu / m_{V_2}}} \times \frac{\sigma_T^2 (V_1 N)}{\sigma_T^2 (V_2 N)} \tag{7}$$

where σ_{el} = elastic cross section.

It is not possible, however, to measure the differential cross section at zero momentum transfer for photon induced reactions. This is because the kinematics of any reaction in which there is a mass change between the incoming and scattered particles requires the process to occur with some minimum momentum transfer. In the high energy limit and in particular for psi-photoproduction in our experiment,

$$|t_{min}| = \frac{1}{4} \frac{m_\psi^4}{E_\gamma^2} \tag{8}$$

where E_γ = energy of the incident photon.

The extrapolation to t = 0 can be done, however, by multiplying the differential cross section as a function of momentum transfer squared evaluated at $p_\perp^2 = 0$ $\left(\frac{d\sigma}{dp_\perp^2}\Big|_{p_\perp^2 = 0}\right)$ by the factor $e^{\alpha|t_{min}|}$, where α is the coherent slope. The extrapolation can also be done by using an expression for the differential cross section as a function of the invariant momentum transfer squared ($d\sigma/dt$) itself.

One such expression is due to Margolis:[8]

$$\frac{d\sigma}{dt} = |v(q)|^2 \{A^2 |F(q)|^2 + A(1 - |F(q)|^2)\} \tag{9}$$

where

$v(\vec{q})$ = two-body scattering amplitude

A = atomic number of nucleus

$F(\vec{q})$ = form factor of nucleus

This expression is derived in the first Born approximation assuming an effective spin and isospin independent potential of the form $v(\vec{r} - \vec{r}_i)$ between the incident particle whose position is denoted by r and a target particle i whose position is denoted by $\vec{r}_i$. The two-body scattering amplitude $v(\vec{q})$ is given by the Fourier transform of the interaction potential:

$$v(q) = \int e^{i\vec{q}\cdot\vec{r}}\, v(\vec{r})\, d^3r \tag{10}$$

Two body correlations are ignored and nuclear states are considered degenerate with the ground state.

The first part of Equation (10) is:

$$A^2 |v(\vec{q})|^2 \, |F(\vec{q})|^2 \tag{11a}$$

which is the square of the coherent sum of scattering amplitudes off of each nucleon. It has an angular distribution characteristic of the size of the target nucleus and hence falls off in the range $q \sim 1/R_{\text{nucleus}}$ where R = radius of nucleus.

The second part of Equation (9) is:

$$A|v(\vec{q})|^2 \, (1 - |F(\vec{q})|^2) \tag{11b}$$

and corresponds to scattering to all nuclear states. As $F(\vec{q})$ falls off to 0, this quantity represents an incoherent sum of elastic scatterings

from each target nucleon. Furthermore, as q^2 goes to 0, this term becomes 0 as would be expected by the fact that very small momentum transfers would not be sufficient to kick a nucleon out of the nucleus.

A final note is added on the possibility of relating the masses of the vector mesons to their total interaction cross sections, the semi-empirical $(1/M)^2$ relationship.

On the basis of a model for hadrons incorporating SU4, Carlson and Freund[9] have extended a relationship originally postulated for the vector mesons ρ, ϕ, and ω. This relation is:

$$\frac{\sigma_{T_V}(\infty)}{\sigma_{T_\rho}(\infty)} = m_\rho^2/m_V^2 \qquad (12)$$

where V is a higher mass vector meson composed of a quark anti-quark pair (in analogy with the ϕ) of the new kind required for the SU4 representation, and ∞ denotes the fact that the cross sections are to be taken at large energy.

III. EXPERIMENTAL DETAILS

A. Beam

The FNAL proton beam, extracted from the main ring about one mile upstream of the PE target box, was transported to the target hall by several series of vertical and horizontal bending magnets and quadrupole focusing magnets [See Fig. 3]. Losses due to scraping and the attendant radiation problem in the PE section of the external proton beam limited the intensities this line could transport to 2-3 $\times 10^{12}$ protons/pulse except for limited periods.

In the pre-target area [Fig. 4], the proton beam was focused by a quadrupole doublet (QH400H, QV401H) and steered by a main ring dipole (BH403H), which provided horizontal sweeping, and by a pair of small magnets which provided vertical pitching (BV402, and BV403).

The intensity of the incident proton beam was measured by a secondary emission monitor (SEM) located 20 feet upstream of the target. The beam position and size were monitored in two places, at the entrance to the target hall before the first quadrupole and about 10 inches in front of the target by segmented wire ion chambers (SWICs).

Typical intensities on the production target were 7-8 $\times 10^{11}$ protons/pulse which over the one second spill generated about 200 event triggers. For the standard running, intensities were limited by the number of 0 degree photoproduced e^+e^- pairs the first multi- wire proportional chambers could take without drawing a dangerous amount of current

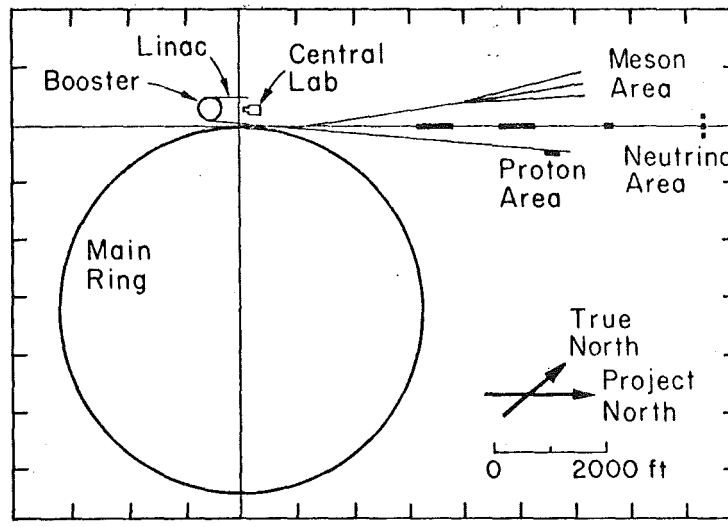

Fig 3a Plan View of FNAL

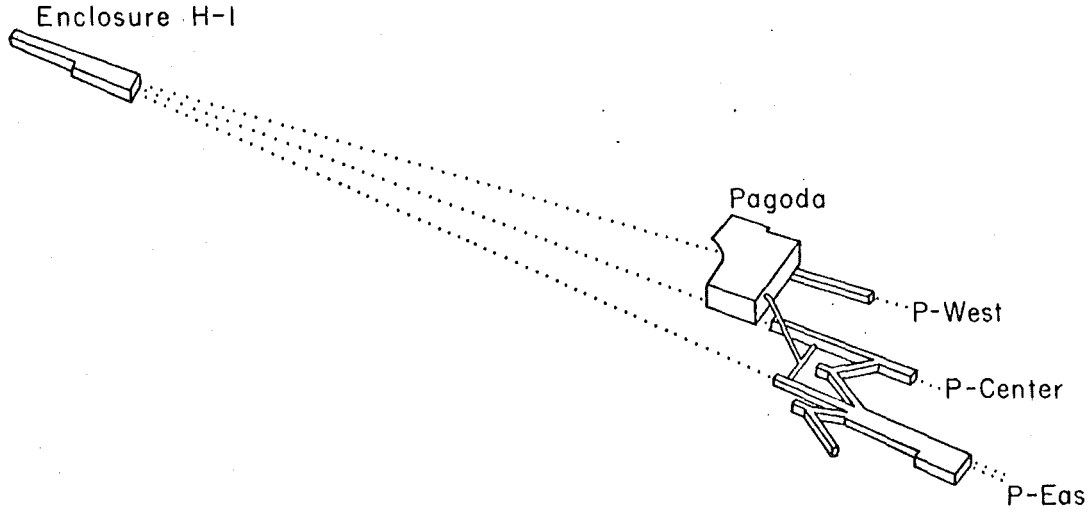

Fig. 3b Diagram showing the upstream half of the Proton Area

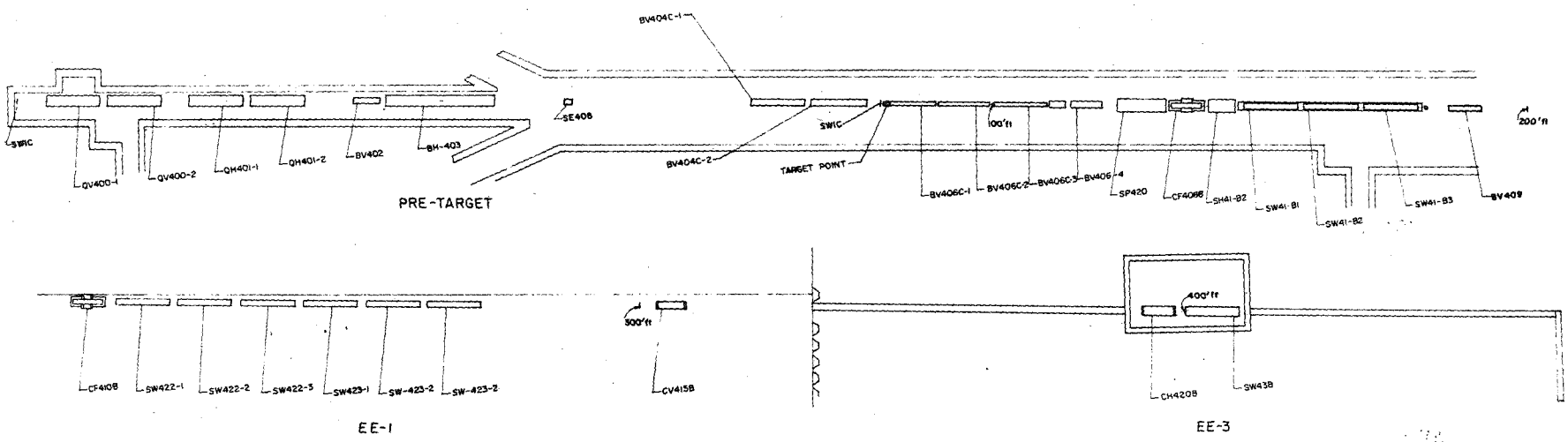

Fig 4-BROAD-BAND PHOTON BEAM EQUIPMENT LAYOUT

(about 40-50 microamps). During periods of bad spill structure, intensities were limited to as little as 1×10^{10} protons/pulse. An earlier problem due to the ambient muon fluxes produced upstream of the target hall by scraping of the beam halo off the magnets had been corrected by replacing some of the upstream magnets with ones of larger aperture and by filling the ground between EE1 and EE4 with battleship steel.

The proton beam impinged on a 12" long, 60 mils wide, 300 mils high beryllium target [Fig. 5]. The surviving protons and charged secondaries were bent downward into tungsten and steel dumps. A hole in the magnets at 0 degrees with respect to the nominal beam line allowed neutral particles to escape the target box. At this point the neutral beam consists primarily of neutrons.

Referring to Fig. 6 or to Fig. 4, the neutral beam then passed through a fixed aperture collimator (CF408B), 35 feet of liquid D_2, a second fixed aperture collimator (CF410B), 68 feet of liquid D_2, and variable aperture vertical and horizontal collimators (CV415B and CH420B). The full length of the deuterium filter was surrounded by sweeping magnets in order to remove charged secondaries from the neutral beam. The collimator (CF408B) serves to define the beam spot, while the remaining collimators serve to remove the halo caused by interactions in the deuterium. The sizes of the holes in the first fixed aperture collimator are given in Table 1. All of the photon running in the fall of 1975 was done with this collimator set at hole #1. This produced a 2" by 2" beam spot on our experimental target.

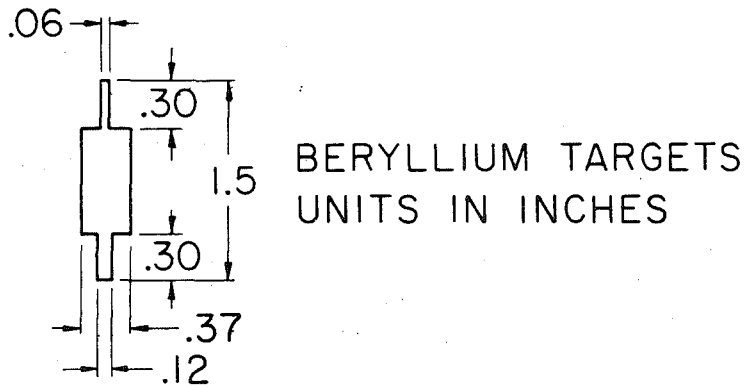

FIG. 87A Production Targets

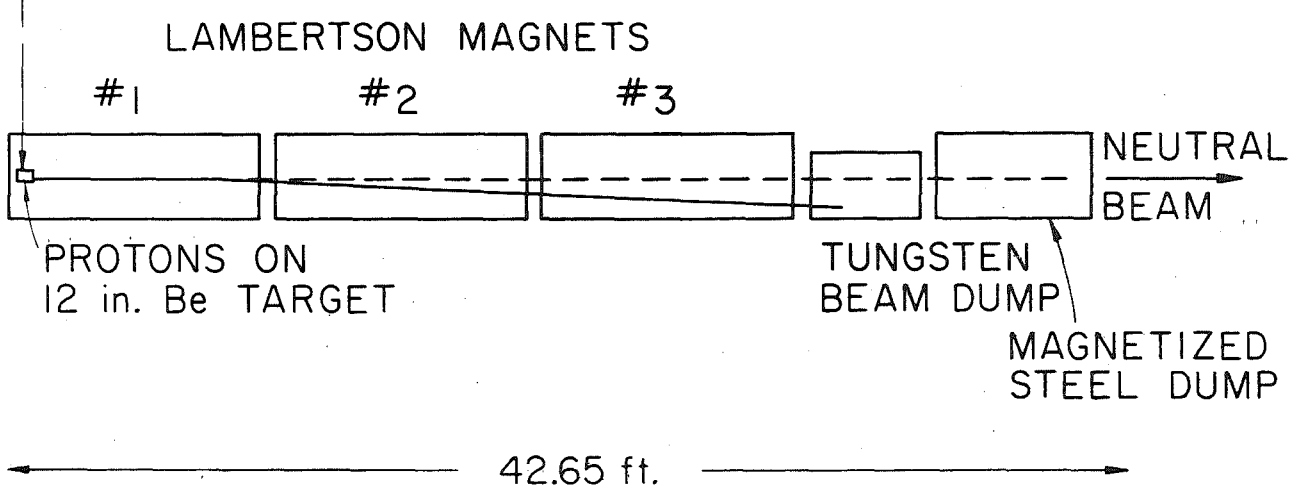

FIG. 5 Target Box Side View

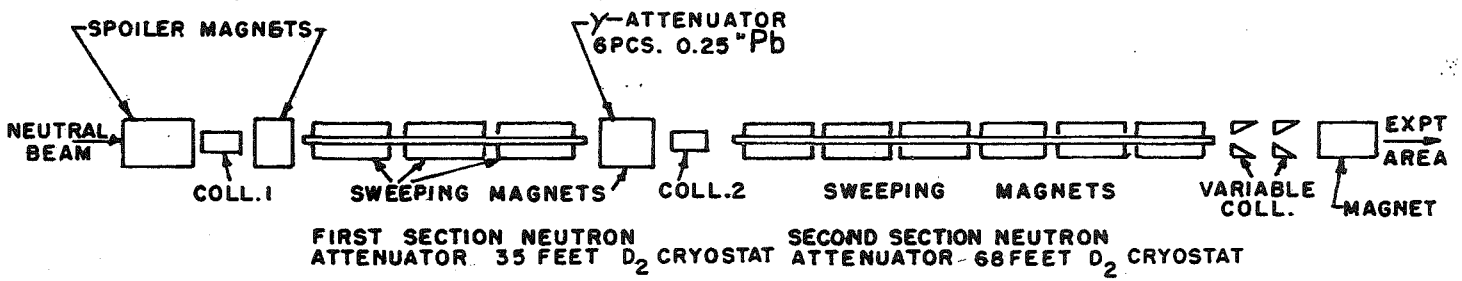

Fig 6 Schematic of Collimators and Deutenium System

TABLE 1

CF408B COLLIMATOR SOLID ANGLE DEFINITION

Hole	Hole Size	Solid Angle of the Beam
1	.250" × .250"	1.5×10^{-7} Sr
2	.040" × .080"	7.3×10^{-9} Sr
3	.040" × .160"	15×10^{-9} Sr
4	.080" × .240"	44×10^{-9} Sr
5	.080" × .320"	60×10^{-9} Sr

The deuterium filter contains about 4 radiation lengths ($4X_o$) and 8.5 interaction lengths (8.5 IL) of D_2. The full length of the filter thus enhances the photon component by a factor of about 200 with respect to the neutron component.

A small bending magnet containing a device which allowed the remote insertion of from one to six radiation lengths of lead into the beam was placed behind the first section of deuterium. The beam power as measured by the quantameter and normalized to the number of incident protons is plotted in Fig. 7 as a function of the number of radiation lengths in the beam for three conditions: no D_2, 35 feet of D_2, and 100 feet of D_2. There is no evidence of neutron power in the beam when the deuterium filter is full.

B. Spectrometer

The experimental equipment is shown in Fig. 8 and consists of a magnetic spectrometer, the particle identification system, and various scintillation counters. The spectrometer consists of five multi-wire

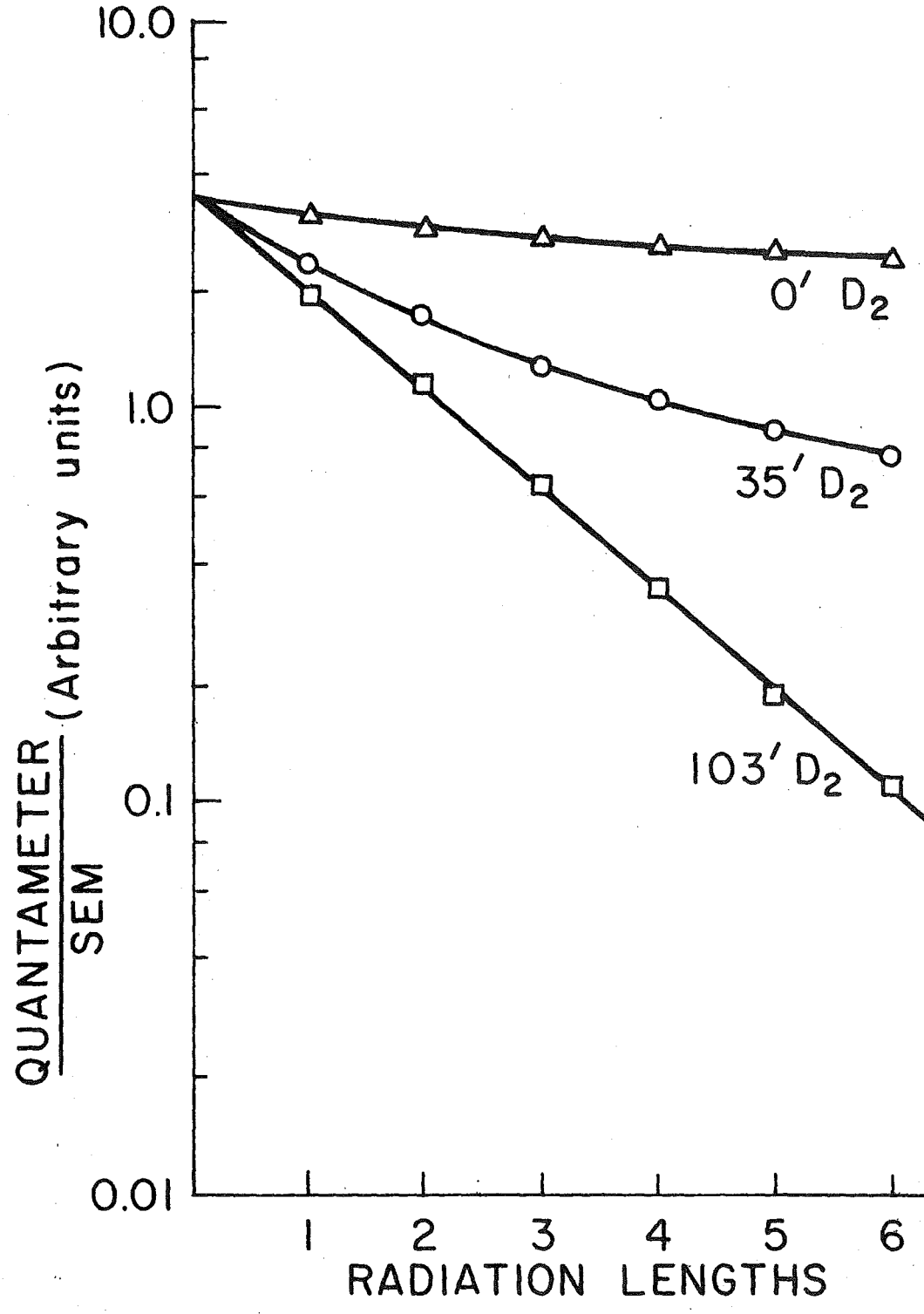

Fig 7 Attenuation of neutral beam through deuterium filter

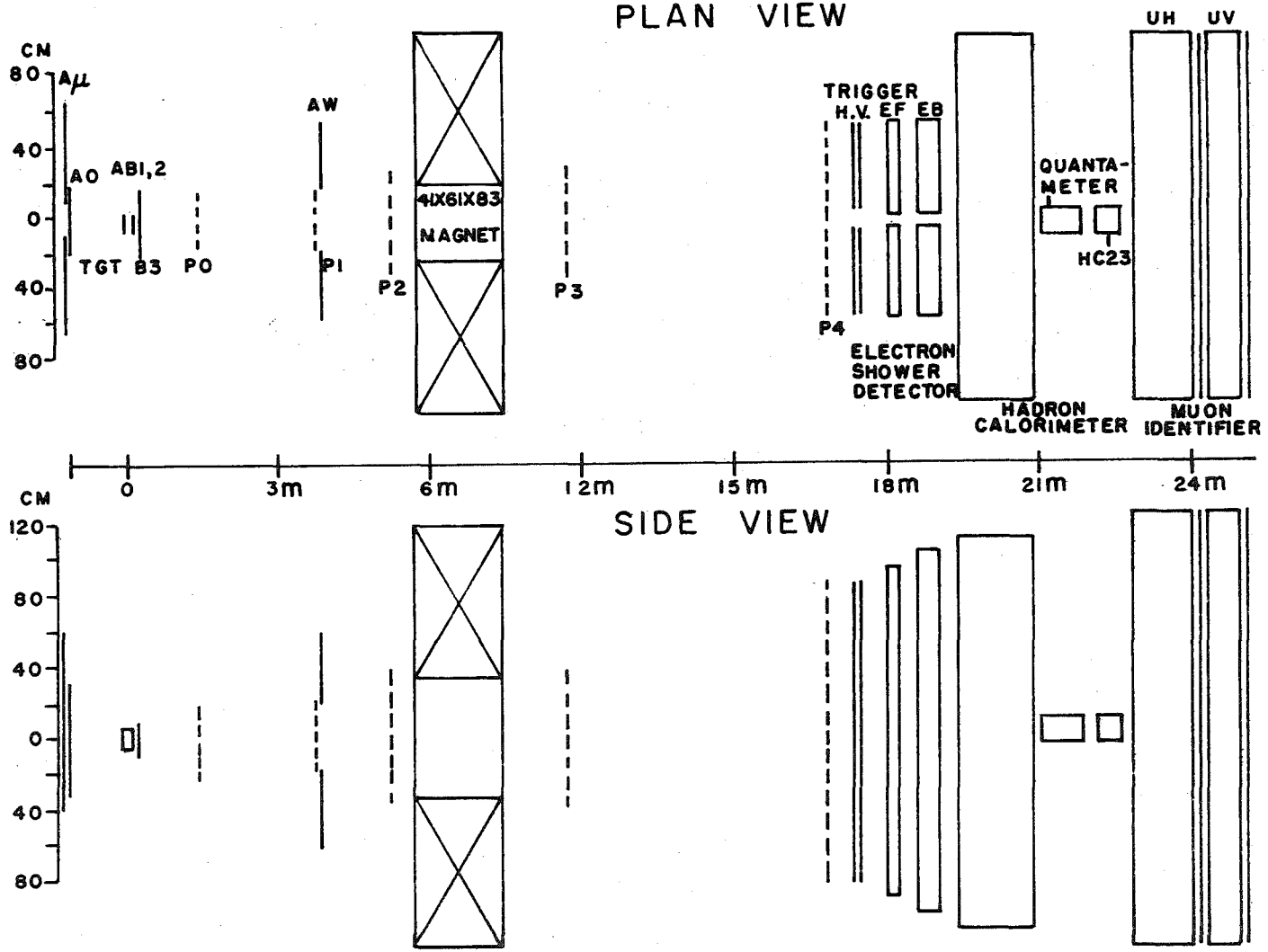

Fig 8 Views of magnetic spectrometer and particle identification system

proportional chambers (MWPC's) identified as PO-P4 in Fig. 8 and an enlarged version of the BM109 bending magnet. This magnet, while not identified as such was also referred to as AN422B.

Each MWPC consists of three wire planes, an x-plane, a v-plane, and a u-plane. The wires in the x-plane run vertically and the wires in the other planes cross the x-plane wires at an angle of 11 degrees with respect to the horizontal. Further details of the construction of the chambers may be found in Reference 10.

Wire chamber readout is accomplished in three steps. First the raw signal of several micro-volts from each wire is amplified at the chamber. The amplified signal of several millivolts is sent to a unique shift register in the Porta-Kamp. Then, if the event is accepted, the address of all the shift registers that have been set in that event are read into an external buffer memory of the Sigma-2 computer and later (between beam pulses) stored on magnetic tape.

The analyzing magnet, which was a standard BM109 magnet with the gap between the pole faces doubled, was turned on its side in order to give a vertical bend. Its aperture was 18" by 24" and had a field integral of roughly 54 Kg-ft. In the analysis program an analytic form of the field, fitted from a field map was used:[11]

$$\int B\cdot dz = \int B\cdot dz\Big|_{x=y=0} \times \{1 + Ax^2 + By^2 + Cx^4 + Dy^4 + Ex^2y^2 + Fx^6 + Gy^6 + Hx^2y^4 + Ix^4y^2\} \qquad (12)$$

where $A = 1.983 \times 10^{-4}$ $D = -4.353 \times 10^{-6}$ $G = 7.2693 \times 10^{-9}$

$B = -2.094 \times 10^{-4}$ $E = 1.7786 \times 10^{-5}$ $H = 1.6128 \times 10^{-7}$

$C = 3.4406 \times 10^{-6}$ $F = -2.723 \times 10^{-5}$ $I = -3.1096 \times 10^{-7}$

The central value was determined by finding the best fit to the mass of the K_L^o meson in the decay $K_L^o \rightarrow \pi^+\pi^-$. [See Fig. 9].

C. Particle Identification System

The particle identification system consists of three pieces of apparatus, an electromagnetic shower detector, a hadronic shower detector or hadron calorimeter, and a muon identifier [See Fig. 10]. The electromagnetic shower detector consists of a front and rear vertical array of lead-scintillator sandwich shower counters with each array split into a right- and left-hand side separated by plus and minus 2" about the beam line. This separation allows the copiously produced e^+e^- pairs to pass through the detector without depositing a significant amount of energy in it. The separation as well as the separation of the trigger counters (see below) was determined by moving the hodoscope arrays together until the counting rates became too high.

The front hodoscope array was made up of 22 counters (11 to each side), each counter consisting of six pieces of scientillator interleaved with the same number of 1/4" thick lead sheets and connected to a 58 AVP photomultiplier tube. The rear array was made up of 24 (12 to a side) counters of similar construction except that the rear counters were made up of 16 pieces of scintillator and the corresponding number of lead sheets. In addition, for the fall running, two 16 radiation length shower counters

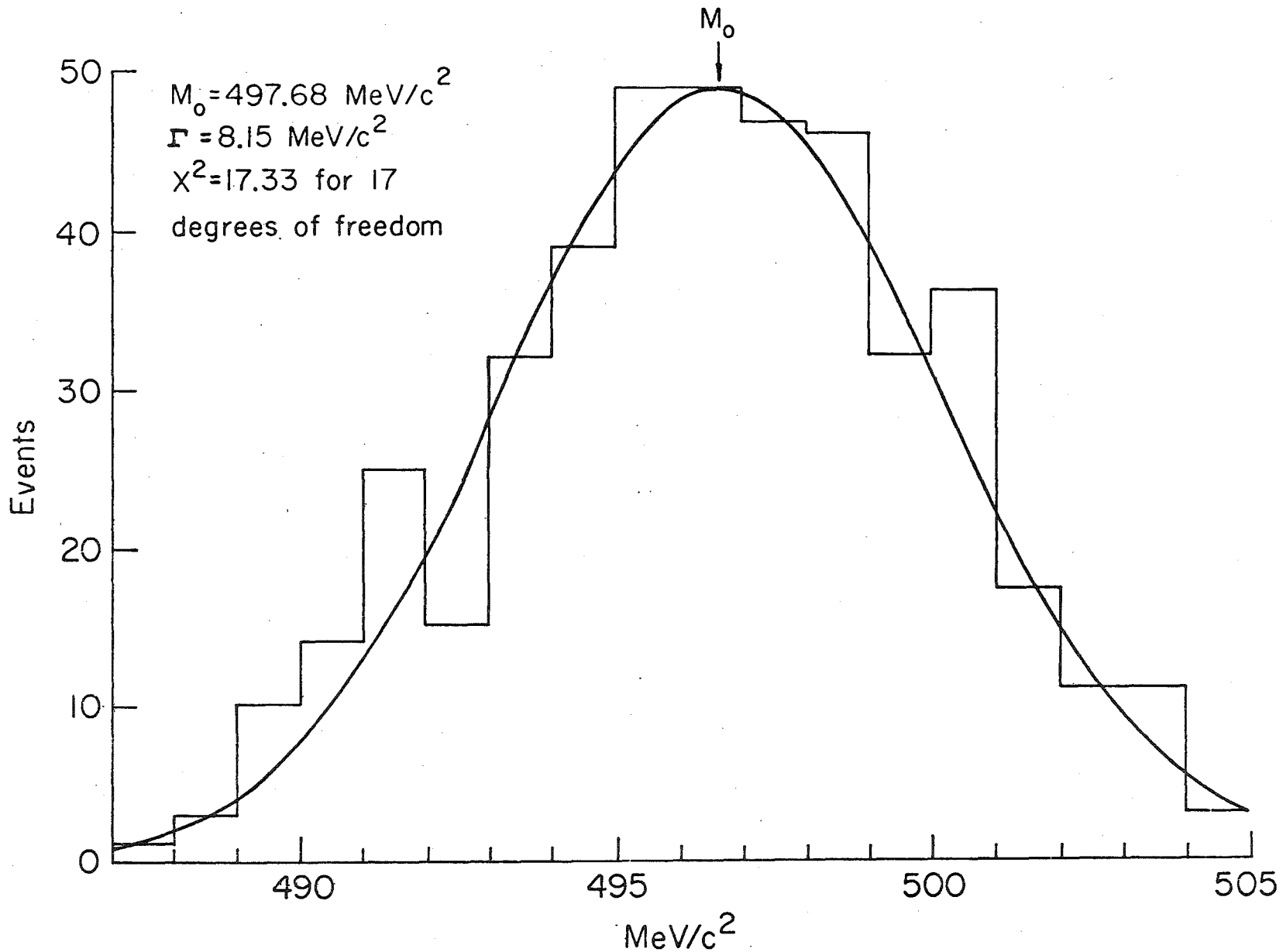

FIG 9 FIT TO MASS OF K_L^0

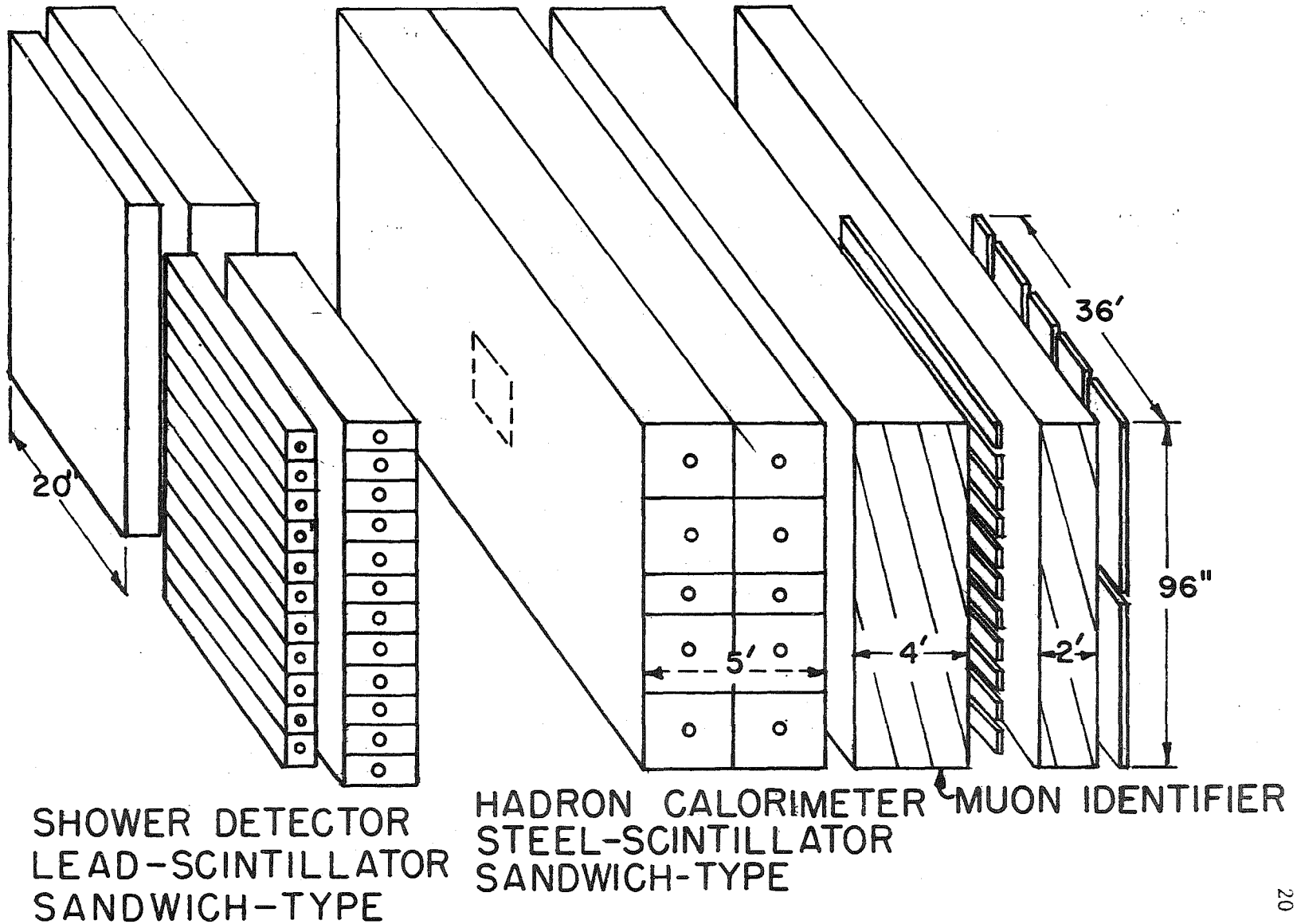

Fig. 10 Schematic of Particle Identification System

were mounted vertically between the shower detector and hadron calorimeter in the gap between the left and right banks of the shower counters. The primary function of these counters is to shield the hadron calorimeter from the Bethe-Heitler pairs and thus make the hadronic trigger more discriminative. Further details of the construction, operation, and calibration of the shower detector may be found in Reference 3.

The hadron calorimeter consists of 16 counters mounted in two vertical arrays and a single calorimeter behind the quantameter in the beam line. The first array consists of 10 counters, 5 to a side. On either side, the middle counter was 6" high and the two top and two bottom ones were 24" high. [See Fig. 11]. The middle counters were offset 3" from the beam line so that a 6" × 6" hole was allowed for the beam to pass through. The rear array consisted of 6 counters, 3 to a side, with the middle counters in each side again being a 6" counter. The single counter behind the quantameter was a 24" counter. Each counter consists of 24 sheets of scintillator tied to a 58 AVP photomultiplier tube through seperate non-adiabatic light pipes and a mixing block [See Fig. 12].

The muon identifier consists of a horizontal and vertical array of scintillation counters seperated by 24" of steel and preceeded by 48" of steel, plus a single downstream counter in the beam line protected by an additional 48" of steel. Thus including the upstream material in the shower counters and hadron calorimeter, there was a minimum of 154 X_o (16 IL) in front of the horizontal array and 178 X_o (19.5 IL) in front of the vertical array. The parts of the array directly behind the quantameter and extra calorimeter were shielded by an additional 63 X_o (6.5 IL). The counter in the beam (Mu-H 23) was shielded by roughly the same amount

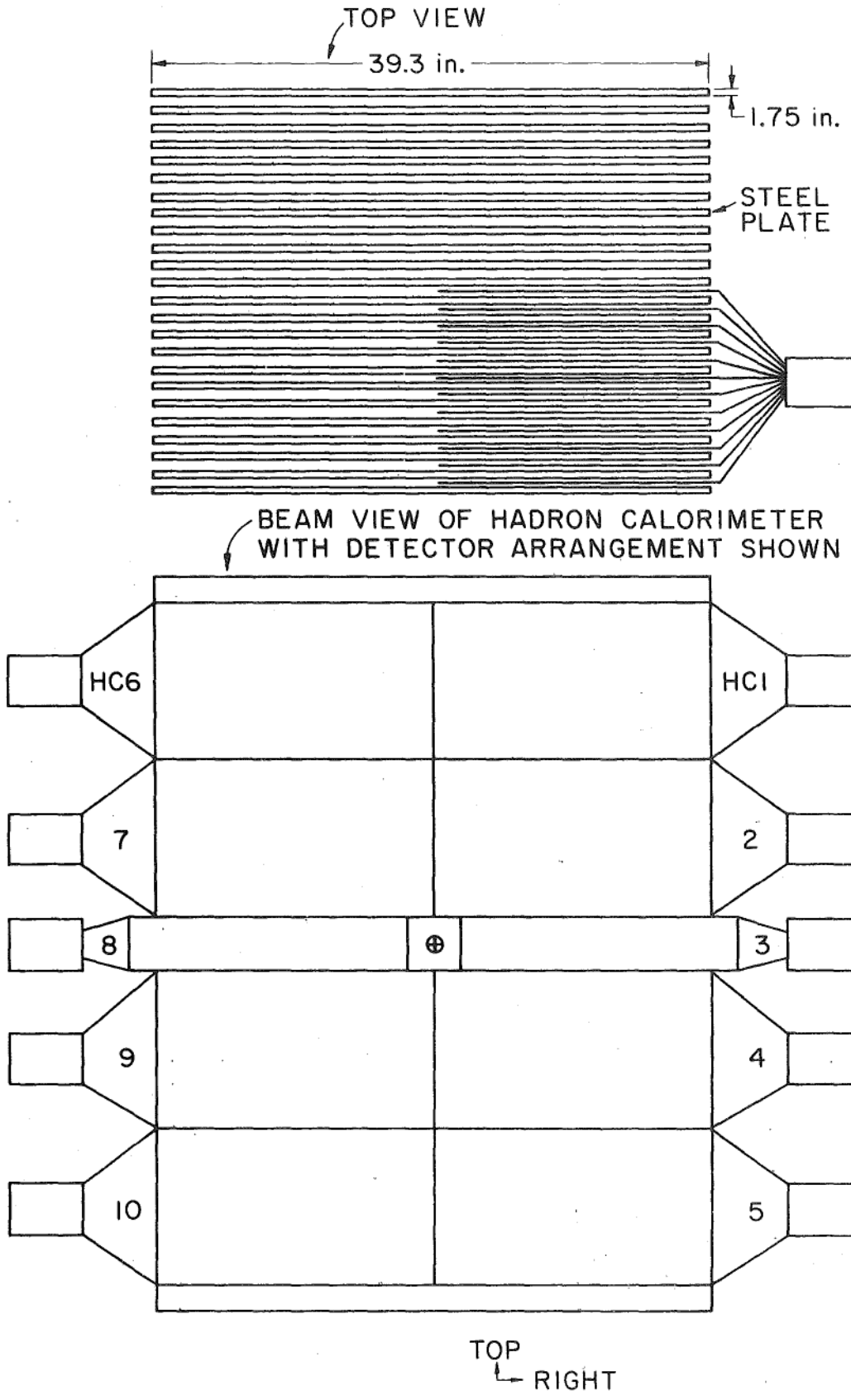

FIG. 11 Hadron Calorimeter

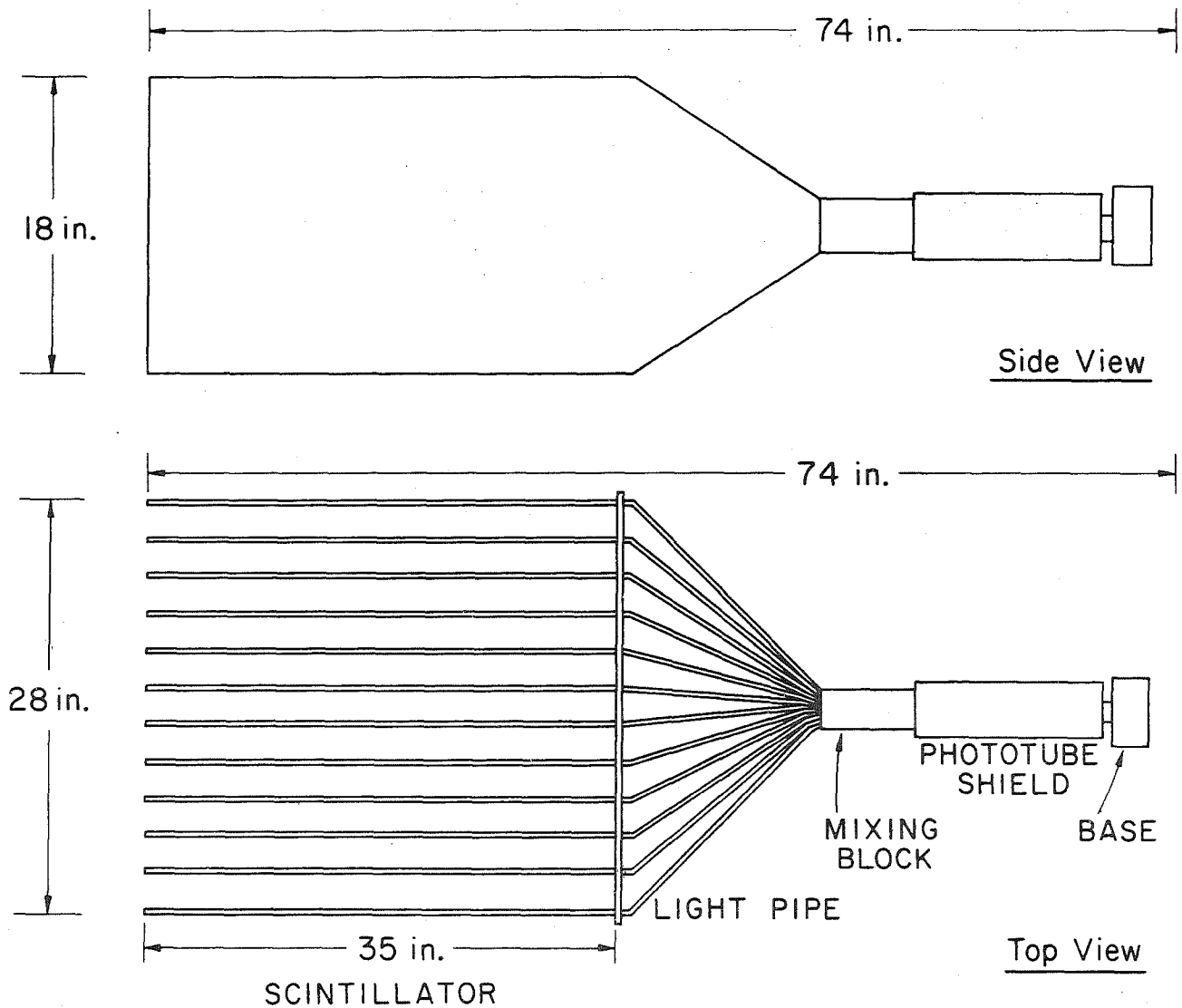

FIG. 12 Details of Large Hadron Calorimeter Counter

of material. The horizontal array consisted of 22 8" × 33" scintillators connected to 8575 photomultiplier tubes and the vertical array of 18 8" × 36" scintillators also connected to 8575 tubes. [See Fig. 13].

D. Quantameter

Photon energy in the beam was monitered by a Wilson-type quantameter located just downstream of the calorimeter. This device was calibrated at SLAC and was found to have a calibration constant of 416 ions/Gev. For further details of the construction, operation, and calibration see Reference 12.

E. Trigger Counters

The master trigger for an event was based in part on signals from a horizontal and vertical scintillation counter hooscope situated behind P4 and in front of the shower detector. Because of the high instantaneous rates these counters had to survive, a DC voltage source ("afterburner") was provided for the last few dynode stages of each tube. The horizontal array consisted of 12 counters, 6 to a side, and the vertical 8, 4 to a side. Each array was separated by 2.5" about the beam line for the standard photon running.

F. B3

The scintillation counter B3 was placed about 20" downstream of the target in order to detect interactions in which a charged particle was produced. As such it was used in forming the master gate and could be used for purposes of normalization. Its photomultiplier was also provided with an afterburner.

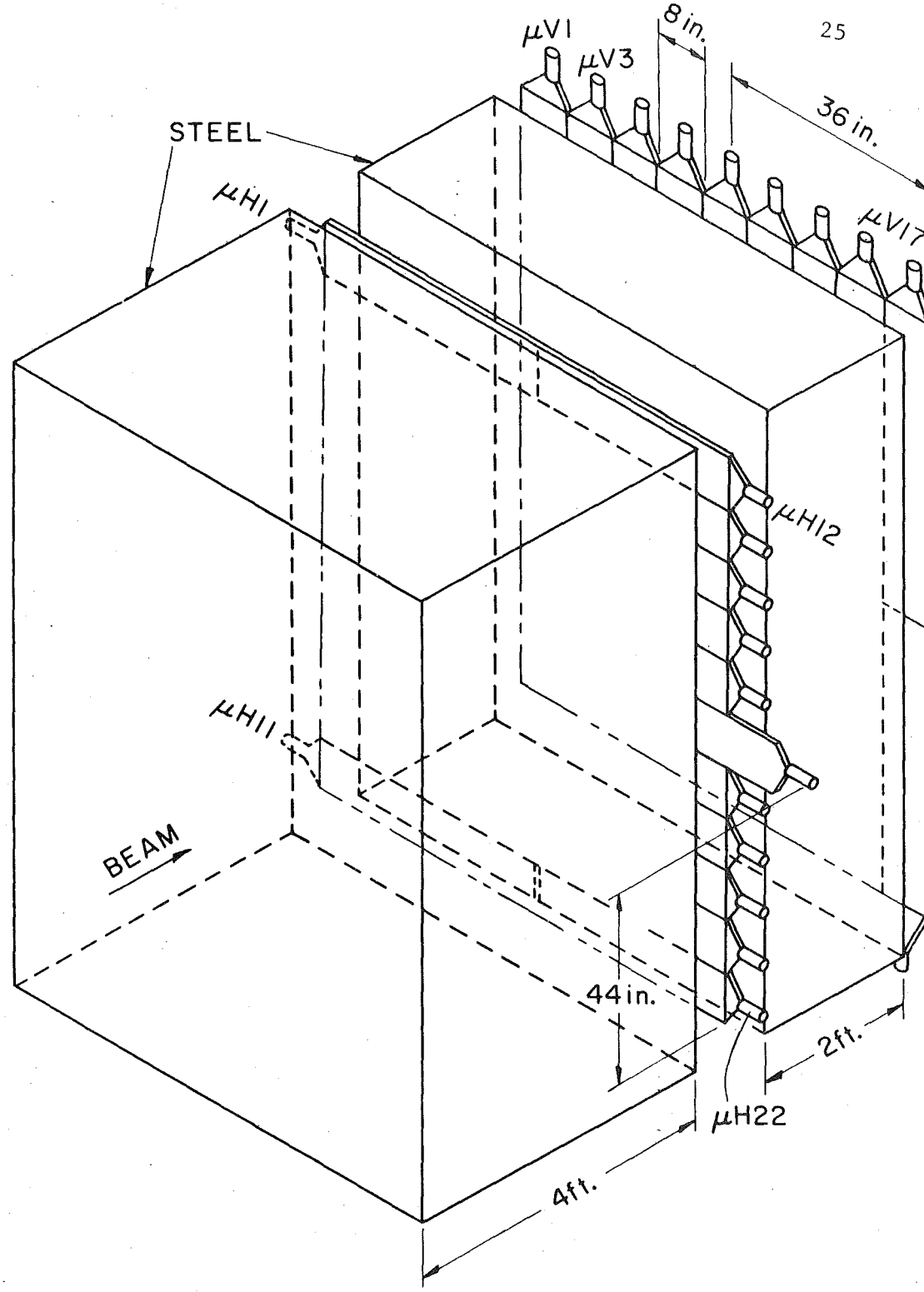

FIG. 13 Muon Identifier
(Beam hole not shown)
(μH - 23 not shown)

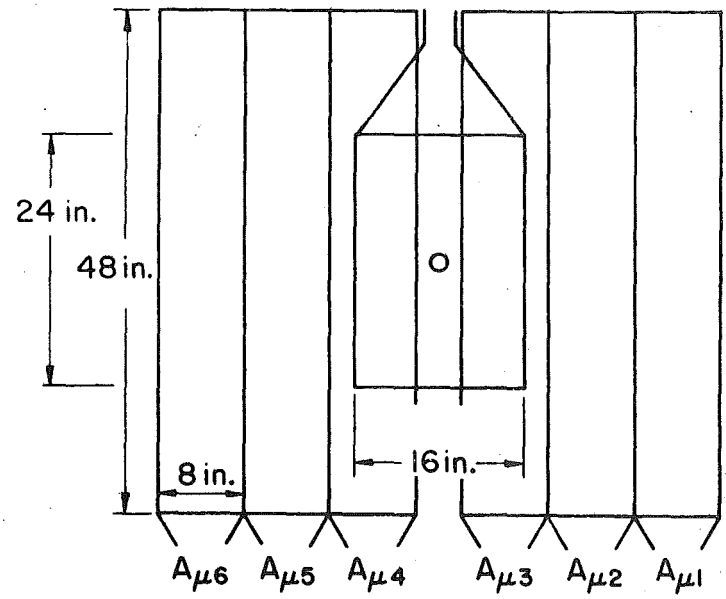

FIG. 14 Upstream View of Muon Anti Counters

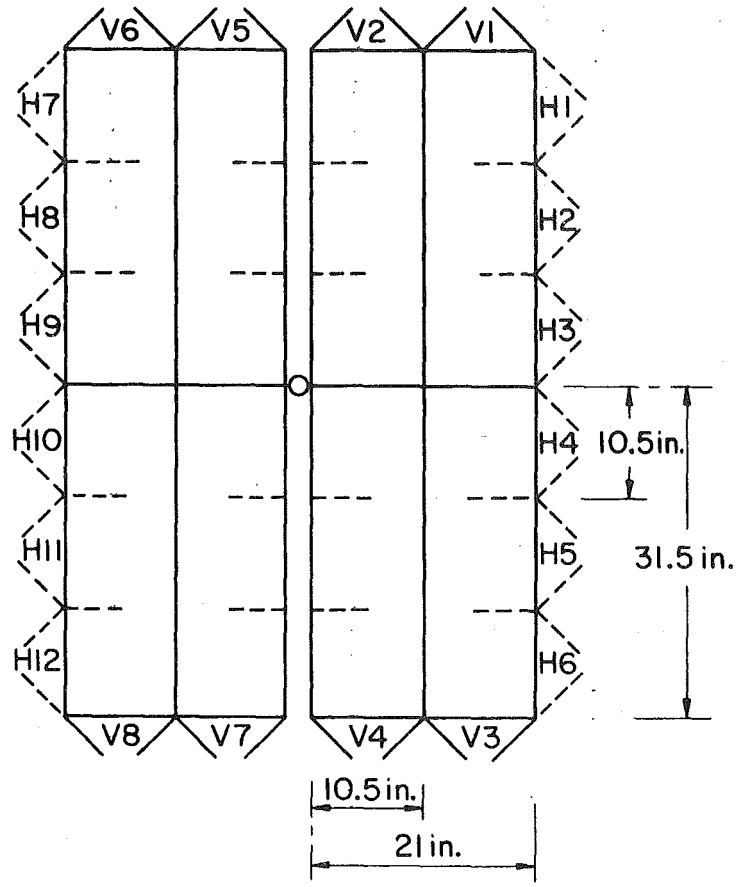

FIG. 15 Downstream View of Trigger Counters

G. Anti's

Counters AB1 and AB2, provided with afterburners, were located above and below B3. Each counter was preceded by a 1/4" of lead to convert photons from pi-zero decay. Counters AW1-AW4 were located around the active area of the second multi-wire proportional chamber (P1). These counters (the AB's and the AW's) when all off define a "diffractive" event, i.e., an event in which 1) all forward going tracks are reconstructable, 2) all forward-going tracks get through the magnet, and 3) there are no slow π^{o}'s. The counters A0, and A1-A6 were located 10" upstream of the target and served to veto muons from the ambient muon flux. See Fig. 15.

H. T-Counters

Finally, the target was surrounded by 8 scintillation counters, each of which was shielded by 1/4" of lead and 3/8" of aluminum. The purpose of these counters was to detect the recoil proton from inelastic events and to detect the photon from pi-zero decay. The minimum kinetic energy required of a recoil nucleon in order for it to escape the target and penetrate the shielding in front of the T-counters was about 100 MeV.

A schematic view of the upstream proportional and scintillation counters is presented in Fig. 16. Further details of the construction of the trigger counters, B3, the anti-counters, and the T-counters may be found in Reference 3.

I. Target

The target was a 2" × 2" × 31/32" piece of beryllium mounted on a remotely controlled holder which provided vertical travel.

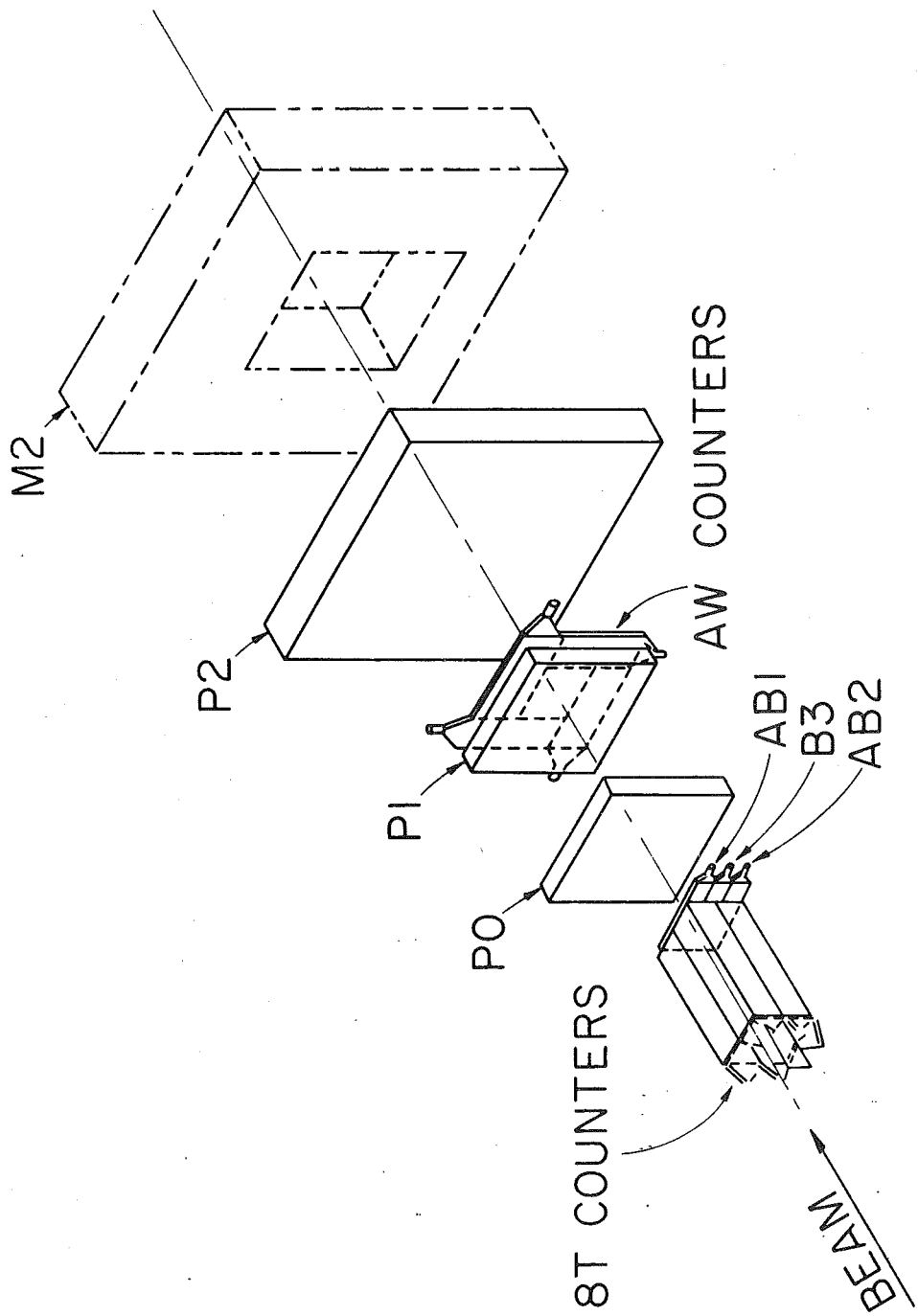

FIG. 16 Upstream Proportional and Scintillation Counters (Schematic)

IV. ELECTRONICS

A. Overview

A block diagram of the electronics is presented in Fig. 17. Master event gates are generated from certain coincidences among scintillation counters and/or pulse height requirements, are processed by the "CONFUSION" logic, and are passed on to the DC (or Nevis) logic. The master gate is made sufficiently loose to include all classes of events to be studied, but sufficiently stringent to prevent a high system deadtime. The DC logic then checks to see if an event satisfies one of up to 16 further sets of requirements defining an event type. If an event satisfies one of these predetermined requirements, all the counter, pulse height, and MWPC information for the event is read into a 32K word (16 bit/word) external buffer memory of a Sigma-2 computer. At the end of each spill, the contents of this memory as well as end-of-spill data are stored on magnetic tape. To see how the event selection system works, I will describe the decision making components, the CONFUSION logic and the DC logic in some detail.

B. Master Gate and CONFUSION Logic

The master gate for events is formed from a two-fold coincidence of

$$(L+R)>0 * B3 * (HC+A0)$$

where $(L+R)>0$ is a two particle trigger in the H and V hodoscopes, B3 indicates a charged track in the counter B3 downstream of the target, HC indicates a pulse height greater than a certain threshhold in the hadron

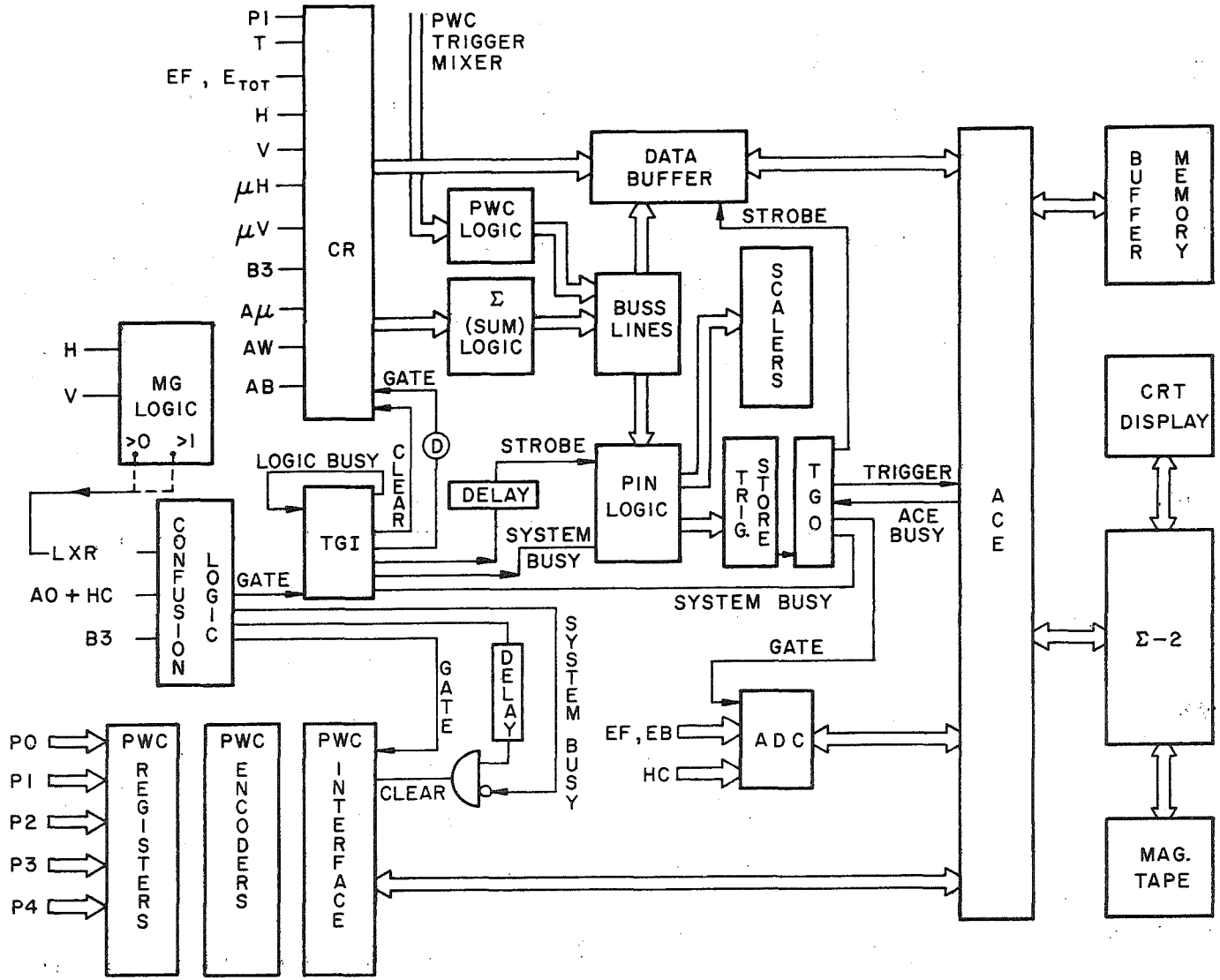

FIG 17 ELECTRONICS BLOCK DIAGRAM

calorimeter, and A0 indicates a charged track in the beam upstream of the target. The pulse height required was found afterward to correspond to requiring 40 GeV of energy to be deposited in the calorimeter. The level was initially set so that the counting rate for triggers with this requirement in them was not too high. [See Fig. 18].

The requirement (L+R)>0 denotes the fact that while a two-particle trigger in the H,V hodoscopes required overlapping counters to fire, it was not necessary for the tracks to pass through separate H and separate V counters. An acceptable trigger could be one in which both tracks passed through the same H counter and separate (but overlapping with H) V counters, or vice versa. Possible combinations yield the following event types:

(L+R)>0*B3	standard charged particle trigger
(L+R)>0*HC	strange particle trigger
B3*A0	charged particle in beam
(L+R)>0*A0	charged particle in halo
B3*HC	one or more charged hadrons down the center; only one outside slit in H,V counters

Most dimuon events satisfy (L+R)>0*B3; the function of the triggers with A0 in them will be discussed below.

All three inputs were fed into a logic module called for historical reasons the "CONFUSION" logic. The purpose of this module was threefold: (1) to generate a master gate for the DC (or Nevis) logic, (2) to provide READ and CLEAR pulses to the MWPC shift registers, and (3) to keep track of logic deadtimes.

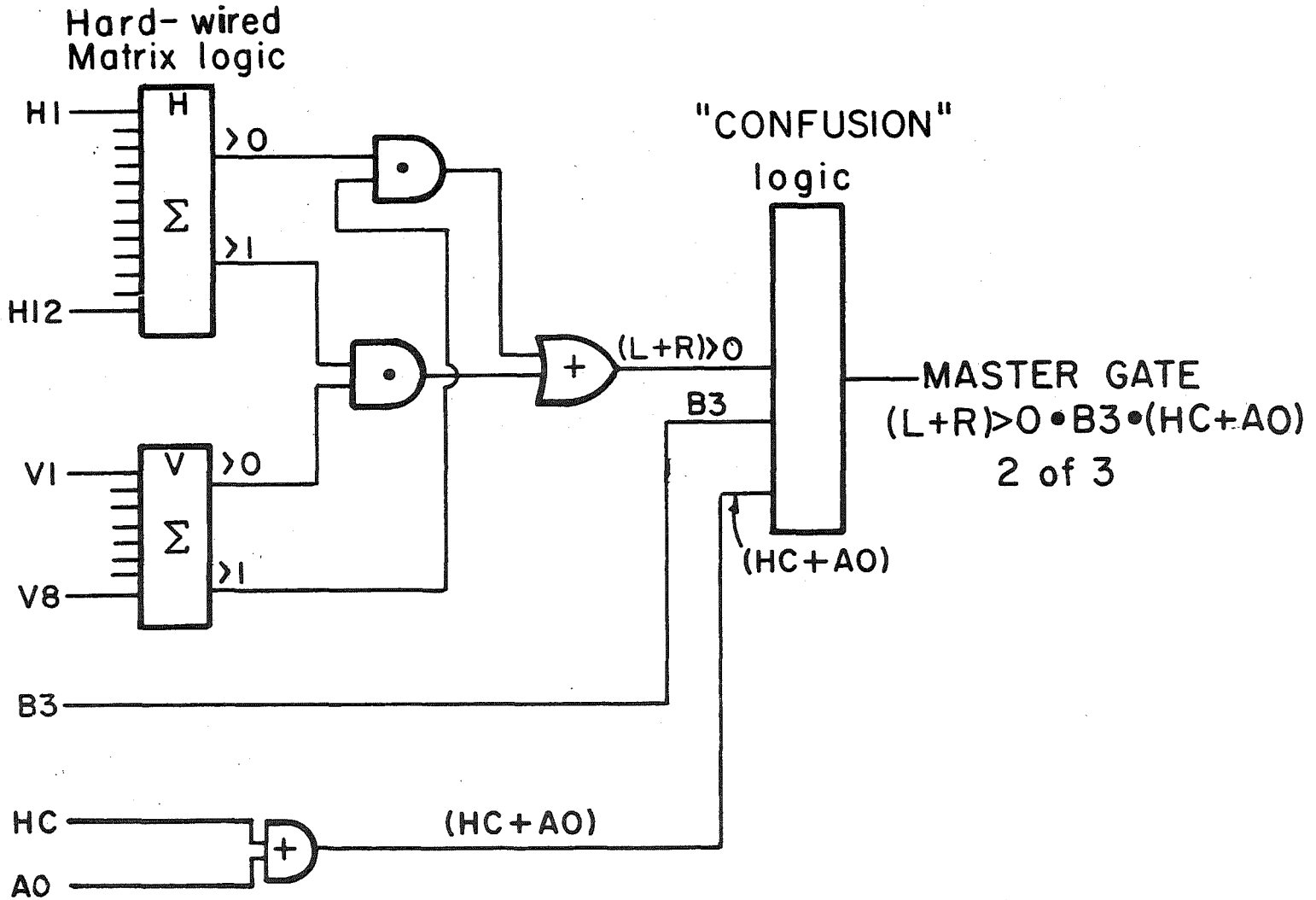

Fig 18 DERIVATION OF MASTER GATE

The CONFUSION logic generates >0 and >1 trigger outputs to the DC logic provided three conditions are met. These are:

1) no input for the previous 100 ns

2) no output for the previous 250 ns

3) no external veto

The >0 output is scaled by 1024 and intermixed with all >1 outputs in order to provide a sampling of >0 events. The scaled >0 output is also available as a separate output, PS>0, where it is used to generate a PS>0 buss line in the DC logic if desired.

The first condition helps reduce the number of times bad data will appear in the coincidence registers (CR's) as when the spill structure is very bad or equivalently when a relatively large number of particles are incident on the experimental target in a relatively short time (within 10 ns). This requirement further reduces the deadtime due to false triggers caused by charged particles in the beam. This is the origin of the triggers with A0 in them; when there is one charged particle in the beam or halo there may be many. The function of the triggers with A0 in them is to turn off the logic for 100 ns. The second condition insures that there will be no master gate sent to the DC logic during the decision time of this logic. The third condition inhibits any master gate generated while the Sigma-2 is reading out an event or while the DC logic is waiting for readout. This is done via the "BUSY" input which comes from the Sigma-2 and via the "HOLD" input which comes from the Output Trigger Generator (TGO--see below). Additionally, the Busy input from the Stigma-2 is passed on to the TGO where it inhibits further event triggers.

The second function of the CONFUSION logic is to provide gates and clear pulses to the MWPC rack. At the same time a >0 or >1 master gate is sent to the DC logic, a GATE and a delayed CLEAR pulse are sent out. The CLEAR pulse is delayed by the decision time of the DC logic and is blocked if the event is to be kept for later off-line analysis. Otherwise the MWPC shift registers are cleared in preparation for the next event trigger.

The third function of the CONFUSION logic is to keep track of the number of >0 and >1 master gates satisfied and the number actually sent to the DC logic for decision. This is done through the scaler outputs >0, >1- no deadtime (number satisfied) and >0, >1- deadtime (number sent to DC logic). By taking the ratio (>1 DT)/(>1 no DT) one can find the live time of the electronics to be used in calculating cross sections.

C. DC Logic

The function of the DC (or Nevis) logic is to make the decision whether to save an event for storage on magnetic tape or whether to throw it away, either decision being made according to some predetermined criteria. This decision is made through a series of coincidence register latches, sum logic (Σ-logic) modules, matrix logic modules, the so-called "Pin Logic" modules, and through some more conventional logic modules of the AND and OR variety. Communication throughout the DC logic is by means of DC current levels, initially set to some quiescent state which I will refer to as "OFF". Once a particular level is set "ON", it remains so until all the levels are cleared in preparation for the next master gate.

Inputs to the system are in the form of discriminator pulses from scintillation counters and threshhold requirements. Outputs of the system are logic signals to scalers, gates to the pulse height digitizing system, and triggers to the computer for the transfer of data and to the CONFUSION logic to inhibit further master gates. A first level of logic defines how many tracks are in each hodoscope plane. A second level of logic distributes these and other logic definitions to a buss to which many independent logic modules connect. Each logic module defines an event classification according to internal, pre-set switch connections to the logic buss. This logic is strobed and outputs are available for direct scaling. At this point the outputs may be used to form output triggers. However, it is often necessary to optimize the readout rates so the more common event types do not exclude the less common ones from generating event triggers. Accordingly, provision is made to pass some or all of the outputs through prescalers before they form output triggers. The output triggers are then mixed in a final level of logic to form the master output trigger from which the gates and event trigger to the computer is derived.

Each time an input trigger is accepted, a deadtime is generated to cover the time to clear the register, to gate the event into the registers, and to propagate the logic and form the output triggers. This deadtime was set to about 250 ns and is extended by the computer for up to several hundred micro-seconds if the logic produces an output trigger.

To see how this logic operates in detail, and in particular to see how it facilitates making what otherwise might seem to be complicated coincidences among many inputs, I will briefly describe the operation of

its components, trace the generation of several representative buss lines, and then present the Pin Logic requirements for a typical running period.

In addition to the types of modules noted above, there are several special purpose modules, the Input Trigger Generator (TGI) and the output Trigger Generator (TGO), the buss line drivers, and the trigger store modules. The TGI accepts master gates from the CONFUSION logic and performs the following functions:

1) sends CLEAR and delayed GATE pulses to the coincidence registers,
2) inhibits itself for a set but externally adjustable time, up to a maximum of 200 ns,
3) sends a strobe to the buss line driver, thus activating it, and
4) sends BUSY signals with a suitable delay to the Pin Logics via the buss line driver.

In normal operation, the gate to the coincidence registers was about 1.5 ns wide in order to avoid information pileup from the next rf bucket in the spill and could be delayed to accommodate the timing of the external inputs into the coincidence registers. Provision is made via a HOLD input from the TGO for extending the inhibit or deadtime required for decision making. The sum of internal inhibit plus external hold times was typical about 250 ns, of which about 200 ns was generated internally to TGI. The function of the strobe will be explained in more detail later.

The coincidence register modules accept up to 8 NIM inputs from standard discrimators. An external voltage allows the threshhold to be

varied between -100 mv and -800 mv and to be set above zero to cause all registers to latch for test purposes. Inputs to the CR's are discriminator pulses from the various scintillation counters and from the pulse height discrimination of shower and calorimeter counters. Once the inputs are properly timed into the CR's, no further time coincidence operations are needed. As noted above, a single trigger causes these inputs to be gated and sorted; this is done with a resolving time equal to the sum of discriminator plus gate widths, usually set for a total of about 15 ns. [See Fig. 19 for a schematic diagram of the coincidence register inputs.]

The CR's come in two types. The first provides an analog output corresponding to the sum of each of two sets of four inputs. The second type of CR provides an output for each input on a one-to-one basis. As might be surmised, CR's of the second type are used when one wishes to handle seperate inputs like B3, A0, and so forth. Coincidence registers of the first type are used to handle the inputs from counter arrays like the muon counters where one might (and does) desire to perform logical operations on parts and/or all of the array.

The function of the Sum Logic modules is to accept the analog outputs of the coincidence registers and to reconvert them to digital signals. This is done by means of DC current comparators to define >0, >1, >2 current increments and whose outputs indicate the number of latches set (=0, >0, >1, etc.). See Fig. 20. The output of a sum-logic module can be used to generate a buss line directly or it can be used as an input for further logic decisions.

Once any buss line requirement has been satisfied, this information is fed into one of two buss line driver modules. Each module accepts up

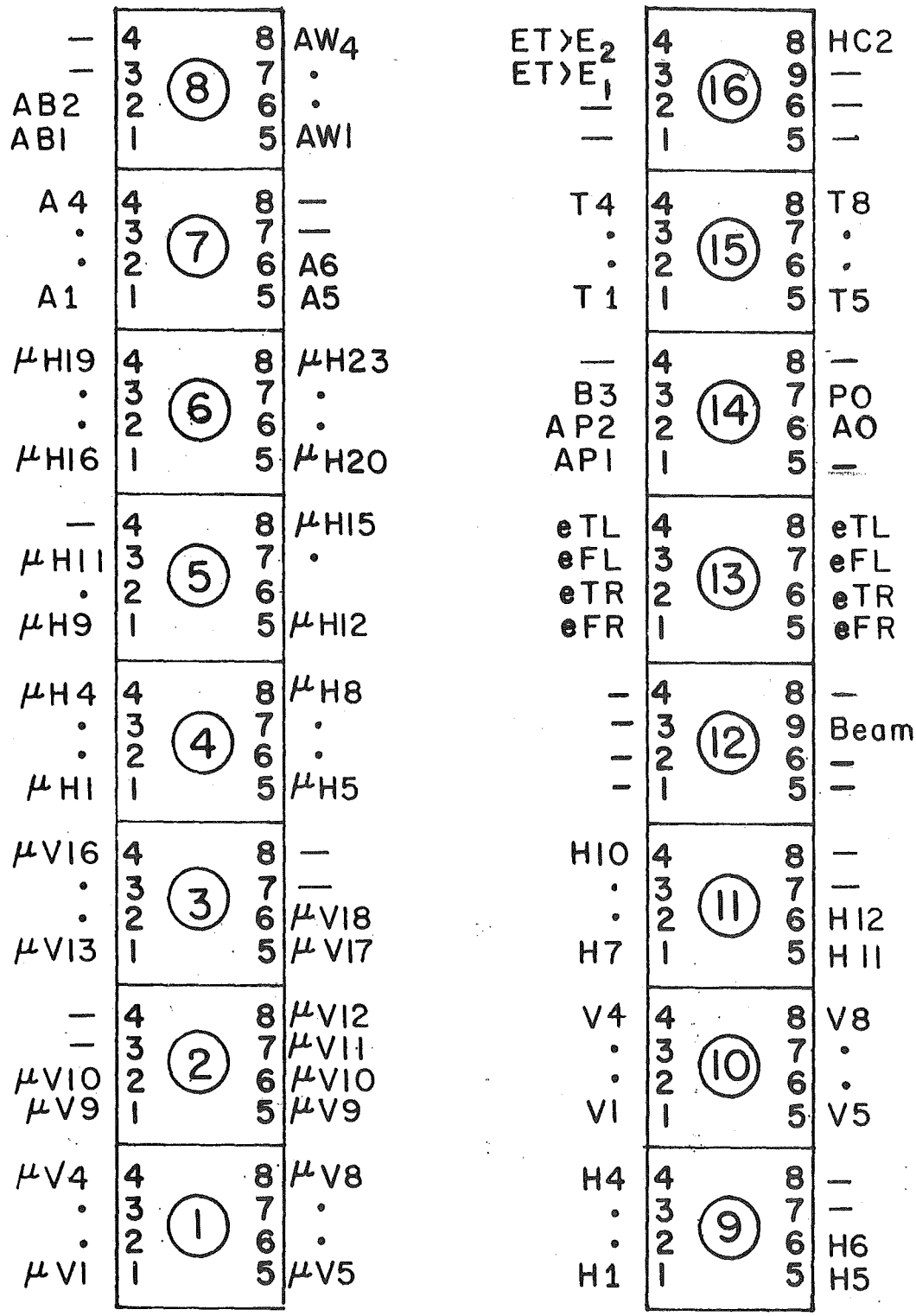

FIG 19 SCHEMATIC OF TYPICAL COINCIDENCE REGISTER INPUTS

"." DENOTES SEQUENTIAL CONTINUATION OF NUMBERING

"-" DENOTES NO INPUT

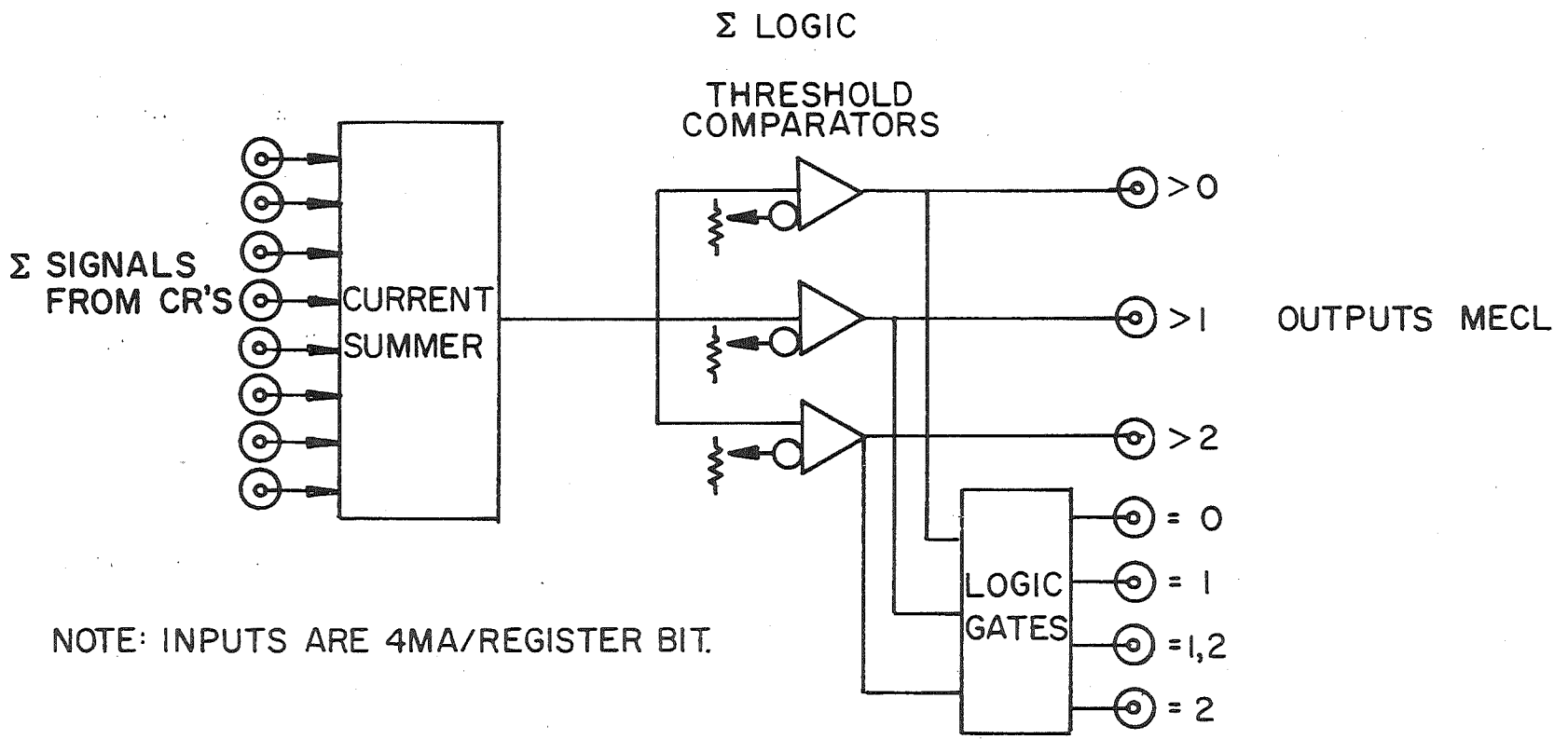

FIG 20 SCHEMATIC LOGIC DIAGRAM OF Σ-LOGIC MODULE

to 8 inputs; one module in addition accepts the STROBE and DEADTIME outputs of the TGI. The modules are mounted in the first two slots of a special bin, the logic buss bin, on which a printed circuit data buss has been attached to the rear. Module connectors are soldered to this data buss to allow the buss line conditions to be sensed by the "Pin Logic" modules. Each line of the data buss is terminated in 50 ohms by a terminator module in the last slot of the bin. The leading edge of the STROBE blocks any further input to the buss line driver. It is for this reason that for a particular event the STROBE must be the last condition to be sensed by the buss line driver modules. The DEADTIME input allows the buss lines to be set and hence the Pin logics to be satisfied even while the system is waiting for computer readout. This allows a comparison of the number of times a Pin Logic actually produces an event trigger with the number of times it is satisfied. The ratio of these two numbers defines a system livetime, which is useful for optimizing readout rates among Pin Logics and is used in the calculation of cross sections.

The Pin Logic module thus accepts up to 16 buss line inputs via the rear connector. During typical running we used up to 14 different Pin Logics although during the neutron and lead-in running we used as few as four. Logic requirements on the 16 buss lines were made with a wire connector (dubbed a "pin") on the Pin Logic PC board. The requirements TRUE, FALSE, and "don't care" are available, the latter condition occurring when no connection was made. [See Fig. 21 for a schematic diagram of a Pin Logic module.] Additional inputs on the front panel allowed an extension of the logic. These provided for an external veto, an inhibit from a prescaler, and for an extra logical TRUE requirement if

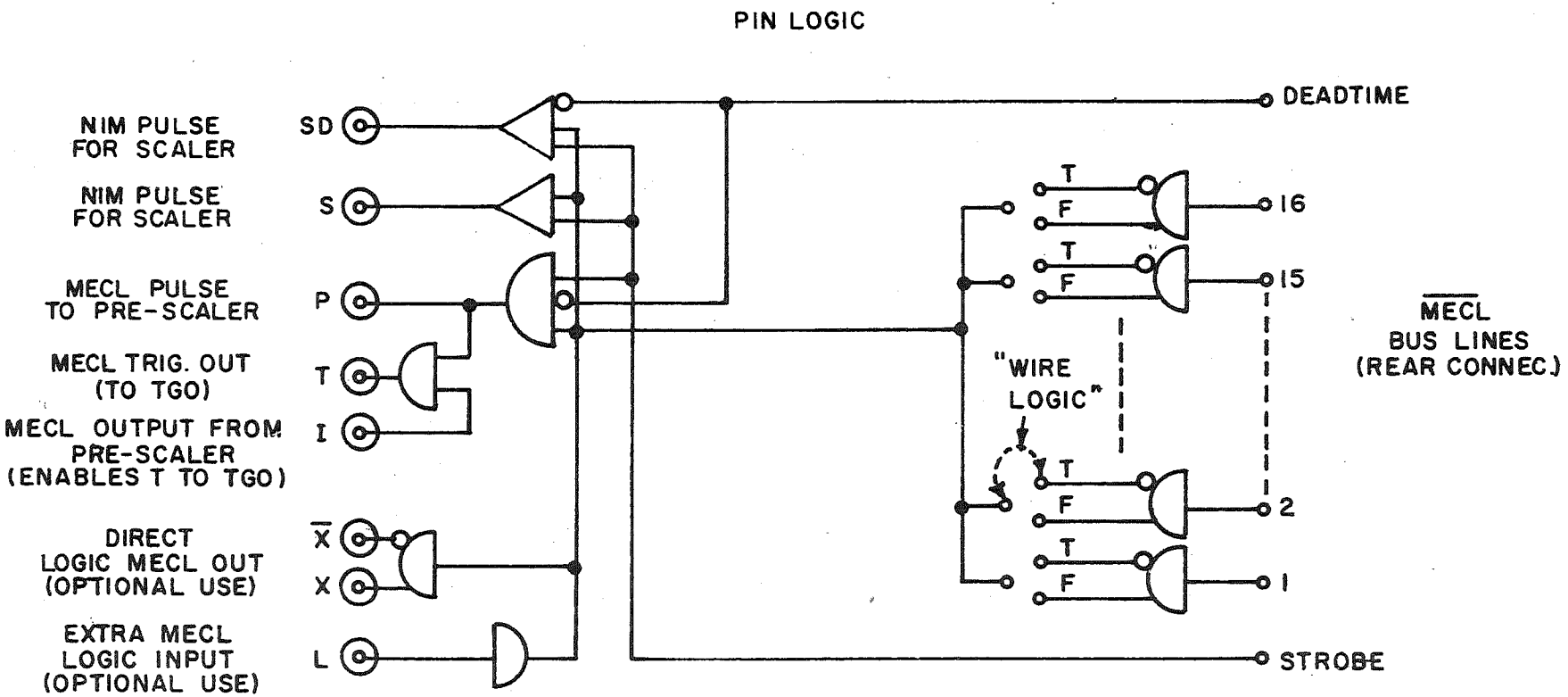

Fig. 21 Schematic logic diagram of Pin Logic Module

connected. The buss line requirements for the Pin Logics during a period of normal photon ("lead out") running will be shown below. As mentioned above, provision was made for scaling the output of the Pin Logic with and without deadtime corrections.

Whenever one or more of the Pin Logics are satisfied, MECL-level "complement true" conditions are sent to the Trigger Store modules, which in turn pass a complement true input to the Output Trigger Generator. The contents of the trigger store modules are transferred via rear connectors to a coincidence register. This information is read out for each event and hence is available for later off-line analysis.

The TGO performs the following operations.

1) Accepts input from the Trigger Store. Provision is made for a MECL-level STROBE input to allow retiming of the READ pulse and for an ANTI input to extend the logic.
2) Generates NIM-level GATES whose width is determined by a front panel "width" cable. The gates are sent to the pulse height digitizing system and through a fanout to other parts of the NIM-level logic and to the CONFUSION logic at the READ input.
3) Sends a MECL-level HOLD condition back to the TGI to prevent further input to the DC logic while the TGO is waiting to send our an event trigger (READ pulse).
4) Generates a NIM-level event trigger from the READ output. The event trigger is sent to the computer and to the "System Busy" input of the TGI and is delayed 15 micro-seconds after the STROBE input ceases in order to allow the analog-to-digital

converters (ADC's) to finish digitizing before the computer begins its read operation. In operation, a READY (NIM complement level) is required to accept an input from the trigger store. A NIM true level, indicating readout, was passed through the CONFUSION logic from the computer and inhibited further input. The MECL-level outputs X and X-bar were also available.

D. Buss Lines and Pin Logics

The sixteen buss lines for the photon running are diagrammed in Fig. 22. In the buss lines involving MWPC requirements, $>0^3$ stands for at least one hit in each of three planes, $>1^2$ stands for at least two hits in two of the three planes, and $>2^2$ stands for at least three hits in two of the three planes. Additionally, P1(2/3) stands for at least two hits in two of the three planes of P1.

The Pin Logics for most of the lead-out photon running are shown in Fig. 23. The symbol "X" requires the buss line in veto and "√" requires the buss line in coincidence.

The 2μ Pin Logic requires that there be no hit in A0 or the muon anti's, that the 2μ and MWPC buss lines be required, and that there be less than 7 GeV of energy deposited in both EV1 and EV2, which were the vertical shower counters.

Fig. 22a Typical Buss Lines for Photon Running

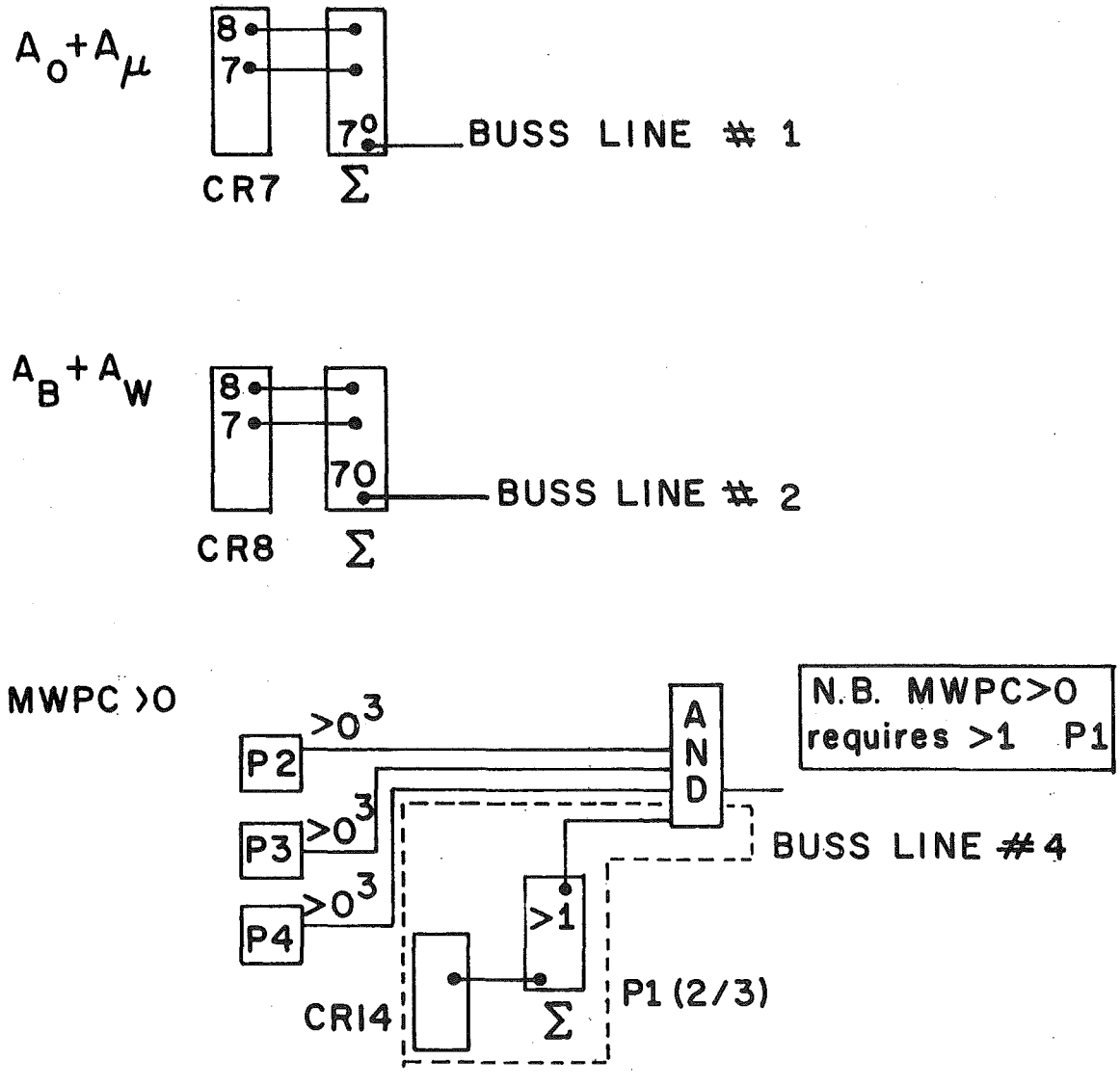

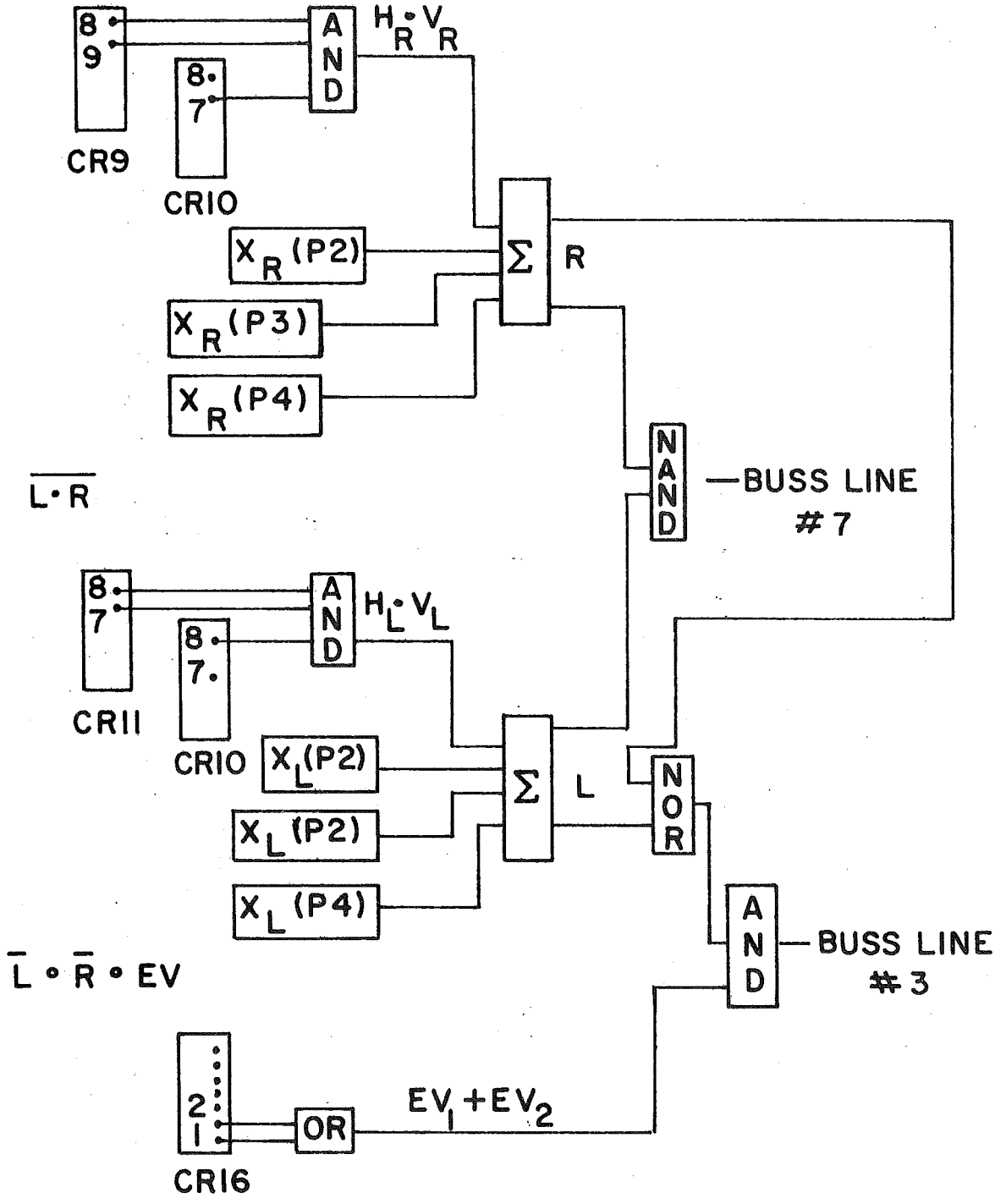

FIG 22b TYPICAL BUSS LINES FOR PHOTON RUNNING

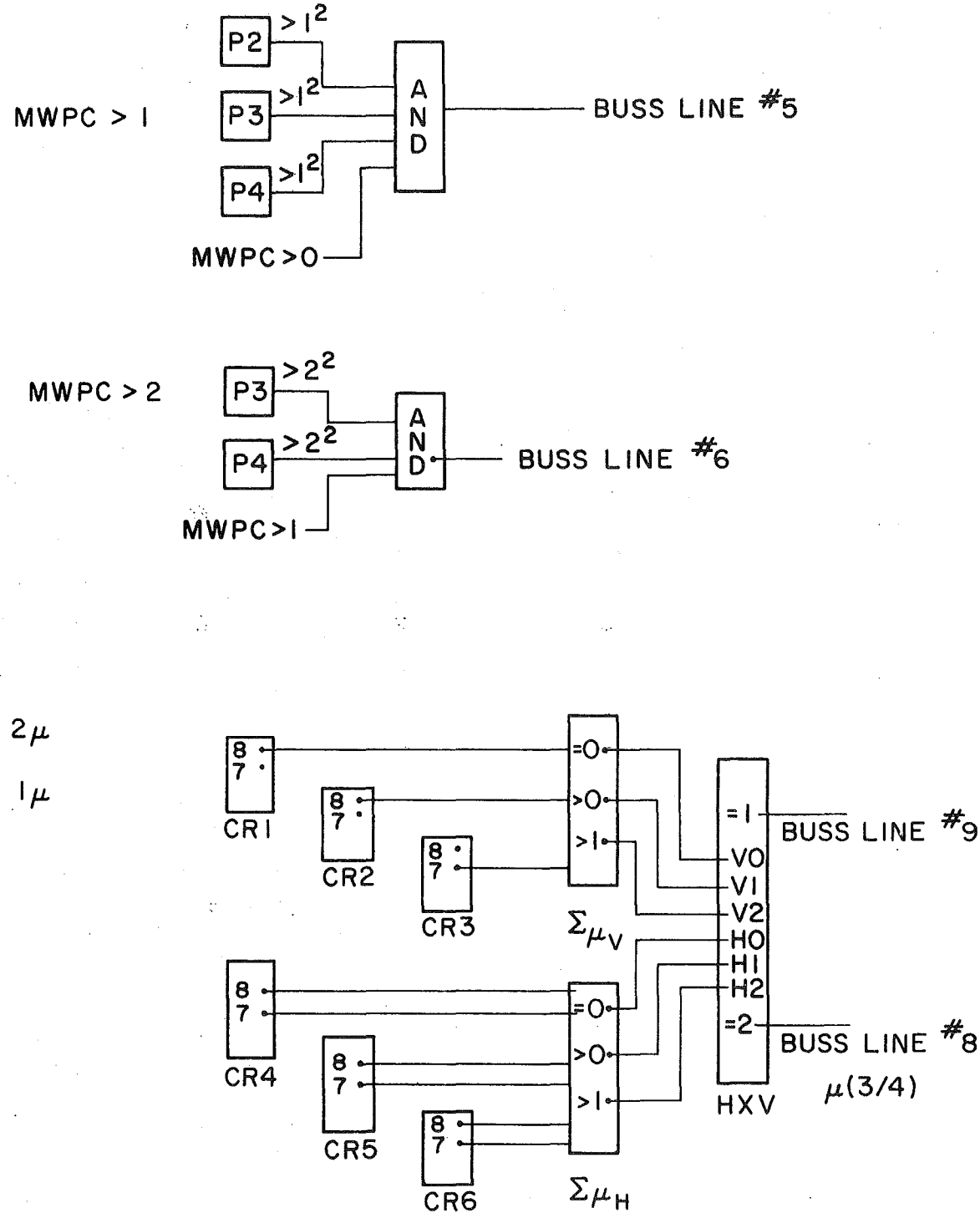

FIG 22C TYPICAL BUSS LINES FOR PHOTON RUNNING

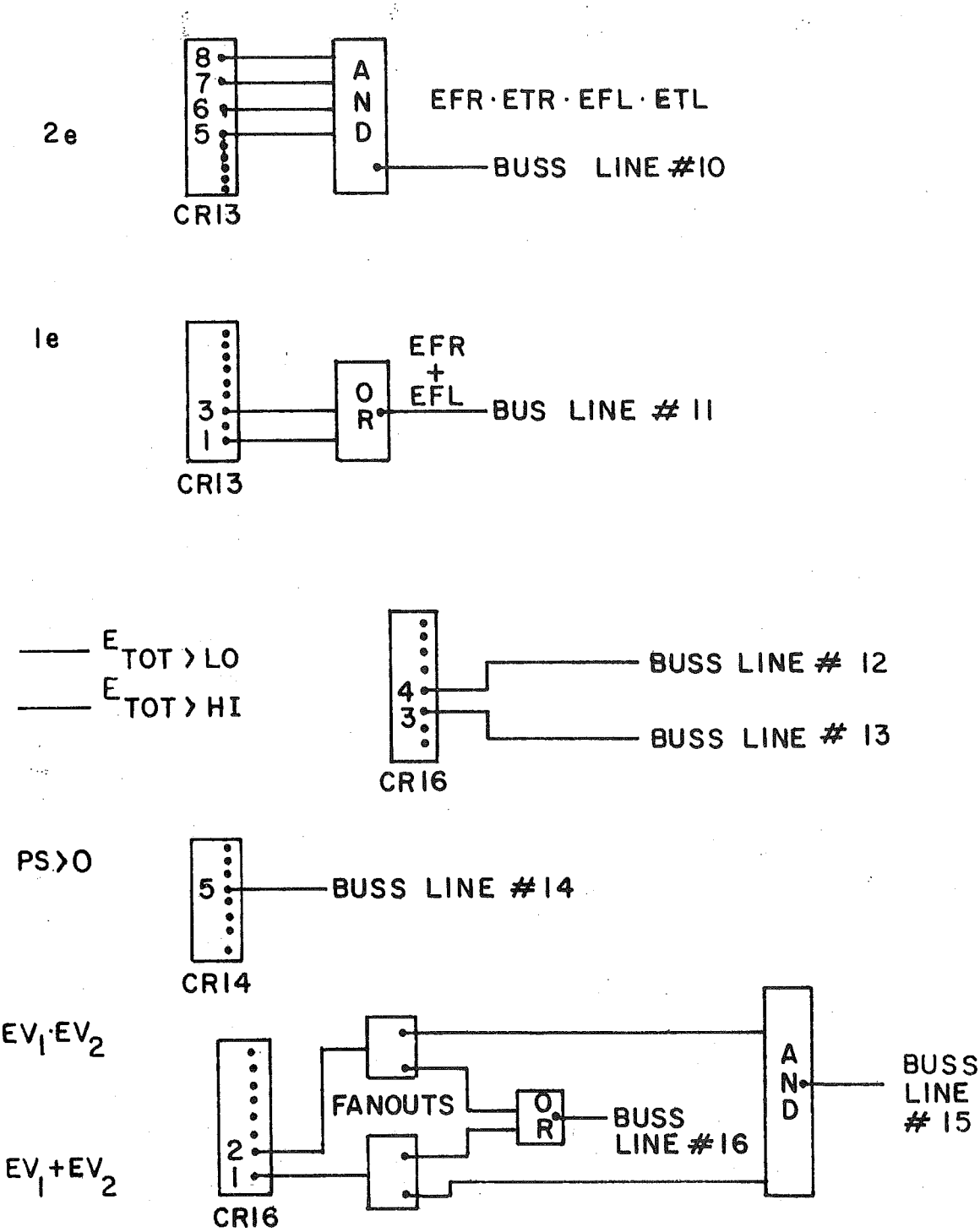

FIG 22d TYPICAL BUSS LINES FOR PHOTON RUNNING

FIG 23 TYPICAL PIN LOGICS FOR PHOTON RUNNING

BUSS LINE \ PIN LOGIC	2e	1e	μe	2μ	2μ	μ	2π	4π	Monitor Pins			2π Hi	1e Hi
$A_O + A_\mu$	×	×	×	×	×	×	×	×				×	×
$A_W + A_B$		×				×	×	×				×	
$\overline{L} \cdot \overline{R} \cdot EV$					×	×	×	×					
MWPC > 0											✓		
MWPC > 1	✓	✓	✓	✓	✓	✓	✓						
MWPC > 2								✓					✓
$\overline{L \cdot R}$	×	×			×	×						×	×
2μ				✓	✓								
1μ			✓			✓							
2e	✓												
1e		✓	✓										
E_{TOT} > Lo					✓	✓	✓	✓					
E_{TOT} > Hi		✓										✓	
PS > 0									✓	✓	✓		
$EV_1 \cdot EV_2$										✓			
$EV_1 + EV_2$				×					✓				

✓ Required in coincidence

× Required in anti-coincidence

V. DATA REDUCTION AND ANALYSIS

A. Spectrum

The photon spectrum was measured periodically throughout the photon running by removing the experimental target and inserting a lead foil of 4% XO in front of the magnet M1 (AN421B). See Fig. 24. Runs were made at different current settings in order to open up e^+e^- pairs from all parts of the spectrum. From each run, the number of events as a function of photon momentum was normalized to 10^{12} protons. The spectrum from each run was then cross-normalized to the spectra from the other runs by using the quantameter for absolute calibration. The resulting photon spectrum is shown in Fig. 25.

B. Monte Carlo

The efficiency for accepting events was calculated by a Monte Carlo program. Events were generated at a given mass (3.095, 3.684 GeV/c, etc.), were given a $1 + \cos^2\theta$ distribution in the center of mass, a flat energy dependence or were distributed according to $e^{-.0215\ E_\gamma}$ and were distributed in the momentum transfer squared ($P_\perp^2$) according to one of two slopes, where one slope is characteristic of coherent scattering off a nucleus and the other is typical of incoherent scattering off single nucleons in the nucleus. The decay angular distribution $1 + \cos^2\theta$ is characteristic of the decay of a 1- particle into two spin 1/2 particles. A flat energy dependence was chosen for calculating the acceptance of the ψ as a function of momentum. The acceptance was then fit to a functional form.

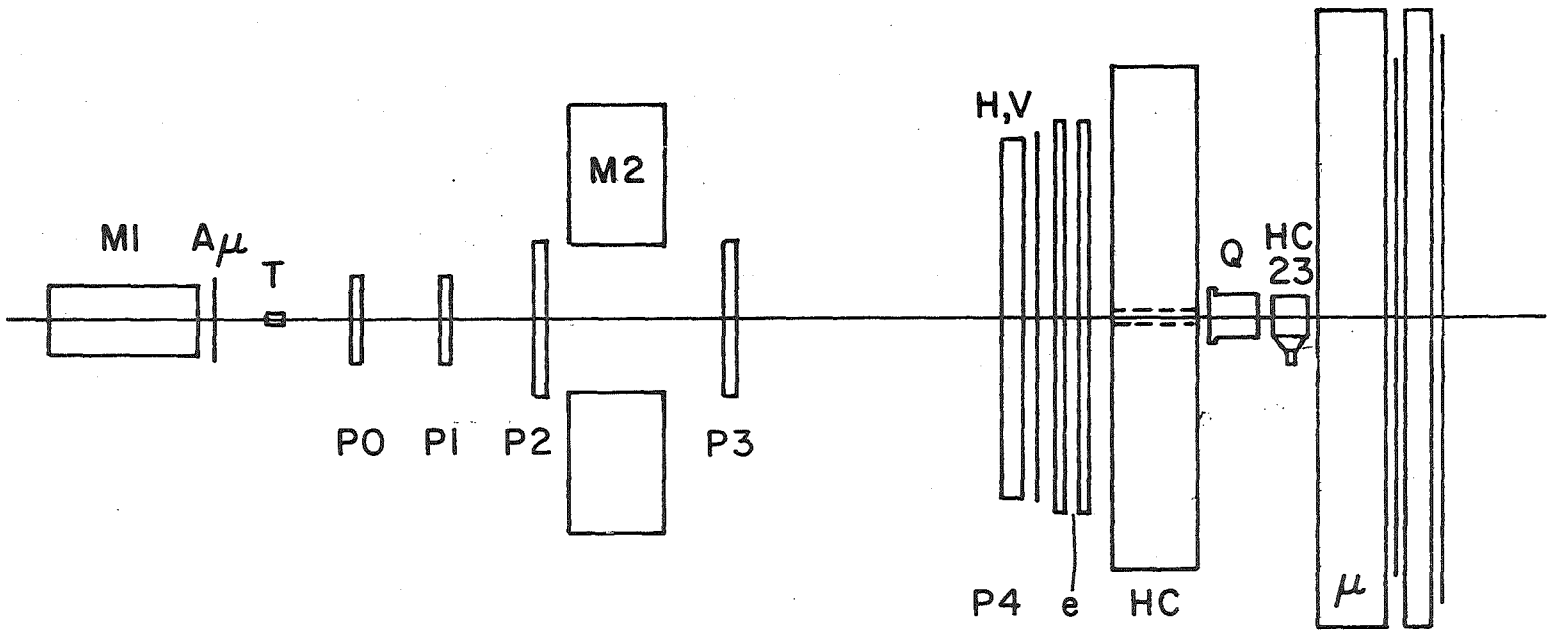

Fig. 24

Schematic diagram of spectrometer Showing magnet M1, used for spectrum measuremet.

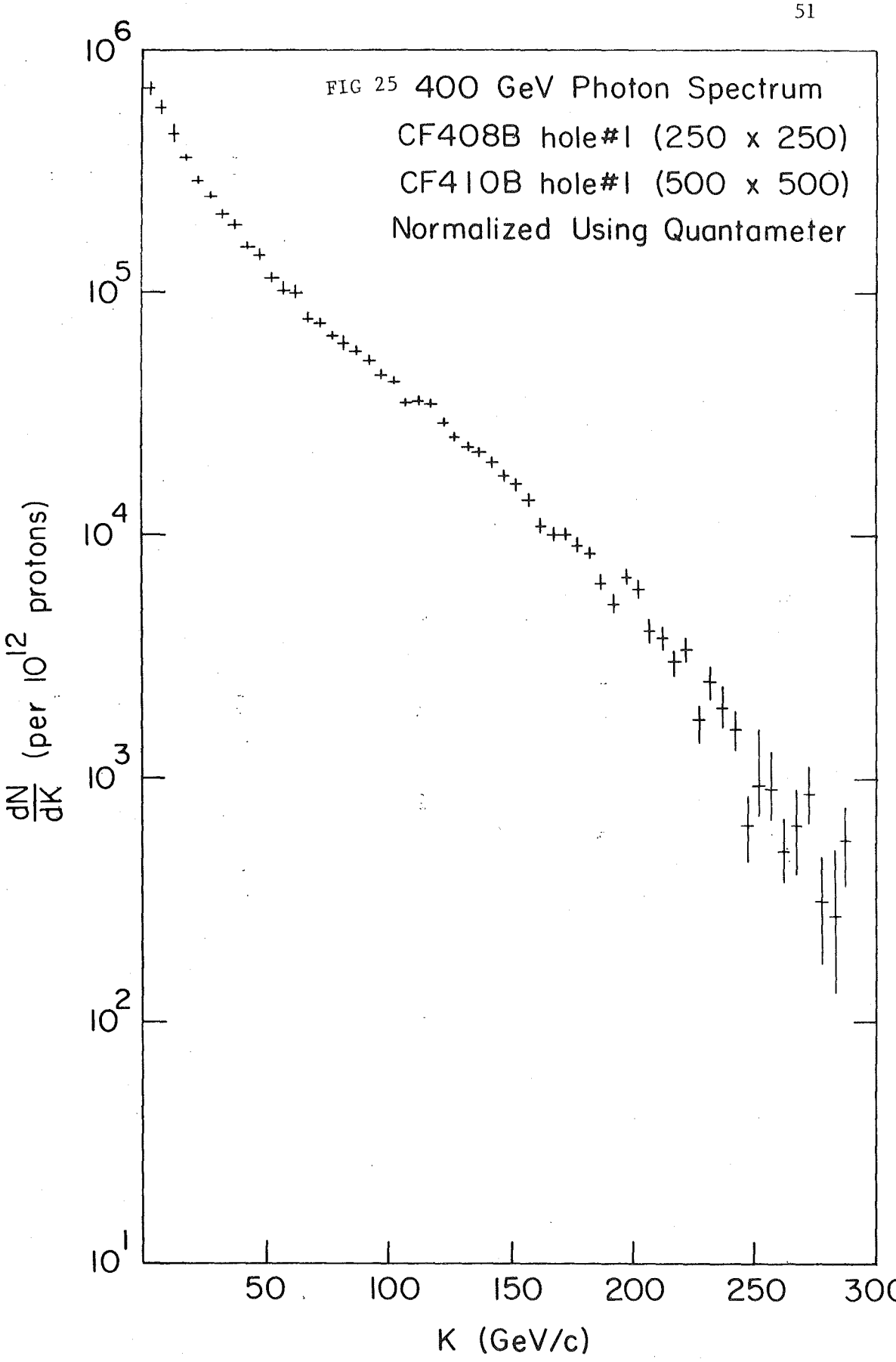
FIG 25 400 GeV Photon Spectrum
CF408B hole#1 (250 x 250)
CF410B hole#1 (500 x 500)
Normalized Using Quantameter
dN/dK (per 10^12 protons)
K (GeV/c)
10^6
10^5
10^4
10^3
10^2
10^1
50
100
150
200
250
300

See Fig. 26. For calculating overall acceptances, resolutions, and other quantities of interest the energy of an event was distributed exponentially according to the average slope of the spectrum above 70 GeV/c. The distribution in $P_\perp^2$ of the events was generated according to the formula of Margolis.

The generated events were then required to pass the following fiducial cuts:

1) within the active area of P1,

2) within the magnet aperture at exit,

3) within the active area of P4

4) within the active area of the H and V counters (excluding the gap between left and right counter banks), and

5) within the active area of the vertical muon counters.

The Monte Carlo events were also required to satisfy the MWPC>1 trigger, which required at least one track to be outside the central 8 wires of the x-planes of P2, P3, and P4. Our acceptance was determined mainly by the magnet aperture.

In order to determine the background due to Bethe-Heitler muon pair-production, a Monte-Carlo program following the prescription due to Y. S. Tsai[13] was written. Events from this Monte Carlo were required to pass the same event cuts as the events from the line spectra Monte Carlo.

In Monte Carlo studies for the cascade decay of the ψ', $\psi' \to \psi\pi\pi \hookrightarrow_{\mu\mu}$ the ψ' was generated with the same energy-angle distributions as was the ψ and was allowed to decay into a ψ and 2 pions which were in a state of relative orbital angular momentum $\ell = 0$ (s-wave). The decay of the ψ into 2 muons followed a $1 + \cos^2\theta$ distribution in the ψ center of mass.

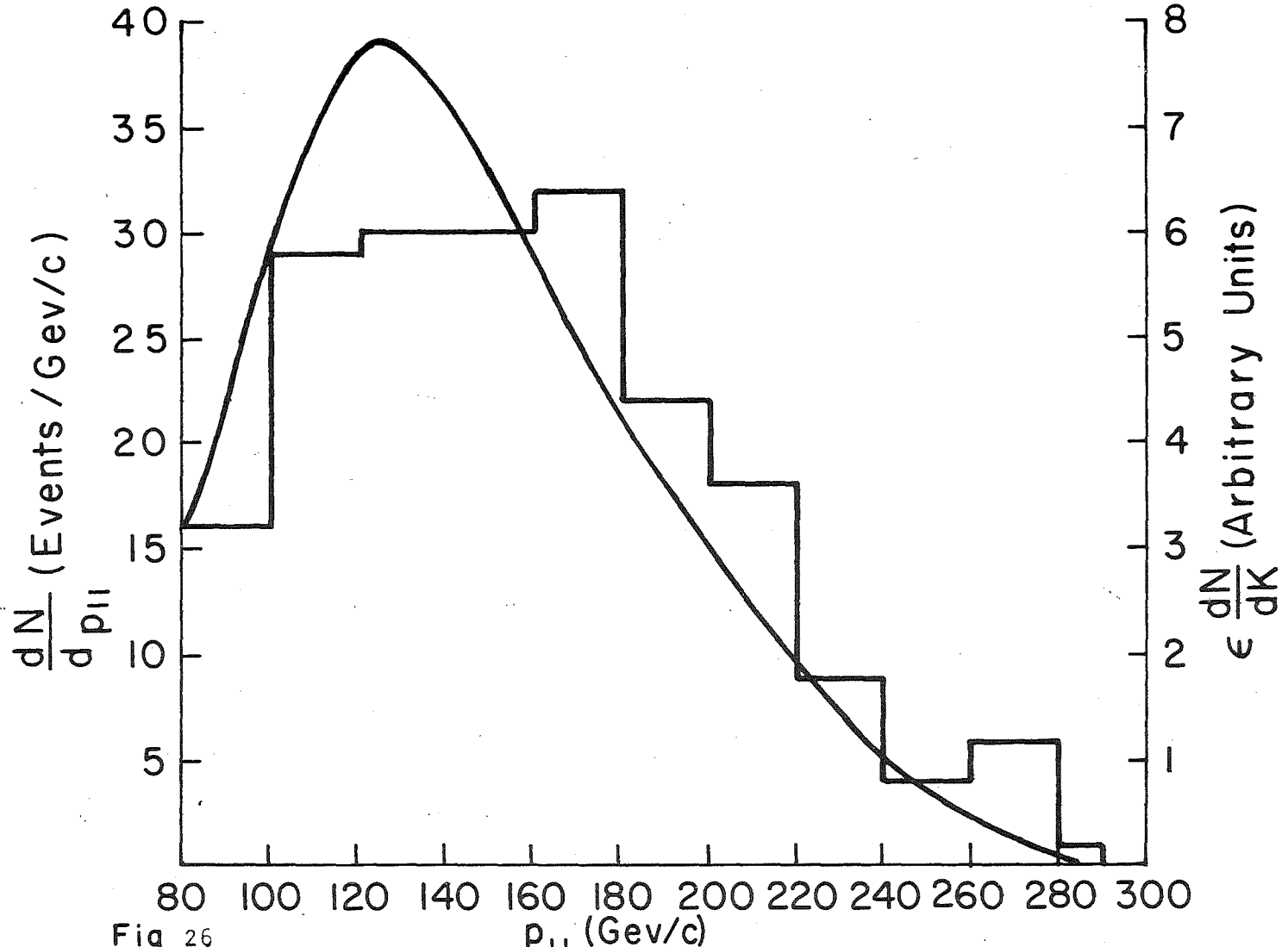

Fig 26

Momentum distribution for "All" Sample $0 \leq t_{\perp} \leq 5.3$ (Gev/c)^2

C. Initial Data Reduction

The raw data for the standard photon running consisted of 337 tapes containing approximately 15 million triggers.

An initial condensation of the data reduced the number of events to a more manageable sample. All two track events that satisfied the following criteria were kept:

1) possess greater than 50 GeV/c in visible momentum

2) possess a vertex

3) possess a mass of at least 1.5 GeV/c^2

In addition, any multi-track event was saved if any two tracks satisfied the above criteria and if any two tracks projected to hit muon counters. The mass cutoff of 1.5 GeV/c^2 was chosen in order to treat the data from the standard photon running, which used a single target, in the same way as the data from the running with three targets followed by a lead absorber. It was not possible to seperate the three targets for events whose mass was less than this value. The cut on momentum was applied because we have almost no acceptance below this momentum for masses above 1.5 GeV/c^2.

A second pass on the above data sample saved all events in which the 2-mu buss line was on. This cut reduced the sample to roughly 10% of its previous size. A third pass selected those events which contained two or more identified muons.

Muons were identified according to the following procedure. First, the expected deviation due to Coulomb multiple scattering in the shower counters, hadron calorimeter and muon steel was calculated for each track. Next each track was projected upon the mu-H and mu-V counter planes in turn. Thirdly, the counter planes were searched for a hit counter within

a radius defined by 3x the expected deviation or 4", whichever was smaller. Four inches is the half-width of the muon counters and this was chosen as a cut-off in the search radius in order to avoid possible confusion resulting from searching too many muon counters.

A two-track event is classified as a dimuon event if the following criteria are satisfied:

1) Each track projects to a hit muon counter and no more than one counter is shared.

2) One track projects to two hit counters and the other projects to only one hit counter but no counters are shared.

Criterion 1) is referred to a "4/4"; criterion 2) as "3/4". A dimuon in a multi-track event is required to be a 4/4 event. To restate, any 4/4 dimuon can have no more than one shared counter between the two tracks. A 3/4 dimuon is not allowed to have any shared counters.

After the cut on the 2-mu buss line, 6450 events remain; of these we have

1806	events	with	no	identified	muons
2711	"	"	one	"	"
1793	"	"	two	"	"
88	"	"	three	"	"
3	"	"	four	"	"

The two muon sample is relatively free from contamination due to pion decay in flight. This is seen from the charge distributions for three mass regions for the momentum interval $80 \leq P_{\mu\mu} \leq 290$ without target requirements as shown in Table 2.

TABLE 2

CHARGE DISTRIBUTIONS FOR EVENTS CONTAINING
TWO IDENTIFIED MUONS -- SEE TEXT

	Mass Interval		
Charge	1.5	1.8-2.6	2.8-3.4
+ -	936	232	226
+ +	42	12	Ø
- -	23	8	Ø

D. Vertex Criteria

Up to this point, a track has referred to a track as found by the reconstruction program.* In order to determine whether a particular track intersected with a second track or other tracks at a common location, a multi-track vertex finding routine was written. The vertex is then defined as the point in the z-direction (beam direction) at which the tracks are closest. This involves minimization of the quantity:

$$D^2 = \sum_{\substack{i=1 \\ j=1 \\ i\neq j}}^{N} \{(x_i-x_j)^2 + (y_i-y_j)^2\} \qquad (14)$$

where the subscripts 1, 2, 3, ..., denote tracks 1, 2, 3, ..., and which for two tracks is the square of the distance between the tracks at point of closest approach. Once this quantity is minimized, the x- and y-coordinates of the vertex, X_V and Y_V, are found and the distance of each track from the vertex is computed.

*Details of the reconstruction program may be found in Reference 10.

If all the tracks are within a specified distance of the vertex, no further computation is necessary and the event is kept as an N-track event, where N is the number of tracks found by the reconstruction program. If one or more tracks are farther away from the vertex than this distance, the track farthest away is flagged and not used in the next or succeeding iterations. The next iteration finds the (N-1)-track vertex, after which the (N-1) tracks are again tested as above. This procedure continues until an acceptable vertex is found or until there is only one track left.

The test distance was chosen to be Δ = .01". Monte Carlo studies indicated for two-track events that all the tracks passed within .05" of the common vertex and 90% of the tracks passed within .005". The distribution of Δ**2 is plotted in Fig. 27. Relaxing the criterion to Δ = .14" results in the "loss" of only 2 two-track ψ events. Relaxing the criterion to up to 1/2" results in no further exclusion of two track ψ events.

Subsequent analysis showed that about 3% of the events in the interval $2.8 \leq M_{\mu\mu} \leq 3.4$ GeV/c^2 (i.e., ψ candidates) were lost by the above procedure. This occurred whenever a vertex of a multi-track event was found which did not contain one of the muons from the decay $\psi \rightarrow \mu\mu$. Accordingly, non-intersecting muon tracks were flagged and after the particular event had been analyzed, were paired with all the other muons in the event. Each pair in turn was reanalyzed.

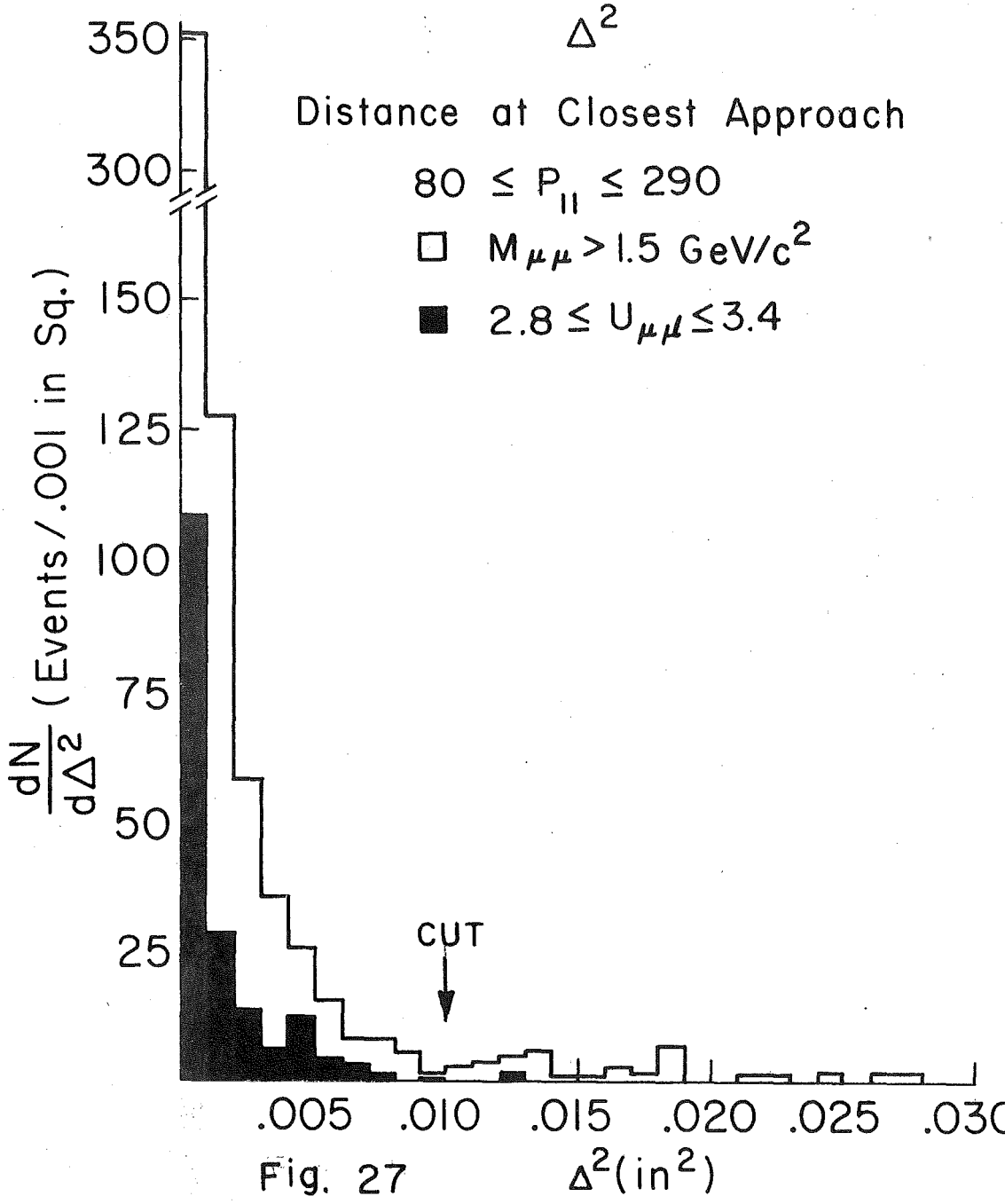
Δ^2
Distance at Closest Approach
$80 \leq P_{11} \leq 290$
$M_{\mu\mu} > 1.5$ GeV/c^2
$2.8 \leq U_{\mu\mu} \leq 3.4$
$\frac{dN}{d\Delta^2}$ (Events/.001 in Sq.)
350
300
150
125
100
75
50
25
CUT
.005
.010
.015
.020
.025
.030
Δ^2(in^2)

Fig. 27

E. Event Cuts

Events with two identified muons are required to pass three further cuts in addition to the fiducial cuts previously described. These are:

1) Vertex within 10" of the nominal position of the target -- see Fig. 28.

2) Dimuon momentum between 90 and 290 GeV/c. The lower limit was chosen because we have almost no acceptance for ψ's below this momentum. The upper limit was chosen because there are virtually no photons above this momentum.

3) Charge 0. 805 events passed all cuts but this one; only 5 events were cut by requiring charge 0, none of which were ψ candidates.

The dimuon mass spectrum for a slightly less restrictive momentum range is plotted in Fig. 29. The resolution of the peak centered about 3.1 GeV/c^2 is about 220 MeV/c, which is consistent with a Monte Carlo calculation. There are 6 events in the range $3.4 \leq M_{\mu\mu} \leq 4.0$ GeV/c^2 and 4 events clustered about 4.7 GeV/c^2.

As a check on muon identification, the 2-track events containing only one identified muon (required to project to two hit counters) were subjected to the same event cuts as the 2-muon sample. The resulting mass spectrum is shown in Fig. 30.

The lack of a accumulation of events in the ψ-mass region indicates that muons are being identified properly.

Figure 31 is a semi-log plot of the dimuon mass spectrum with the solid curve representing the background due to Bethe-Heitler muon pair production. The curve has been normalized to the number of events in the mass region $1.8 \leq M_{\mu\mu} \leq 2.6$ GeV/c^2.

Fig 28 Dimuon Vertex Distribution

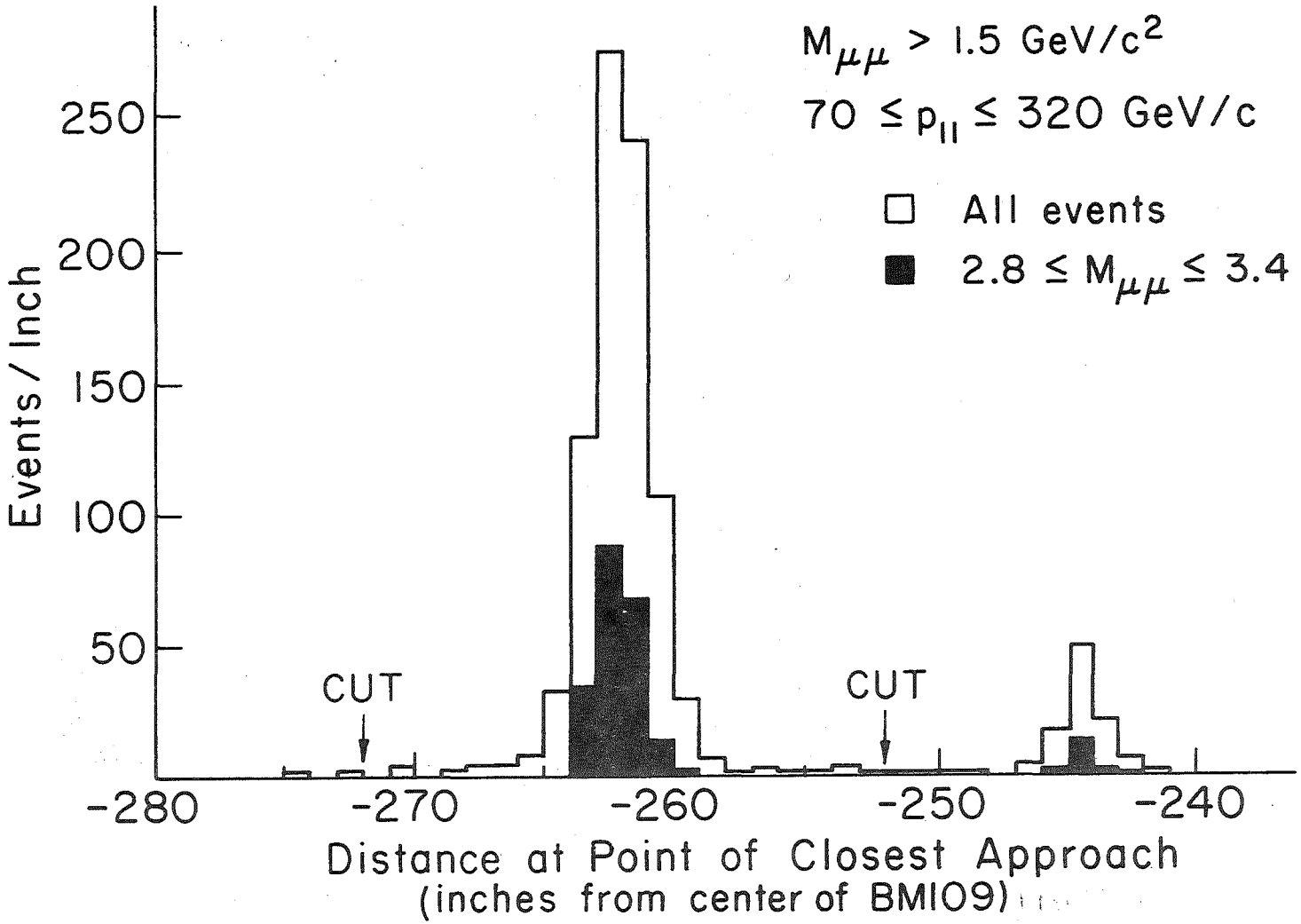

Fig. 29

Dimuon Mass Spectrum

$70 \leq p''_{\mu\mu} \leq 320$

1" Be Target

$Q = 4.99 \times 10^{13}$ GeV

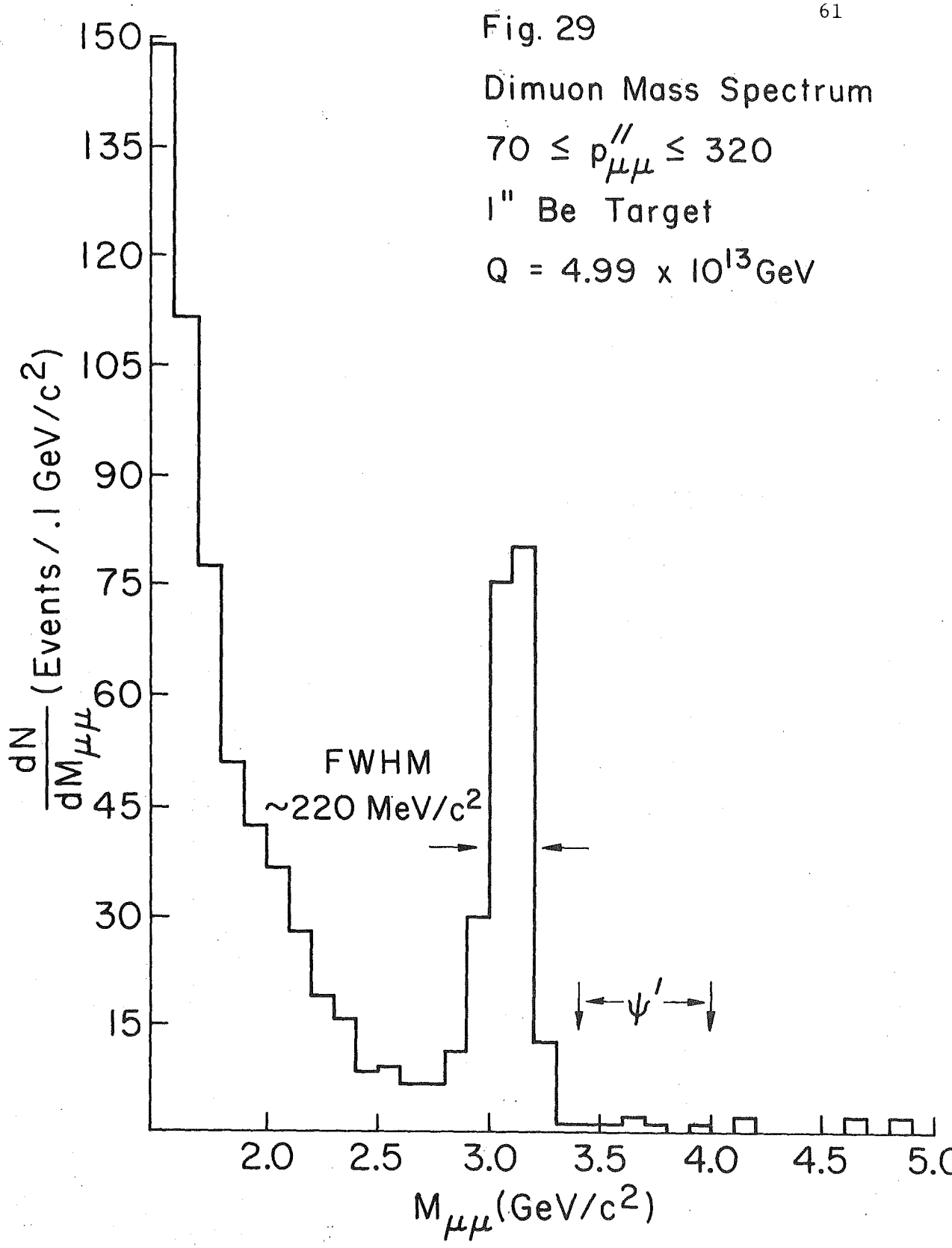

Fig 30

Mu - Pi Mass Spectrum

Two - Mu Buss Line on 1" Be Target

$Q = 4.99 \times 10^{13}$ GeV

$70 \leq p^{11}_{\mu\mu} \leq 320$

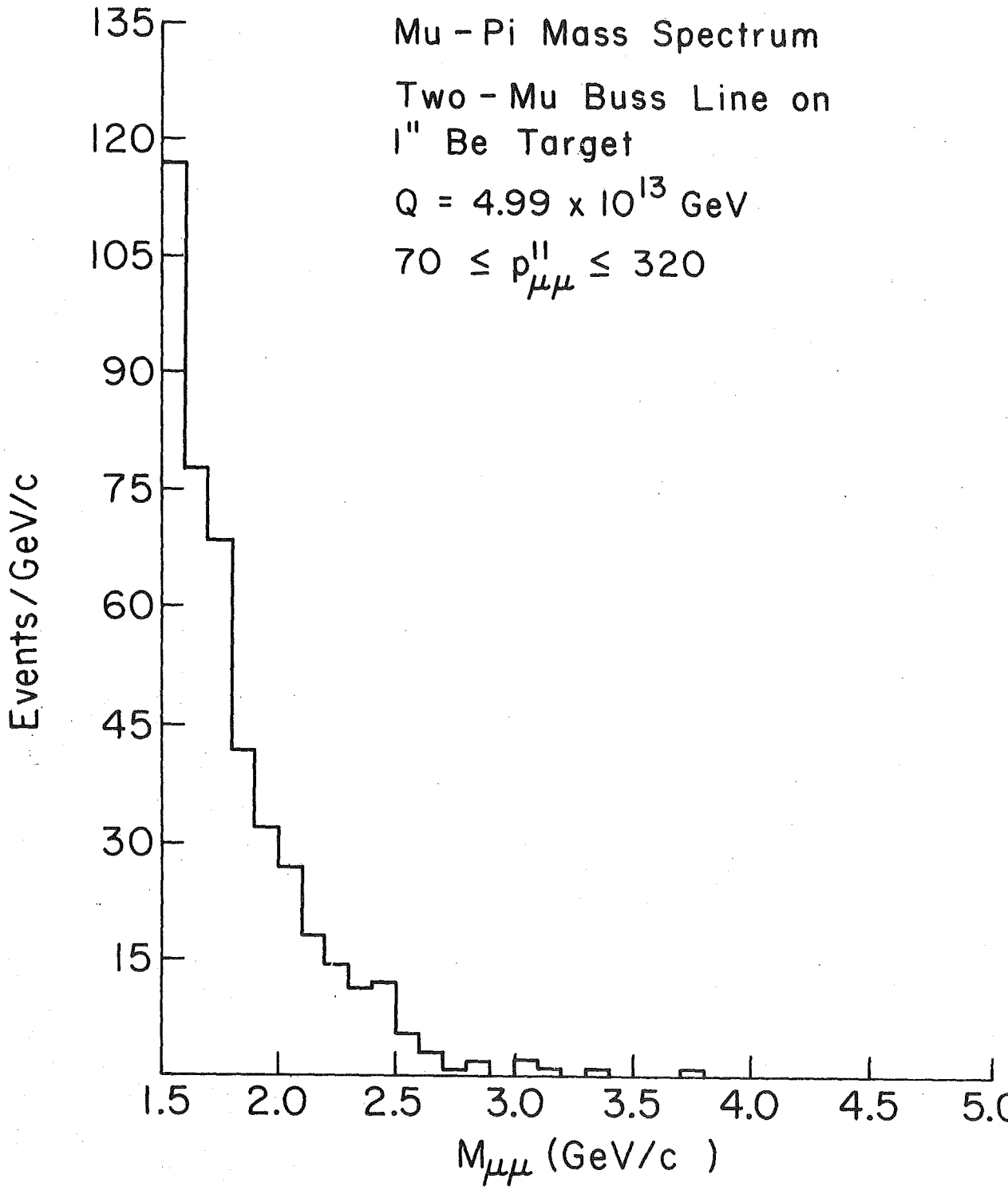

FIG 31 DIMUON MASS DISTRIBUTION FOR "CLEAN" SAMPLE

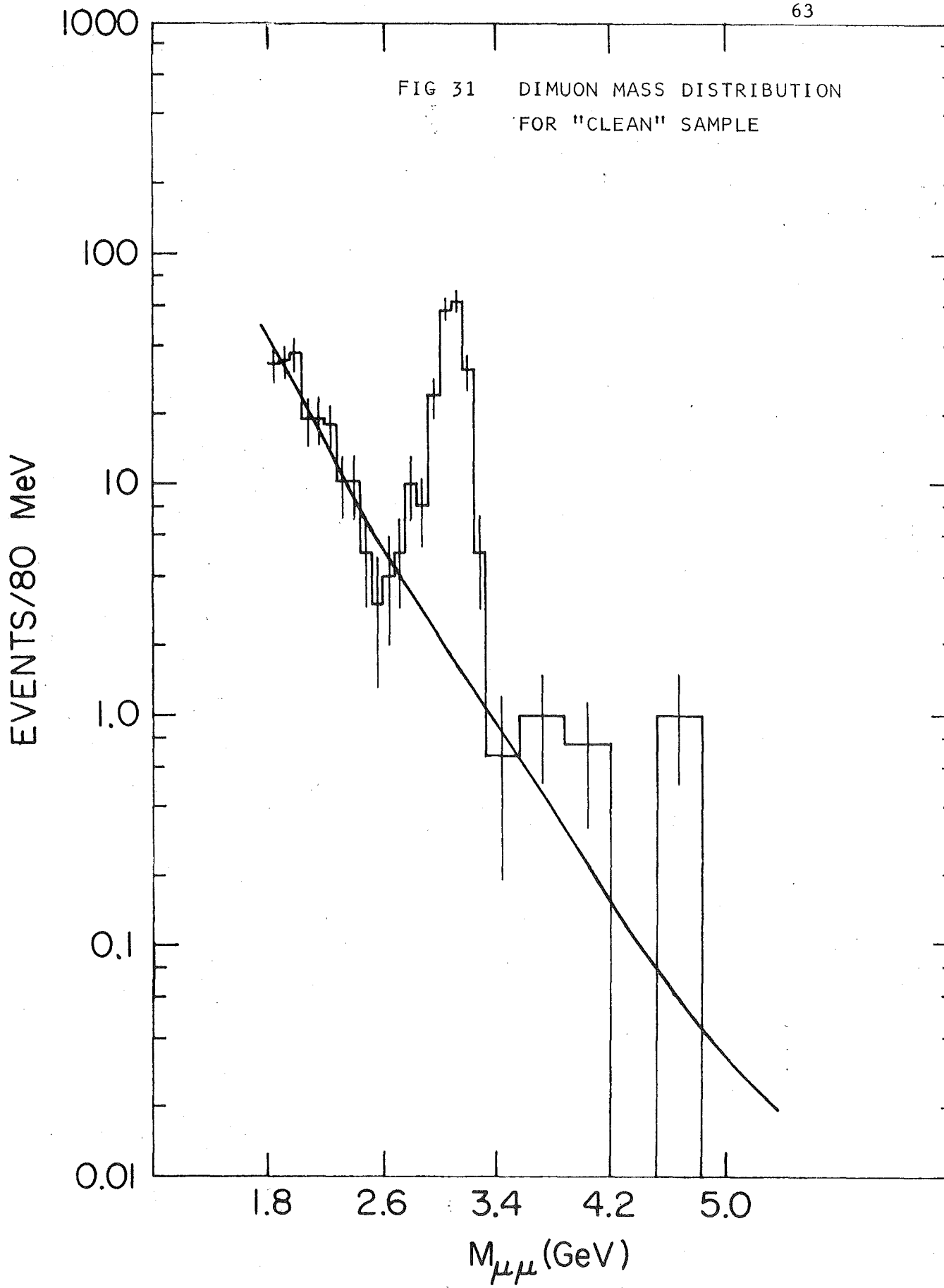

F. "Clean" and "All" Samples

After the above cuts, 195 two-track events remain in the ψ region. In deference to past practice, this sample will be designated the "all" sample. It contains events of three types, elastic, quasi-elastic, and inelastic as well as background from the Bethe-Heitler process and from the sequential decay of ψ's. Elastic scatterings involve no additional production of particles other than the ψ. In elastic events the nucleus as a whole absorbs the momentum transfer of the photoproduction process while in quasi-elastic events the momentum transfer is absorbed by individual nucleons in the nucleus. Inelastic events are those in which additional particles are produced. The inelastic contamination may be quite high* and will necessarily complicate a determination of the overall normalization of a "clean" sample to be described below.

Possible inelastic events as well as products of ψ' decay will readily be identified if an extra intersecting track or tracks accompany the dimuon; these will be identified as multi-track events and hence will be automatically excluded from the "all" sample. The two possible multiple track events included in the "all" sample by the choice of Δ = .01" as the cut in the vertex routine will be discussed below.

Inelastic events in which neutral pions are produced and/or in which the charged particles are not reconstructed as tracks are harder

*The inelastic contribution at $t = t_{min}$ has been estimated to be 20-30% at SLAC energies.[14]

to identify and the number of such events may be subject to relatively large systematic errors. The upstream scintillation counters and proportional chambers provide an aid in identifying the presence of neutral and charged pions. These counters, the T counters, AW counters and MWPC chambers P0, P1, P2 are shown schematically in Fig. 16. The T counters detect π^o's via the decay $\pi^o \rightarrow \gamma\gamma$ and recoil protons or other charged particles having sufficient kinetic energy to penetrate the shielding around them (about 100-150 MeV). Additionally, the T counters have a small profile for muons in the beam halo and hence are not subject to high singles rates. The AW counters detect charged particles. Unused hits in the chambers P0, P1, and P2 can be ascribed to a variety of sources. A large number of unused hits in P0 alone would indicate the presence of spallation products and/or soft electrons from the target, target box walls, target holder, lead in front of the AB's, etc. A large number of unused hits in P2 might reflect splash-back from tracks hitting the magnet face. A relatively small number of unused hits in P0 and P2 but no unused hits in P1 would indicate the presence of a charged particle from the target that missed P1 and hence was not reconstructed. [See Fig. 32].

The AB counters were also designed to detect π^o's and charged tracks that would not enter the magnet aperature and as such were designed as an aid in identifying inelastic events. An examination of the counting rates in these counters leads to the conclusion, however, that they cannot be used for this purpose with this data sample. See Table 3. There are several interpretations of the difference in counting rates; the most natural one is that the beam was scraping the target holder.

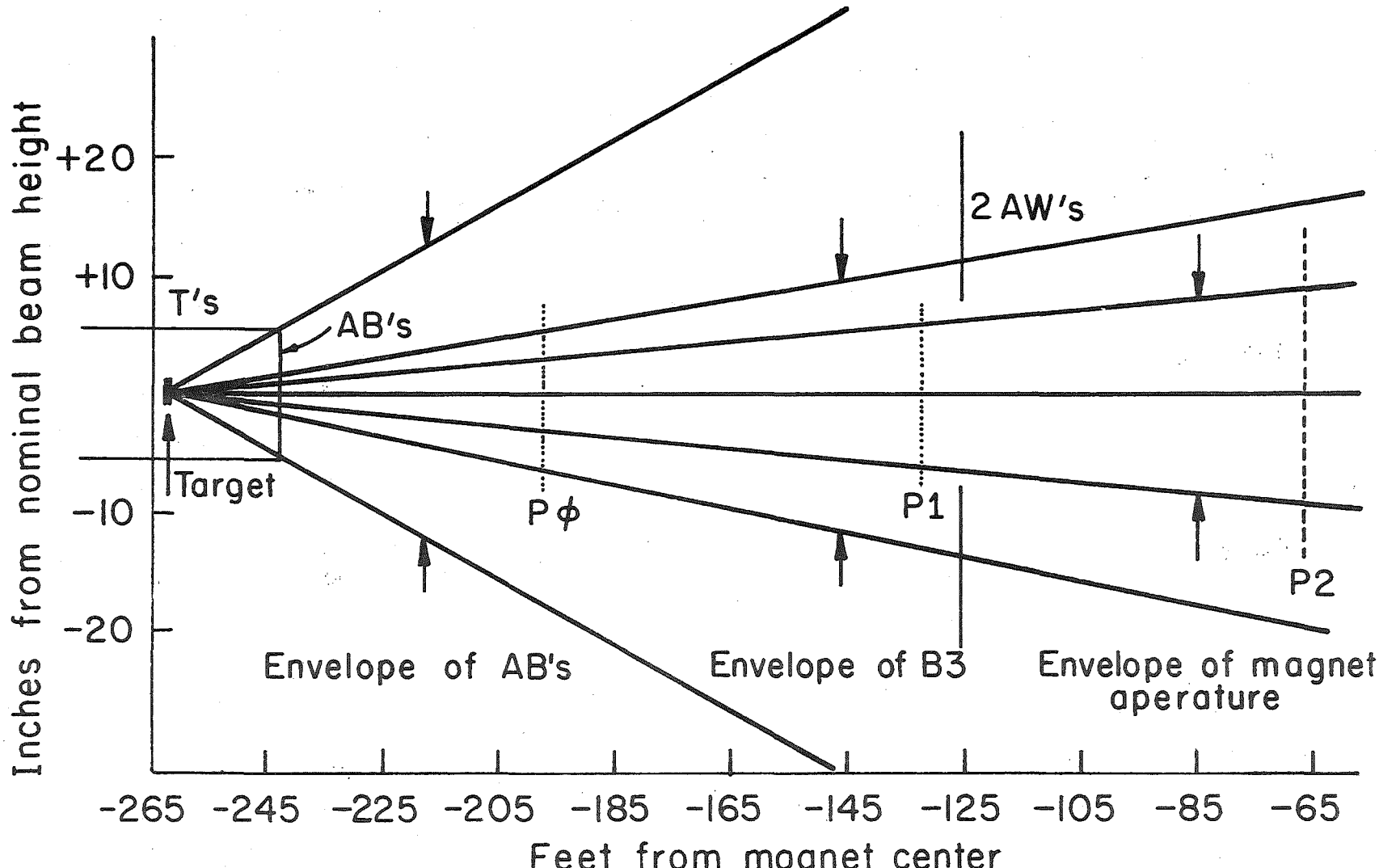

Fig. 32 Side view of upstream chambers

TABLE 3

FREQUENCY OF AB COUNTERS FOR TWO-TRACK EVENTS
IN THE MOMENTUM INTERVAL $80 \leq p_{11} \leq 290$ GeV/c.
2-MU BUSS LINE REQUIRED.

	$M_{\mu\mu} > 1.5$ MeV/c^2	$2.8 \leq M_{\mu\mu} \leq 3.4$
No AB	1573	198
AB1 only	167	7
AB2 only	485	31
AB1 + AB2	330	7

Accordingly, we will make the following cuts on the "all" sample in order to generate a sample relatively free from contamination due to inelastic events or events from the decay of the ψ'.

We first eliminate all events in which three or more T counters fire. There are 24 such events; they are listed in Appendix B as Class I events. The average $p_\perp^2$ of these events is 1.66 $(GeV/c)^2$, which is to be contrasted with the average $p_\perp^2$ of the "all sample, which is .58 $(GeV/c)^2$. We note that half of these events are also accompanied by hits in the AW counters and a large number of unused hits in the first three proportional chambers.

We next eliminate events in which 2 T counters have fired. These are 1) events in which neither T counter subtends the direction of a possible nucleon recoil, 2) events in which the presumed energy of the recoil would be insufficient to penetrate the shielding around the T counters, and 3) events in which a T counter not adjacent to the one in the path of a nucleon recoil also fires and which in addition are accompanied by some

activity in the AW counters. Under the assumption of a quasi-elastic scattering, the direction of the nucleon recoil is determined uniquely, i.e. opposite in azimuthal direction to that of the dimuon. In order to allow for the effects of Fermi motion, counters on either side of the T counter to which the nucleon recoil points are also considered to subtend the direction of recoil. The maximum Fermi energy of nucleons in the Be nucleus is about 25 MeV; the corresponding momentum is about 200 MeV/c. The minimum energy needed to penetrate the shielding around the T counters corresponds to a $p_\perp^2$ of about .20 $(GeV/c)^2$. This cut eliminates 6 additional events. The cut events are called Class II events and are tabulated in Appendix B.

The final cut on the "all" sample eliminates events which have more than a certain number of unused hits in the first three proportional chambers, provided either 1) the wrong T counter or more than 1 T counter fired, or 2) one or more AW counters fired. The average number of unused hits in a sample of events in which no T, AW, and AB counters fired was less than 1. This sample constituted 103 events or more than half of the "all sample". We therefore feel safe in setting the number of unused hits to test on at 10. Any number of hits greater than this, if they were associated with one track, would be used in the reconstruction program. Further discussion of this determination will be found below under the topic of systematic errors. This cut reduces the "all" sample by another 9 events. The events eliminated by this cut are referred to as Class III events and are listed in Appendix B.

There are 156 events left after the above cuts, the average $p_\perp^2$ of which is .32 $(GeV/c)^2$. The average $p_\perp^2$ of events eliminated from the

"all" sample is 1.6 $(GeV/c)^2$. The reduced sample will be referred to as the "clean" sample. The "clean" sample may be subject to relatively large systematic errors as discussed below.

G. Cross Section

The number of events we observe in a particular momentum range (80-290 GeV/c say) is given by the following:

$$N(80\text{-}290) = B\sigma \times \text{Flux factors} \times \text{Acceptance} \times \text{Live time} \quad (15)$$

where $N(80\text{-}290)$ is the number of events, and

$B\sigma$ is the cross section times branching ratio for the appropriate decay channel.

The flux factors reflect the number of particles in the beam as well as the number of available scattering centers in the target.

$$\text{Flux} = \frac{\rho A_o}{A} \times \ell \times \int_{80}^{290} \frac{dN}{dK}\, dK \quad (16)$$

where, ρ = density of target

A = atomic weight of target

A_o = Avagadro's number

$\int_{80}^{290} \frac{dN}{dK}\, dK$ = number of photons between 80 and 290 GeV/c

In order to determine the latter quantity, we use the shape of the spectrum in conjunction with the total photon power in the beam, as determined by the quantameter and corrected for target losses.

That is, the spectrum measurement can be expressed as

$$\frac{dN}{dK} = C\, f(k) \quad (17)$$

where C is some scale factor and f(k) is the shape.

The quantameter integrates the photon spectrum and once the shape is known determines C:

$$Q = \int_o^\infty k \frac{dN}{dK} dK = C \int_o^\infty kf(k)dK \tag{18}$$

To correct for large losses, we multiply the Q reading by a factor $e^{+7/9\ x/x_o}$, where x is the length of the target and x_o is the radiation length of Be.

After some rearranging, equation (15) can be written as:

$$B\sigma = \frac{N(80\to290)}{\rho \frac{A_o}{A} \ell} \times \frac{1}{Q} \times \frac{1}{Acc^{\times}LT} \times \frac{\int_o^{290} k\ f(k)dk}{\int_{80}^{290} f(k)dk} \tag{15a}$$

The last term in this equation can be determined graphically from the spectrum measurement in Fig. 25, and was found to be 2.7×10^2 or $(.00370)^{-1}$. The live time was found to be about 61%. The average acceptance in the momentum interval $80 \leq p_{||} \leq 290$ GeV/c was determined to be about 20.6%; for a determination of the differential cross section $\frac{d\sigma}{dp_{||}}$, events were individually weighted using the previously mentioned fit to the acceptance. In the momentum range considered, no significant variation was found in the efficiency as a function of $p_\perp^2$ out to a value of about 4.5 $(GeV/c)^2$.

The production cross-sections for the "all" and "clean" samples are 29.5 ± 2.1 nb/nucleus and 23.5 ± 1.9 nb/nucleus, respectively. Results are expressed in terms of nb/nucleus because of the possibility of coherence effects. Errors are statistical only.

The momentum distribution for the "all" sample has been shown in Fig. 26. Differential cross section in $p_{||}$ and $p_\perp^2$ or $t_\perp$ for both the

"clean" and "all" samples are presented in Fig's 33-40. Errors are statistical only. The data in $p_\perp^2$ was fit to three functional forms using the least squares fitting routine LSQ. The first form was

$$N_1(72e^{-\alpha p_\perp^2}+9)e^{-\beta p_\perp^2} \tag{19}$$

motivated by the formula due to Margolis, where N1, α, and β are the free parameters. This fit is referred to as the three-parameter fit. The other two fits are free parameter fits in two or three exponentials:

$$N_1e^{-\alpha' p_\perp^2} + N_2e^{-\beta' p_\perp^2} + (N_3e^{-\gamma p_\perp^2}) \tag{20}$$

where N_1, N_2, α', β' and (N_3 and γ) are the free parameters. These fits are referred to as the four- and six-parameter fits respectively. For a summary of the results of these fits, see Appendix C.

The three- and four-parameter fits were found to give excellent results out to both .6 and 1.0 $(GeV/c)^2$ in $p_\perp^2$. Beyond 1.0 $(GeV/c)^2$, the quality of either fit became relatively poor. For instance, the four-parameter fit to the data out to 2.0 $(GeV/c)^2$ for the "clean" sample resulted in a χ^2 of 3.86 for 5 degrees of freedom. This is to be compared to a χ^2 of 1.93 for 4 degrees of freedom when the fit is restricted to $p_\perp^2 \leq 1.0$ $(GeV/c)^2$.

The six-parameter fit gave excellent results out to a $p_\perp^2$ of 3.5 $(GeV/c)^2$, and on the basis of χ^2 is preferred to the 4-parameter fit. An attempt to fit the data for a $p_\perp^2 \leq 2.0$ $(GeV/c)^2$ with the six-parameter fit was unsuccessful.

The resolution of the coherent peak in our apparatus was studied using Monte Carlo techniques. For values in α between 40 and 60 $(GeV/c)^{-2}$,

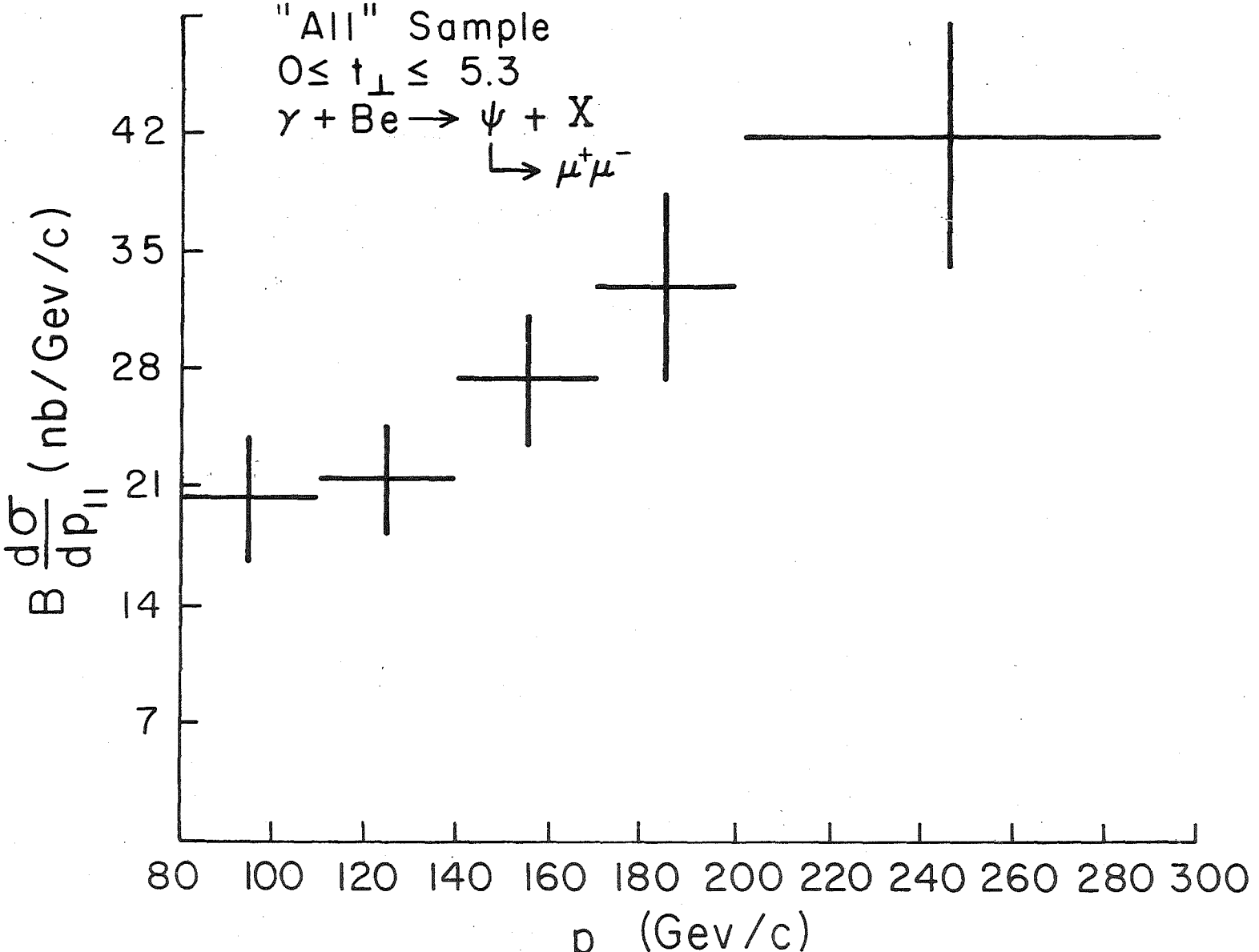

Fig. 33 $B\sigma(p_{11})$ for "all" sample $0 \leq t_\perp \leq 5.3$

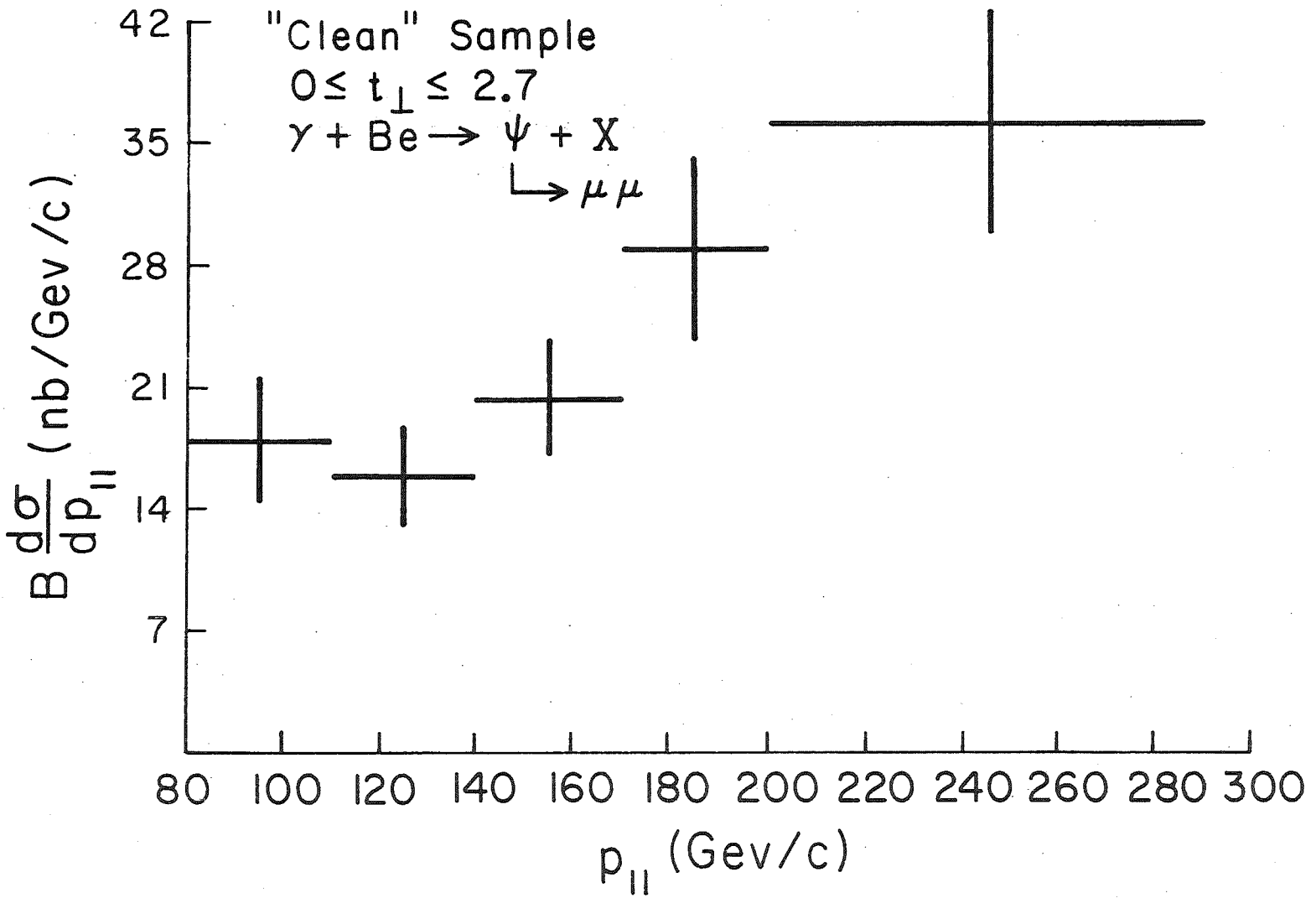

Fig 34 $B\sigma(p_{11})$ for "clean" sample $0 \leq t_\perp \leq 2.7$

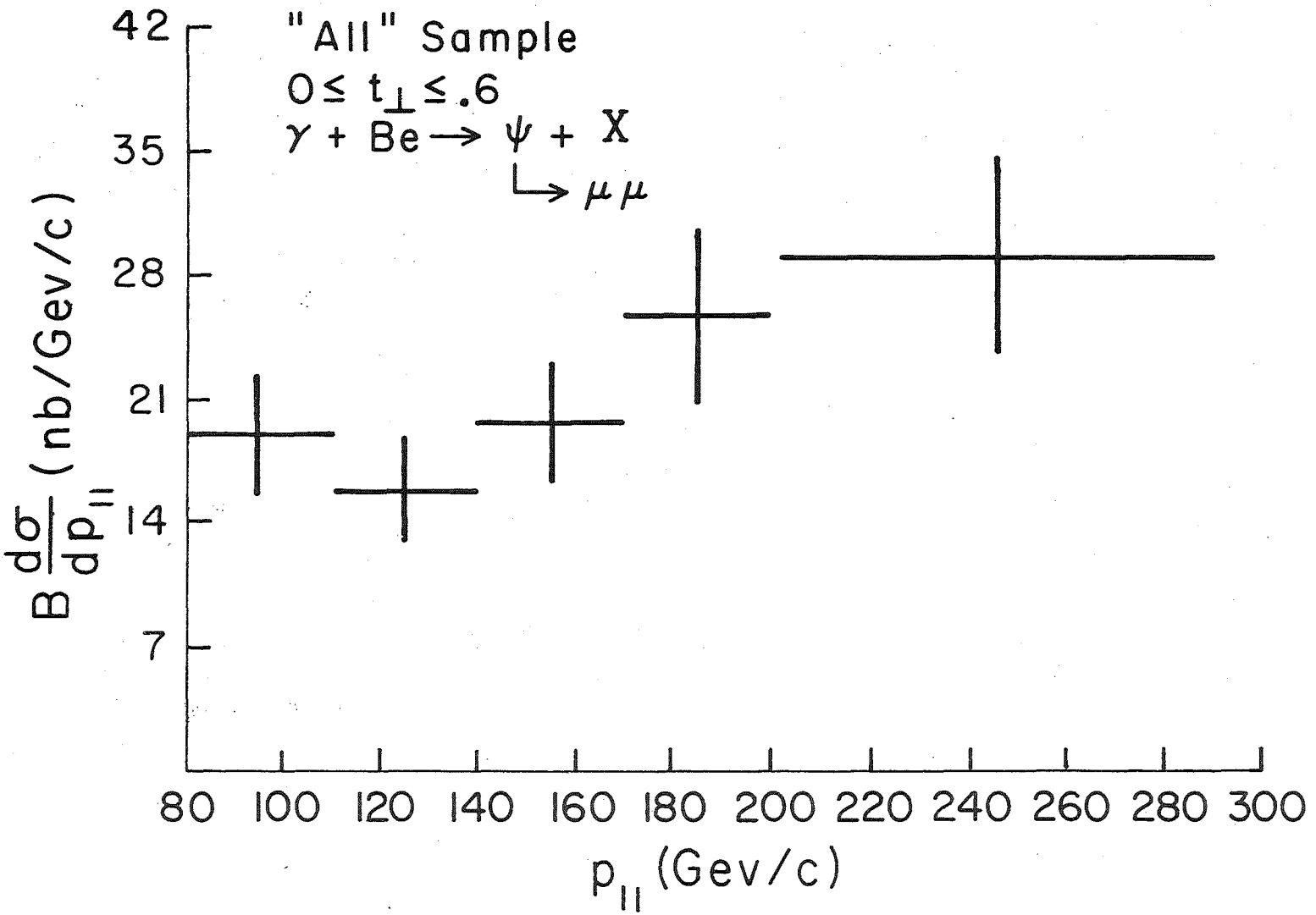

Fig 35 $B\sigma(p_{11})$ for "all" sample $0 \leq t_\perp \leq .6$

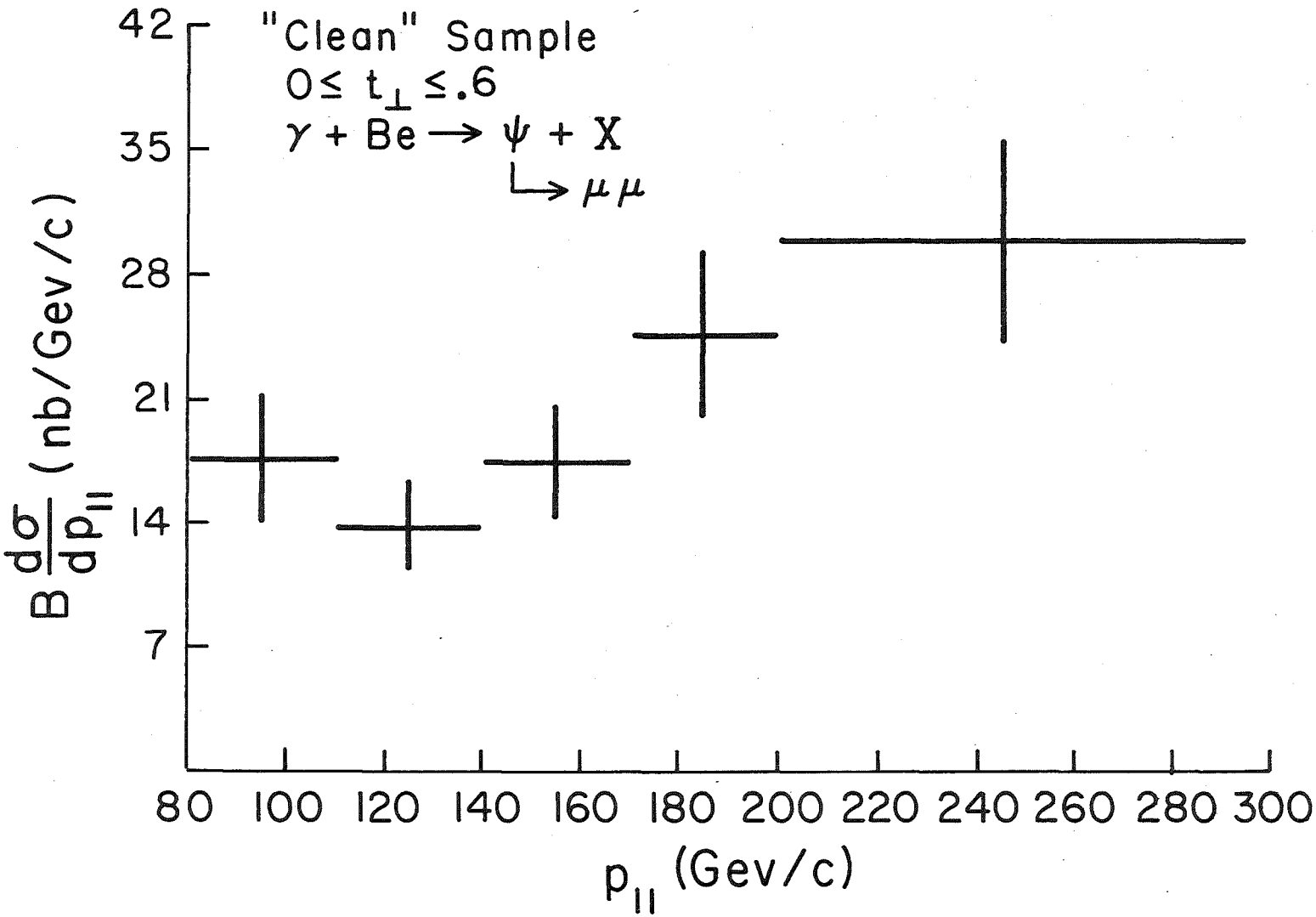

Fig 36 $B\sigma(p_{11})$ for "clean" sample--$0 \leq t \leq .6$

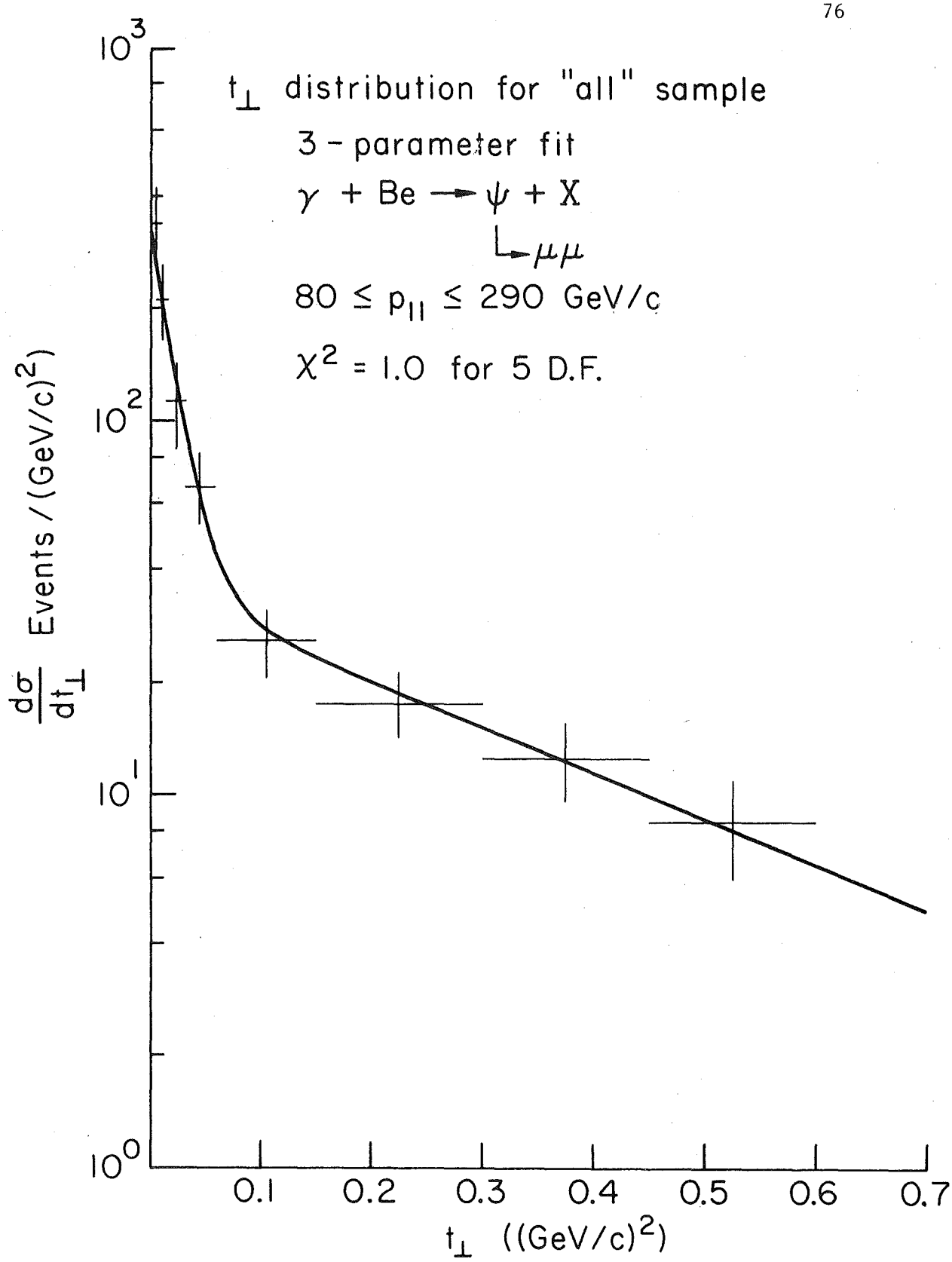
$t_\perp$ distribution for "all" sample
3 - parameter fit
γ + Be → ψ + X
↳ $\mu\mu$
$80 \leq p_{11} \leq 290$ GeV/c
χ^2 = 1.0 for 5 D.F.
$\frac{d\sigma}{dt_\perp}$ Events / (GeV/c)^2)
10^3
10^2
10^1
10^0
0.1
0.2
0.3
0.4
0.5
0.6
0.7
$t_\perp$ ((GeV/c)^2)

FIG 37

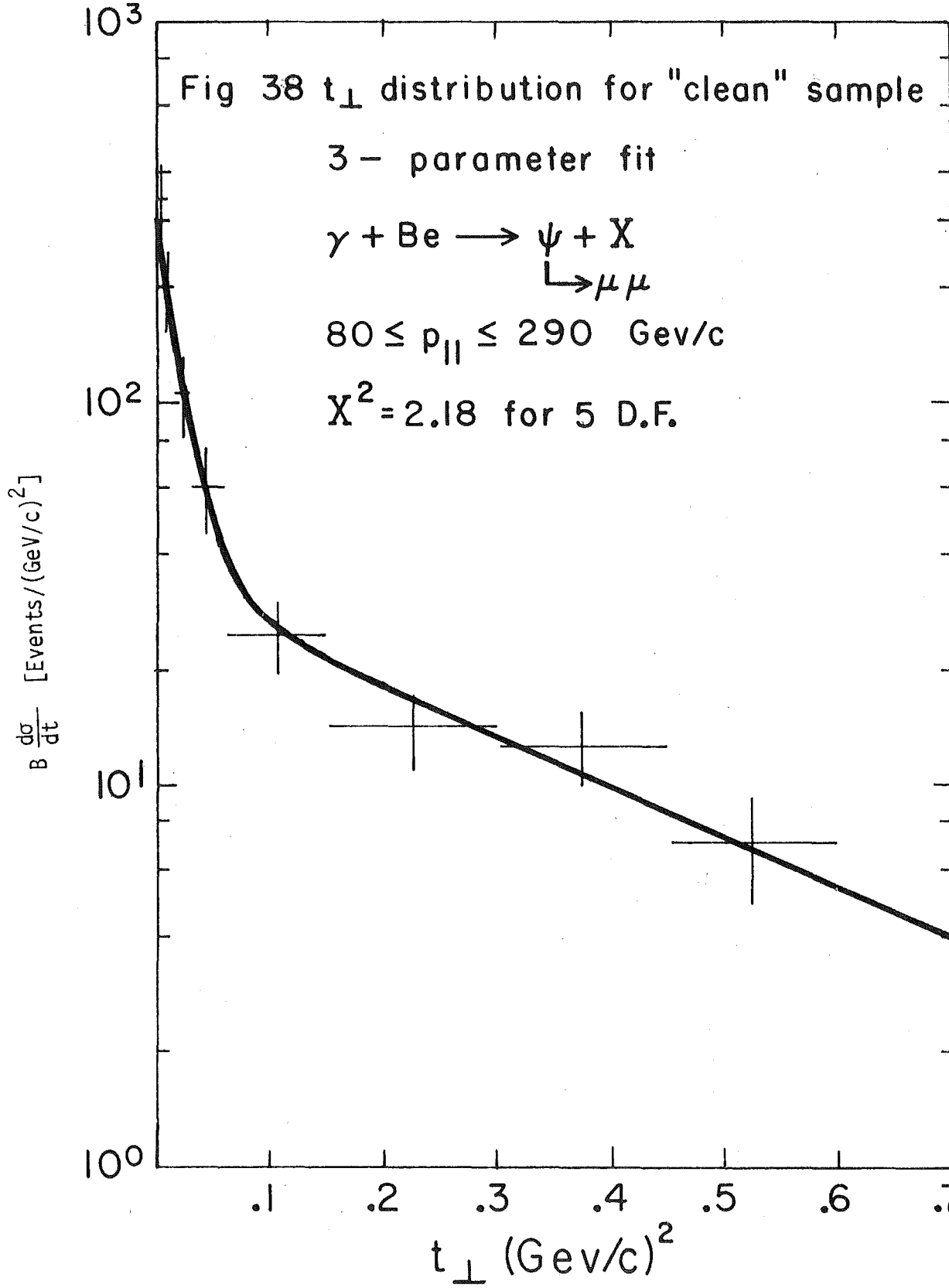
Fig 38 $t_\perp$ distribution for "clean" sample
3 – parameter fit
$\gamma + Be \longrightarrow \psi + X$
$\hookrightarrow \mu\mu$
$80 \leq p_{||} \leq 290$ Gev/c
$X^2 = 2.18$ for 5 D.F.
$B \frac{d\sigma}{dt}$ [Events/(GeV/c)^2]
10^3
10^2
10^1
10^0
.1
.2
.3
.4
.5
.6
.7
$t_\perp$ (Gev/c)^2

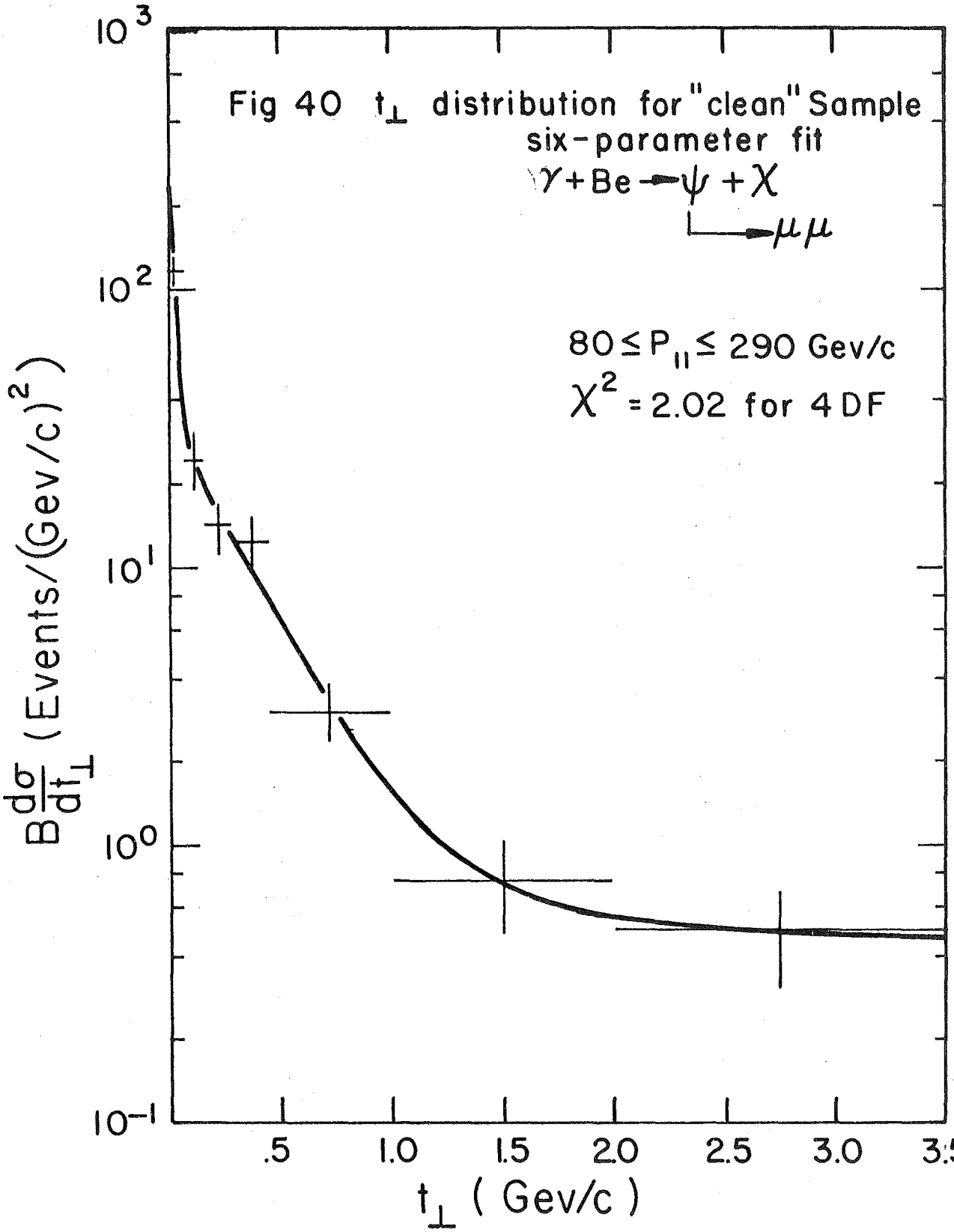
Fig 40 $t_\perp$ distribution for "clean" Sample
six-parameter fit
$\gamma + Be \rightarrow \psi + \chi$
$\psi \rightarrow \mu\mu$
$80 \leq P_{11} \leq 290$ Gev/c
$\chi^2 = 2.02$ for 4 DF
$B\frac{d\sigma}{dt_\perp}$ (Events/(Gev/c)^2)
10^3
10^2
10^1
10^0
10^{-1}
.5
1.0
1.5
2.0
2.5
3.0
3.5
$t_\perp$ (Gev/c)

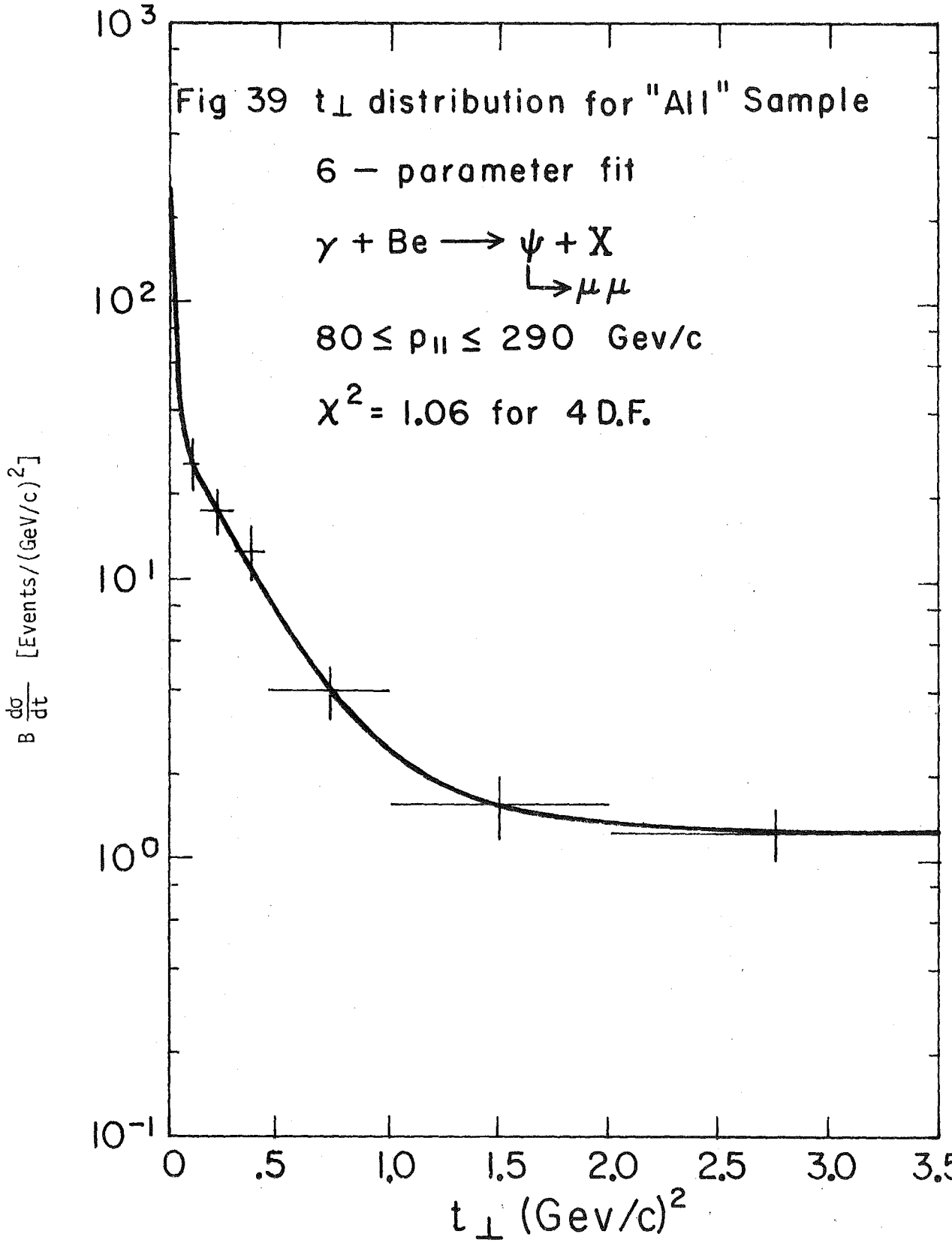
Fig 39 $t_\perp$ distribution for "All" Sample
6 – parameter fit
$\gamma + Be \longrightarrow \psi + X$
$\hookrightarrow \mu\mu$
$80 \leq p_{11} \leq 290$ Gev/c
$\chi^2 = 1.06$ for 4 D.F.
$B \frac{d\sigma}{dt}$ [Events/(GeV/c)^2]
10^3
10^2
10^1
10^0
10^{-1}
0
.5
1.0
1.5
2.0
2.5
3.0
3.5
$t_\perp$ (Gev/c)^2

it was found that the observed slopes were about factor of 1.4 ± .2 less than the generated slopes. This factor was determined by comparing the fitted value of the generated slope to the fitted value of the slopes of events which were accepted and whose particle momentum vectors had been recalculated to take into account the MWPC wire spacing.

H. Systematic Errors

We will now estimate possible systematic errors arising from the selection criteria used in defining the "clean" sample of events. Thirteen (13) events have a $p_\perp^2$ of less than .6. Since only 2 events are expected to come from ψ' decay into $\psi\pi^+\pi^-$ followed by the decay of the ψ into a $\mu^+\mu^-$ pair, if we have made a mistake in excluding these events, the maximum error would be about +8%. There are in addition 12 events which are otherwise "clean" events but in which an excess of T counters fire. If the hits in the T counters were suprious in all cases, then the maximum error we would make is +8%. There is some overlap between these two sets of events. We estimate the systematic error to be about 9% in the positive direction.

If, on the other hand, we were to exclude from consideration events which would otherwise be excluded if the AB's were considered reliable, we would cut an additional 9 events. This yields a systematic error of 6% in the negative direction.

Hence, the systematic error on the number of events in the "clean" sample is estimated to be +9%/-6%, rounded to ±9%.

I. Discussion of the Data for ψ Photoproduction

Figures 33-36, which show the differential cross section $\frac{d\sigma}{dp_{||}}$ for the "all" and "clean" samples, indicate that the ψ photoproduction cross section to be rising with energy. Other members of the group have obtained the same result.[15] We believe we have calculated the acceptance properly; in addition, weighing each event individually helps avoid the problem inherent in averaging a rapidly varying acceptance over too wide a momentum interval. The other possibility is that the slope of the photon spectrum is incorrect, that is, there are really more high energy photons (in the momentum interval above 170 GeV/c say) than indicated by the spectrum in Fig. 25. We have double-checked the calculation of the spectrum, done by R. Coleman, and can find no obvious error.

One further test can be made and is in progress as this thesis is written. That is to calculate the photoproduction cross section of the rho meson. The pi-p cross sections are nearly constant in the momentum interval 140-290 GeV/c.[16] Hence we would expect to find $d\sigma/dp_{||}$ $(\gamma+Be\rightarrow\rho Be)$ and $\sigma_T(\rho N)$ to be constant or very nearly so.

The coherent slopes off Be when corrected for the resolution are in the range 65-85$(GeV/c)^2$. This is in reasonable agreement with previous lower statistics data from this experiment.[2,3,4,10] Assuming the Be nucleus to be a black body, we find the radius to be 3.2 - 3.6 fm.* Taking into account differences in treatments, this is in good agreement with the electron scattering data,[17] the neutron elastic scattering data,[18] and the rho photoproduction data.[19]

*See Appendix D for this calculation.

The single nucleon slope is in the range (2.6-3.6) as determined by the three- and four-parameter fits and are in agreement with previous determinations. See Appendix E.

As far as we know, this is the first determination of a third slope in $p_\perp^2$. It is consistent with being 0 in as much as the errors on the slope are larger than the fitted value itself.

We now extract $\sigma_T(N)$ using the formula (6) and the branching ratio for ψ decay into muons as determined at SPEAR.[20] We first use the value $d\sigma/dt\ p_\perp^{2=0}$ for the "clean" sample obtained from the three-parameter fit for events with a $p_\perp^2 \leq .6(\text{GeV/c})^2$. This fit is used in order to require explicitly that the incoherent contribution to the differential cross section vanish at $p_\perp^2 = 0$. The fit is restricted to $.6(\text{GeV/c})^2$ in order to further minimize any possible inelastic contamination of the data sample.*

The average ψ momentum is 161 GeV/c; hence the average t_{min} is $8.85 \times 10^{-4}\ (\text{GeV/c})^2$. We extrapolate to t = 0 by use of the formula

$$\left.\frac{d\sigma}{dt}\right|_{t=0} = \left.\frac{d\sigma}{dt}\right|_{p_\perp^2=0} \times e^{\alpha_{Res}\langle t_{min}\rangle} \qquad (21)$$

where ω is the correction factor for the resolution and $\alpha_{Res} = \alpha \times \omega$.

Thus will all acceptances and resolutions folded in, we obtain:

$$\left.\frac{d\sigma}{dt}\right|_{t=0} = 80 \pm 17\ \text{nb/(GeV/c)}^2 \quad \text{per nucleon}$$

where the error is statistical only.

*In the text, we use $t_\perp$ and $p_\perp^2$ interchangeably.

It is also possible to calculate $\left.\frac{d\sigma}{dt}\right|_{t=0}$ using the $t_\perp$-dependence as determined by the four parameter fits:

$$B\sigma = B \int \frac{d\sigma}{dt_\perp} dt_\perp = B \left.\frac{d\sigma}{dt}\right|_{t=0} \times \int t_\perp \text{ dependence} \tag{22}$$

where $B \int \frac{d\sigma}{dt_\perp} dt_\perp$ is the number of events between the limits of integration.

Taking $\left.\frac{d\sigma}{dt}\right|_{t=0}$ to be extrapolated from $p_\perp^2 = 0$ as in Equation (21) and using $A^2 e^{-\alpha t_\perp} + A e^{-\beta t_\perp}$ for the $t_\perp$ dependence as suggested by an optical model approach, we obtain

$$\left.\frac{d\sigma}{dt}\right|_{t=0} = \frac{1}{B} \times B\sigma(0 \to 2.7) \frac{\#\text{ events } (0 \to .6)}{\#\text{ events } (0 \to 2.7)} \frac{e^{+\alpha_{Res}\langle t_{min}\rangle}}{\int_0^{.6} p_\perp^2 \text{ dependence}}$$

$$= \frac{23.5}{.069} \times \frac{136}{156} \times \frac{1.07}{3.85} = 83 \pm 7 \text{ nb/(GeV/c)}^2 \tag{22a}$$

where we have used $\alpha_{Res} = 74$ and $\beta = 2.6$. (See Appendix C.)

Using the same procedure, we can also calculate $\left.\frac{d\sigma}{dt}\right|_{t=0}$ from the single nucleon contribution alone:

$$\left.\frac{d\sigma}{dt}\right|_{p_\perp^2=.15} = \frac{B\sigma(0 \to 2.7)}{B} \frac{\#\text{events } (.15 \to 1.0)}{\#\text{events } (0 \to 2.7)} \times \frac{1}{\int_{.15}^{1.0} p_\perp^2 \text{ dependence}} \tag{23}$$

Using $\beta = 2.6$, we find:

$$\left.\frac{d\sigma}{dt}\right|_{p_\perp^2=.15} = \frac{23.5}{.069} \times \frac{54}{156} \times \frac{1.002}{2.09} = 56.6 \pm 7.7 \text{ nb/(GeV/c)}^2. \tag{23a}$$

To extrapolate to t = 0, multiply by the factor $e^{2.6\times.15} = 1.48$ to get:

$$\left.\frac{d\sigma}{dt}\right|_{t=0} = 84 \pm 11 \text{ nb/(GeV/c)}^2 \text{ per nucleon,}$$

in good agreement with the previous results.

Taking the average of the three results and folding in the systematic errors, we obtain

$$\left.\frac{d\sigma}{dt}\right|_{t=0} = 82 \pm 10 \text{ nb/(GeV/c)}^2 \text{ per nucleon} \quad .$$

Of the three seperate determinations of $\left.\frac{d\sigma}{dt}\right|_{t=0}$, the first was derived mainly from the coherent part of the p^2 distribution, the second from a sum of the coherent and incoherent parts, and the third predominantly from the incoherent part.

Using equation (6) in conjunction with equation (3) we obtain for the ψ-nucleon total cross section

$$\sigma_T(\psi N) = 1.6 \pm .2 \text{ mb}$$

assuming $R_\psi = 0$.

For a comparison of the total cross sections for the vector mesons, see Fig. 41. The ρN total cross section is taken from Reference 21, the ωN total cross section from Reference 22, the ϕN total cross section from Reference 23, and previous determinations of the ψN total cross section from References 2, 14, and 24.

We can also determine the ψ-nucleon elastic cross section from VMD.

Squaring Equation (4) yields

$$\frac{d\sigma}{dt}(\gamma\to v) = \frac{e_o^2}{g_v^2}\frac{d\sigma}{dt}(v\to v) \tag{4a}$$

which coupled with Equation (3)

$$\Gamma(\psi\to\mu\mu) = \frac{\alpha^2}{3}\frac{4\pi}{g_v^2}M_\psi \tag{3}$$

gives:

$$\frac{d\sigma}{dt}(v\to v) = \frac{d\sigma}{dt}(\gamma\to v)\left[\frac{4\pi}{g_v^2}\right]^{-1}\frac{1}{\alpha}$$

$$= \frac{d\sigma}{dt}(\gamma\to v)\,\frac{\alpha}{3}\,\frac{M_\psi}{\Gamma(\psi\to\mu\mu)} \tag{24}$$

We next integrate from $p_\perp^2 = .15$ to $p_\perp^2 = 1.0$ and allow the number of events in the "clean" sample to determine the normalization:

$$\sigma_{el}(\psi N\to\psi N;\ .15 \le p^2 \le 1.) = \int_{.15}^{1.0}\frac{d\sigma}{dt}(\psi\to\psi)\,dt \tag{25}$$

$$= \int_{.15}^{1.0}\frac{d\sigma}{dt}(\gamma Be\to\psi Be)\,dt \times \frac{\alpha}{3}\,\frac{M_\psi}{\Gamma(\psi\to\mu\mu)}$$

$$= \frac{B\sigma(0\to 2.7)}{B(\psi\to\mu\mu)} \times \frac{\#\text{events } (.15\to 1.0)}{\#\text{events } (0\to 2.7)} \times \frac{\alpha}{3}\,\frac{M_\psi}{\Gamma(\psi\to\mu\mu)}$$

$$= \frac{(23.5 \pm 1.9)}{.069} \times \frac{54}{156} \times \frac{\alpha}{3}\,\frac{M_\psi}{\Gamma\ \psi\to\mu\mu}$$

$$= .185 \pm .015 \text{ nb/nucleus}$$

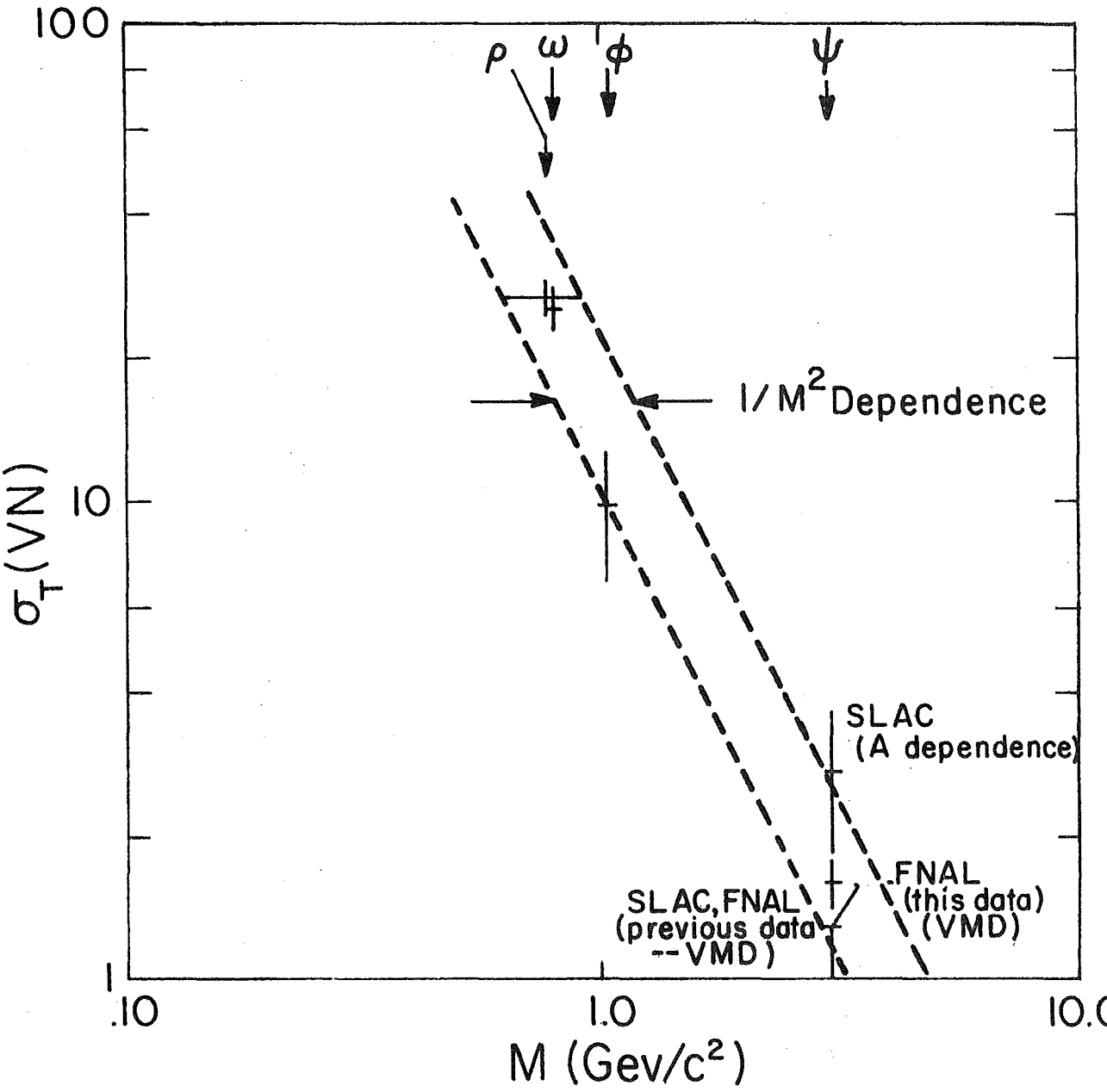

FIG 41 VECTOR MESON TOTAL CROSS SECTIONS

Per nucleon, the elastic cross section is determined to be

$$\sigma_{el}(\psi N) = .021 \pm .002 \text{ mb} \quad .$$

J. ψ' Photoproduction

There are six dimuon events in the mass interval 3.4 - 4.0 GeV/c^2. One of these has a $p_\perp^2$ of > 16 $(GeV/c)^2$, so we will throw it out. The remaining 5 events satisfy the "clean" criteria as defined for the sample; furthermore, 4 of the events possess a $p_\perp^2$ of less than $6(GeV/c)^2$. We observe no events of the cascade process in which a ψ' decays into a ψ and two charged pions followed by the dimuon decay of the ψ.

Background for the dimuon (direct) decay of the ψ' can come from two sources, the tail of the ψ and BH pair production. The estimated background from these sources based on Monte Carlo studies is .75 and 1.0 events, respectively. This leaves us with 3.25 events for a full $p_\perp^2$ range (≤ 2.7 $(GeV/c)^2$ and 2.25 events for the restricted range ($p_\perp^2 \leq .6$ $(GeV/c)^2$.

The three and four track events in which a dimuon in the mass range of the ψ(2.8 - 3.4 GeV/c^2) is present are listed in Appendix F. The only candidate for the process $\gamma + Be \rightarrow \psi' + X \rightarrow \psi \pi^+\pi^- + X$ ($\psi \hookrightarrow \mu^+\mu^-$) has a mass of > 3.9 GeV/c^2. Based on Monte Carlo studies, this mass is rather high. Furthermore, the momenta of the pions while a possible combination, is again an unlikely one. The mass of the dipion is .328 GeV/c^2, which is rather low. Finally, while the dimuon and dipion separately have good vertices ($\Delta^2 \sim 10^{-5}$" squared in both instances), the four particle vertex is rather poor. In fact, the event is not normally considered to be a four-track event as neither pion passes within .01" sq. of the common vertex.

We therefore feel justified in stating that we observe no event of the type $\gamma + Be \rightarrow \psi' + X$ followed by the sequential decay $\psi' \rightarrow \psi\pi^+\pi^-$ (with $\psi \rightarrow \mu^+\mu^-$).

We now ask how many ψ' events we expect to see in either decay mode.

For the direct decay, we make the comparison based on the total cross section for ψ-nucleon scattering, $\sigma_T(\psi N)$:

$$\#\psi' \underset{\rightarrow \mu\mu}{\simeq} \sqrt{\#\psi \underset{\rightarrow \mu\mu}{} \times \frac{BR(\psi' \rightarrow \mu\mu)}{BR(\psi \rightarrow \mu\mu)} \times \frac{Acc(\psi' \rightarrow \mu\mu)}{Acc(\psi \rightarrow \mu\mu)}} \tag{26}$$

$$\simeq \sqrt{131 \times \frac{.0093}{.069} \times \frac{.169}{.206}} \simeq 3.9$$

where we have used the number of ψ's in the "clean" sample between $0 \leq p_\perp^2 \leq .6$; i.e. the sample used in determining $\sigma_T(\psi N)$. We have used $\psi' \rightarrow \mu^+\mu^- = .0093$.[25]

The above calculation assumes $\sigma_T(\psi N) \simeq \sigma_T(\psi' N)$. If, however, we assume a $1/m^2$ dependence for the cross sections, the number of ψ''s we expect is

$$\#\psi's \simeq 3.9 \times \frac{m_\psi^2}{m_{\psi'}^2} \simeq 2.8 \tag{26a}$$

Both numbers are in rough agreement with the number seen, namely 2.25. The statistics are too limited, however, to allow us to distinguish between an equality and a $1/m^2$ dependence for the cross sections.

For the cascade decay $\psi' \rightarrow \psi\pi^+\pi^-$ (with $\psi \rightarrow \mu^+\mu^-$), we make the comparison assuming the 3.25 dimuon events are from the direct decay of the ψ'.

In this case, the number of cascade decays expected is:

$$\#\psi' \to \psi\pi\pi = \#\psi' \to \mu\mu \times \frac{Acc(\psi' \to \psi\pi\pi)}{Acc(\psi \to \mu\mu)} \times \frac{BR(\psi' \to \psi\pi\pi)}{BR(\psi' \to \mu\mu)} \qquad (27)$$

$$= 3.25 \times \frac{.051}{.169} \times \frac{.022}{.0053} \simeq 2.3 \pm 1.3$$

which is consistent with seeing none. We have assumed an isotropic decay distribution for the ψ' into a ψ and an S-wave $\pi\pi$ pair in calculating the acceptance and have used .32 for the branching ratio for $\psi' \to \psi\,\pi^+\pi^-$.[26]

The cross section × branching ratio for the direct decay process $\psi' \to \mu^+\mu^-$ is:

$$B\sigma(\psi' \to \mu\mu) = B\sigma(\psi \to \mu\mu) \times \frac{Acc(\psi \to \mu\mu)}{Acc(\psi' \to \mu\mu} \times \frac{\#\psi' \to \mu\mu}{\#\psi \to \mu\mu} \qquad (28)$$

$$= 23.5 \times \frac{.206}{.169} \times \frac{3.25}{156}$$

$$\simeq .60 \text{ nb/nucleus}$$

This implies a production cross section of

$$\sigma(\gamma + Be \to \underset{\hookrightarrow \text{anything}}{\psi'} + x) \quad \sim \quad 64 \text{ nb/nucleus}$$

The branching ratio × cross section for the cascade decay process, $\psi' \to \underset{\hookrightarrow \mu^+\mu^-}{\psi\pi^+\pi^-}$ is

$$B\sigma(\psi' \to \underset{\hookrightarrow \mu\mu}{\psi\pi^+\pi^-}) = B\sigma(\psi' \to \mu\mu) \times \frac{Acc(\psi' \to \mu\mu)}{Acc(\psi' \to \underset{\hookrightarrow \mu\mu}{\psi\pi^+\pi^-})} \times \frac{1}{\#\psi' \to \mu\mu} \qquad (29)$$

$$= .597 \times \frac{.169}{.061} \times \frac{1}{3.25}$$

$$\simeq .51 \text{ nb/nucleus/event}$$

Therefore, we can say at the 90% confidence level

$$B\sigma(\psi' \rightarrow \psi\pi^+\pi^-) \leq 1.2 \text{ nb/nucleus (90\% confidence)}$$
$$\hookrightarrow \mu\mu$$

This implies at the 90% confidence level the production cross section is

$$\sigma(\gamma + Be \rightarrow \psi' + X) \leq 54 \text{ nb/nucleus (90\% confidence)}$$
$$\hookrightarrow \text{anything}$$

Because these results are only in qualitative agreement and because of the few number of events involved, we calculate a confidence level for the cross section based on the direct decay candidates:*

$$B\sigma(\gamma + Be \rightarrow \psi' + X) \leq 1.4 \text{ nb/nucleus (90\% confidence)}$$
$$\hookrightarrow \mu\ \mu$$

K. Summary

From data obtained during the 400 GeV/c running of Experiment 87A in the broad-band photon beam at the Fermi National Accelerator Laboratory in the Fall of 1975, we have obtained new values for $\psi(3095)$-photoproduction cross sections.

*The 90% confidence level is roughly 7.75 times the cross section per event.

Including all errors, statistical and systematic, these are

$$B\sigma(\gamma + Be \rightarrow \psi + X) \underset{\rightarrow \mu^+\mu^-}{} = 23.5 \pm 2.7 \text{ nb per nucleus}$$

$$\left.\frac{d\sigma}{dt}\right|_{t=o} = 82 \pm 10 \text{ nb/(GeV/c)}^2 \text{ per nucleon}$$

The momentum range over which these cross sections are measured is between 80 and 290 GeV/c. The average ψ momentum in this interval was found to be about 160 GeV/c.

The differential cross section $\frac{d\sigma}{dp_\perp^2}$ can be paramatarized by three slopes over the range $0 \leq p_\perp^2 \leq 2.7$. The slope of the forward peak, corrected for resolution and acceptance, was found to be 75 ± 25 $(GeV/c)^{-2}$. The secondary slope was found to be $3.5 \pm .5$ $(GeV/c)^{-2}$. A third slope is consistent with being flat.

We have also seen that the ψ-photoproduction cross section $\sigma(\gamma + Be \rightarrow \psi + X)_{\hookrightarrow \mu^+\mu^-}$ appears to be rising as a function of energy.

Using the ideas of Vector Meson Dominence, we have extracted the ψ-nucleon total and elastic cross sections under the assumption that the real part of the scattering amplitude is zero. The values are:

$$\sigma_{tot}(\psi N) = 1.6 \pm 0.2 \text{ mb}$$
$$\sigma_{el}(\psi N) = 0.021 \quad 0.002 \text{ mb}$$

We have observed several candidates for the direct dimuon decay of the $\psi'(3684)$, $\psi' \rightarrow \mu^+\mu^-$ and no events consistent with the cascade decay $\psi' \rightarrow \psi\pi^+\pi^-_{\hookrightarrow \mu^+\mu^-}$. Under the assumption that all the candidates for

the direct decay are in fact real events, we conclude

$$B\sigma(\gamma + Be \rightarrow \psi' + X) \leq 1.4 \text{ nb/nucleus}$$
$$\hookrightarrow \mu^+\mu^-$$

at the 90% confidence level.

REFERENCES

1. "Performance of the Wide-Band Neutral Beam," 87A Internal Report (1974).

2. B. Knapp et al., "Photoproduction of Narrow Resonances," Phys. Rev. Lett., 34, 1040 (1975).

3. L. Cormell, "Photoproduction of Electron Pairs at High Energy," Ph.D. Thesis, U. of Illinois (1975).

4. D. Nease, Ph.D. thesis, Cornell University (1975).

5. A. Wattenberg, "High Energy Photoproduction of New Massive Particles," talk presented at the International Conference on High Energy Physics, Palermo, Italy (June 1975) unpublished.

6. W. L. Lee, "Photoproduction of New Particles at Fermilab," in the Proceedings of the 1975 International Symposium on Lepton and Photon Interactions at High Energies, 213 (Aug. 1975).

7. A. Wattenberg, "High Energy Photoproduction of $\mu\mu$ and μe Events," talk presented at the XVIII International Conference on High Energy Physics, Tbilisi, USSR (July 1976), unpublished.

8. B. Margolis, "Coherent and Incoherent Reactions and Diffraction," Acta Phys. Polonica, B2, 57 (1971).

9. C. E. Carlson and P. G. O. Freund, "The Case for a Quartet Model of Hadrons," Phys. Lett., 39B 349 (1972).

10. A. R. Wijanco, Ph.D. Thesis, Columbia University (1976).

11. R. Messner, private communication.

12. F. Harris and D. Yount, "A High Precision Quantameter for NAL," Nucl. Inst. and Meth. 114, 357 (1974).

13. Y. S. Trai, "Pair Production and Bremsstrahlung of Charged Leptons," Reviews of Modern Physics 46, 815 (1974).

14. U. Camerini, et al., "Photoproduction of the ψ Particles," Phys. Rev. Lett. 35, 483 (1975).

15. M. Binkley, private communication.

16. A. S. Carrol et al., "Total Cross Sections of $\pi^{\pm}$ and $K^{\pm}$ on Protons and Deuterons between 50 and 200 GeV/c," Phys. Rev. Lett., 33, 932 (1974).

17. Herman & Hoffstader, High Energy Electron Scattering Tables, Stanford University Press, 62 (1960).

18. G. Bellittini et al., "Proton Nucleon Cross-Section at 20 GeV," Nucl. Phys. 79, 609 (1966).

19. H. Alvensleben et al., "Photoproduction of Neutral Rho Mesons," Nucl. Phys. B18, 333 (1970).

20. A. M. Boyarski, "Quantum Numbers and Decay Widths of the $\psi(3095)$," Phys. Rev. Lett. 34, 1357 (1975).

21. G. McClellan et al., "Photoproduction of Neutral ρ Mesons," Phys. Rev. D4, 2683 (1971).

H. Alvensleben et al., "Photoproduction of Neutral Rho Mesons," Nucl. Phys. B18, 333 (1970).

H. J. Behrend et al., "Photoproduction of 8-Gev Rho Mesons from Nuclei," Phys. Rev. Lett., 24, 336 (1970).

22. J. Abramson et al., "Elastic Photoproduction of ω Mesons from Hydrogen, Deuterium, and Complex Nuclei," Phys. Rev. Lett., 36, 1428 (1976).

P. L. Braccini et al., "Photoproduction of ω-Mesons from Nuclei," Nucl. Phys. B24, 173 (1970).

23. H. Alvensleben et al., "Photoproduction and Forbidden Decays of ϕ Mesons," Phys. Rev. Lett., 28, 66 (1972).

G. McClellan et al., "Photoproduction of ϕ° Mesons from Hydrogen, Deuterium, and Complex Nuclei," Phys. Rev. Lett., 26, 1593 (1971).

24. D. M. Ritson, "ψ and Excess Leptons in Photoproduction," SLAC-PUB-1728 (March 1976).

25. V. Lüth, et al., "Quantum Numbers and Decay Widths of the $\psi(3684)$," Phys. Rev. Lett., 35, 1124 (1975).

26. G. S. Abrams, et al., "Decay of $\psi(3684)$ into $\psi(3095)$," Phys. Rev. Lett. 34, 1181 (1975).

27. B. Gittleman et al., "Photoproduction of the $\psi(3100)$ Meson at 11 GeV," Phys. Rev. Lett. 35, 1616 (1975).

28. T. Nash et al., "Measurement of $J/\psi(3100)$ Photoproduction in Deuterium at a Mean Energy of 55 GeV," Phys. Rev. Lett. 36, 1233 (1976).

APPENDIX A

CALCULATION OF DECAY RATE OF A VECTOR MESON INTO TWO LEPTONS

Notation

P	four-vector of particle
ϵ	four-vector polarization of photon
$\vec{\epsilon}$	three-vector polarization of photon
$E_{v,1,2}; k_{v,1,2}$	energy and momentum vector of vector meson, lepton, and anti lepton, respectively.
m_ℓ	mass of the lepton
M_v	mass of vector meson
M	matrix element for the decay

The differential decay rate for the decay is:

$$d\omega = \frac{1}{2M_v} |M|^2 \frac{d^3k_1}{E_1/m_\ell (2\pi)^3} \frac{d^3k_2}{E_2/m_\ell (2\pi)^3} (2\pi)^4 \delta^4(P_v - p_1 - p_2) \tag{30}$$

The two-body phase-space factor is:

$$D = (2\pi)^4 \, {}^4(P_v - P_1 - P_2) \frac{d^3k_1}{(2\pi)^3} \frac{d^3k_2}{(2\pi)^3} \tag{31}$$

$$= \frac{E_1 E_2 k_1^3}{4\pi^2} \frac{d\Omega_1}{|E_v k_1^2 - E_1 \vec{k}_v \cdot \vec{k}_1|}$$

In the center of mass $k_1 = k_2$, $k_v = 0$

$$E_1 = E_2 = \frac{M_v}{2} = \frac{E_v}{2}$$

Hence $$D = \frac{E_1 E_2}{4\pi^2} \frac{k_1}{M_v} d\Omega_1 \tag{31a}$$

Substituting (30a) into 29:

$$d\omega = \frac{m_\ell^2}{M_v^2} \frac{k_1}{8\pi^2} |M|^2 d\Omega_1 \tag{30a}$$

The matrix element is given by

$$\frac{M_v^2}{g_v} \frac{e_o^2}{M_v^2} \bar{u}(p_1,s_1) \not{\epsilon} v(p_2,s_2) \tag{32}$$

Hence $|M|^2$ is

$$\frac{(4\pi\alpha)^2}{g_v^2} \bar{u}(p_1,s_1) \not{\epsilon} v(p_2,s_2) \bar{v}(p_2^*,s_2) \not{\epsilon} u(p_1,s_1) \tag{33}$$

Averaging over initial spins and summing over final spins allows one to take the trace. Hence

$$|M|^2 = \frac{(4\pi)^2}{g_v^2} \alpha^2 \text{ Tr } \{\bar{u} \not{\epsilon} v \bar{v} \not{\epsilon} u\} \tag{34}$$

$$= \frac{(4\pi)^2}{g_v^2} \alpha^2 \text{ Tr } \{\not{\epsilon}(\frac{-\not{p}_2+m_\ell}{2m_\ell}) \not{\epsilon} (\frac{\not{p}_1+m}{2m_\ell}) \}$$

$$= \frac{(4\pi)^2}{g_v^2} \frac{\alpha^2}{4m_\ell^2} \text{ Tr } \{- \not{\epsilon} \not{p}_2 \not{\epsilon} \not{p}_1 + \not{\epsilon} \not{\epsilon} m_\ell^2 \}$$

Recall that $\mathrm{Tr}\ \not{a}\not{b} = 4\ a\cdot b$

$$\mathrm{Tr}\ \not{a}\not{b}\not{c}\not{d} = 4\{a\cdot bc\cdot d - a\cdot cb\cdot d + a\cdot db\cdot c\}$$

Let the z axis be the axis of quantization and take $\vec{\epsilon}$ = , i.e. the unit vector along the x-axis

$$\mathrm{Tr}\ \not{\epsilon}\not{\epsilon} = 4$$

$$\mathrm{Tr}\ \not{\epsilon}\not{p}_2\not{\epsilon}\not{p}_1 = 4(-2k_1^2\sin^2\theta\cos^2\phi + dk_1^2)$$

Combining (34a) and (33):

$$d\omega = \frac{m_\ell^2}{M_v^2}\ k_1\ \frac{4\pi}{g_v^2}\ \frac{4\pi}{8\pi^2}\ \frac{\alpha^2}{m_\ell^2}$$

$$\times\ (2k_1 - 2k_1\sin^2\theta\cos^2\phi)\,d\Omega_1$$

Integrate with respect to ϕ:

$$d\omega \sim 2\pi(2k_1^2 - 2k_1^2\sin^2\theta \times 1/2) \qquad (37)$$

$$\sim 2\pi(1 + \cos^2\theta)$$

Hence

$$d\omega = \frac{4\pi}{g_v^2}\ \frac{k_1^3}{M_v^2}\ \alpha^2\ (1 + \cos^2\theta)\,d(\cos\theta) \qquad (37a)$$

Integrate with respect to θ

$$\Gamma = \frac{4\pi}{g_v^2}\ \alpha^2\ \frac{8k_1^3}{3M_v^2} \qquad (38)$$

Since $k_1 \simeq \frac{M_V}{2}$, we obtain

$$\Gamma(\psi \to \mu^+ \mu^-) = \frac{4\pi}{g_V^2} \alpha^2 \frac{M_V}{3} \tag{39}$$

APPENDIX B

EVENTS REMOVED TO FORM THE "CLEAN" SAMPLE

$P_\perp^2$	T	AW	Unused hits P0, P1, P2
	Class I Events		
.007	1, 3*, 7	2, 3	3, 1, 6
.055	2, 3*, 4, 5, 6	1, 2	3, 0, 0
.060	1, 2, 6*, 7	---	1, 0, 0
.159	3, 5, 6, 7 (4)	---	0, 0, 0
.164	2, 4, 5, 7, 8 (3)	3, 4	1, 0, 12
.177	1, 2, 5 (3)	---	0, 1, 0
.184	1, 5, 8 (3)	---	0, 0, 0
.218	1, 2, 3, 6 (4)	---	0, 1, 0
.754	3, 4, 8 (6)	1, 2, 3, 4	9, 0, 6
.880	1, 2, 3*	---	0, 1, 0
1.301	1, 4, 7 (3)	1	0, 0, 3
1.559	2, 3, 4, 6	2, 4	7, 0, 1
1.804	2, 3*, 4	1	0, 1, 0
1.934	2, 4, 7, 8 (3)	2, 4	3, 4, 0
2.101	1*, 2, 4, 5, 7	1, 4	10, 0, 13
2.110	2, 4, 6, 7, 8 (1)	---	1, 0, 0
2.355	2, 3, 4	---	5, 0, 0
2.450	1, 3, 4*, 6	---	0, 0, 0
2.928	3*, 5, 8	4	5, 0, 3

*denotes T counter which fired and is in direction of possible recoil.

( )denotes T counter in direction of possible recoil but which did not fire.

APPENDIX B, continued

$P_\perp^2$	T	AW	Unused hits P0, P1, P2
	Class I Events		
3.231	2, 3, 5, 7, 8 (1)	3, 4	0, 1, 7
3.310	1, 2, 4, 5, 8 (3)	---	6, 1, 0
3.415	8*, 1, 2, 6	---	3, 0, 0
3.625	8, 1, 2*	---	0, 0, 0
5.145	1, 4, 5*, 4	3, 4	0, 1, 0
	Class II Events		
.032	1*, 2	1, 4	3, 1, 6
.476	2*, 6	4	0, 0, 0
1.188	4, 8 (3)	3, 4	6, 3, 0
1.845	5, 6 (3)	2, 3, 4	18, 11, 21
1.867	2, 7 (3)	2	0, 1, 0
4.173	3, 7 (8)	3, 4	4, 0, 0
	Class III Events		
.048	4	---	1, 0, 13
.068	- (4)	2, 4	23, 15, 19
.596	2 (7)	1, 2, 3	20, 8, 18
.690	1, 2 (8)	1, 4	0, 0, 13
1.632	2 (7)	1, 2, 3, 4	21, 0, 3
2.154	6, 7*	4	4, 7, 6
2.394	4 (7)	1, 2, 3	17, 8, 26
2.605	- (6)	1, 2, 3, 4	29, 5, 49
4.051	5,6*	4	3, 6, 4

APPENDIX C

RESULTS OF FITS FOR "CLEAN" AND "ALL" SAMPLES

"Clean Sample"

$p_\perp^2$ Range	Param	α	α_{Res}	β	N_1	N_2	γ	N_3	χ^2 - D.F.
0- .6	3	47.6±14.7	67±23	3.03±.72	5.26±1.08				2.18 - 5
0-1.	3	54.2±15.1	76±24	3.70±.47	5.92±1.01				3.24 - 6
0-1.	3	50.0±14.2	70±22	3.33±.47	5.51± .97				2.18 - 5
0- .6	4	52.9±14.1	74±22	2.59±.90	434 ±107	40.9±167			1.59 - 4
0-1.	4	59.4±16.2	83±23	3.65±.53	447 ±116	52.0±10.8			3.19 - 5
0-1.	4	56.3±15.0	79±24	3.21±.51	441 ±112	46.9±10.0			1.93 - 4
0-2.	4	52.0±13.2	73±21	2.27±.37	430 ±106	40.9± 8.1			3.86 - 5
0-3.5	4	50.9±12.9	71±21	2.68±.36	427 ±104	38.9± 7.9			10.44 - 6
0-2.	6	51.3±12.7	72±21	2.76±.37	427 ±103	40.1± .81	Fit unsuccessful		3.87 - 3
0-3.5	6	57.1±15.5	80±25	3.48±.80	443 ±113	47.6± 110	.077±.673	.87±1.47	2.02 - 4
					"All Sample"				
0- .6	3	46.4±14.1	65±22	2.78±.68	5.50±1.10				1.54 - 5
0-1.	3	51.9±14.1	73±20	3.29±.43	6.06± .99				2.29 - 6
0-1.	3	48.3±13.4	68±21	3.01±.41	5.71± .97				1.50 - 5
0- .6	4	50.3±13.9	70±22	2.55±.86	426 ±105	45.8±12.6			1.35 - 4
0-1.	4	55.1±15.3	77±24	3.30±.49	436 ±112	59.6±10.8			2.29 - 5
0-1.	4	52.3±14.3	72±23	2.96±.47	431 ±108	50.1±10.3			1.45 - 4
0-2.	4	42.7±10.6		2.12±.30	400 ± 93	35.8± 7.2			6.74 - 5
0-3.5	4	37.5± 9.0		1.76±.26	379 ± 86	28.8± 6.2			2.13 - 6
0-2.	6	Fit unsuccessful							
0-3.5	6	54.4±15.4	77±22	3.56±.88	433 ±111	51.8±12.2	.071±.362	2.2 ±1.9	1.63 - 4

APPENDIX D

CALCULATION OF RADIUS OF Be NUCLEUS

The form factor of a black disc (or sphere) as a function of the scattering angle θ, the incident momentum k, and the radius of the disc is given by

$$F_{BB} = \frac{2\ J_1(k\ R\ \theta)}{k\ R\ \theta} \tag{40}$$

where $J_1(x)$ is a Bessel function of the first kind.

The differential cross section is then

$$\frac{d\sigma}{dt} \sim F_{BB}^{\ 2} = \left(\frac{2J_1(kR\theta)}{k\ R\ \theta}\right)^2 \tag{41}$$

and is parameterized as $e^{-\alpha|t|}$ for small $|t|$.

Expanding $J_1(x)$ and $e^{-\alpha x}$ for small x and equating like powers of x yields

$$R = 2\sqrt{\alpha} \equiv 2\ hc\sqrt{\alpha} \tag{42}$$

Taking $\alpha = \alpha_{RES} = 67 \pm 23$, we obtain

$$R = 3.2 \pm .6 \text{ fm}$$

The neutron elastic scattering data[18] yields

$$R = 3.47 \pm .015 \text{ fm}$$

which corresponds to a slope of

$$\alpha = 77.6 \pm .2 \ (\text{GeV/c})^{-2}$$

APPENDIX E

COMPARISON OF ψ PHOTOPRODUCTION RESULTS

Experiment	$\langle E\psi \rangle$ (GeV)	K_{max} or range (GeV/c)	A_{tgt}	α $(GeV/c)^{-2}$	β $(GeV/c)^{-2}$	$\frac{d\sigma}{dt}\Big\|_{t=o}$ (nb per nucleon)	$\sigma_T(\psi N)$ (mb)
Cornell[27]	11.0	11.8	9	-----	1.25±0.2	1.01±0.2	≃ 0.18*
SLAC[14]	19	20	2		2.9 ±0.3	19.4±1.3**	≃ 0.8
SLAC[24]	20	-----	9,180	-----	-----	-----	2.75±1.03***
Fermilab[28] (tagged photon)	55	31-30	2	-----	1.8 ±0.4	68±19	≃ 1.4*
Fermilab (Broad Band photon)	116[4]	50-210	9	48±16	1.8 ±0.6	56±19(μμ)	1.3±0.25
	129[3]	70-250	9	~ 40	~ 3	59±15(ee)	1.3±0.3
Fermilab (this data)	161	80-290	9	75±25	3.5 ±0.5	82±10	1.6±0.2

*Calculated from the published value of $\frac{d\sigma}{dt}\Big|_{t=o}$.

**Extrapolated from $t = t_{min}$ from the data in Ref. 14.

***Systematic error quoted in Ref. 24 included.

APPENDIX F

$\psi' \rightarrow \psi\pi\pi$ Candidates
$\mu\mu$

$M_{2\mu}$	$p_{\perp}^2$ $_{\mu\mu}$	p_1	p_2	p_{12}	$M_{2\mu\pi(\pi)}$	$p_{\perp}^2$ $_{2\mu\pi(\pi)}$	$p_{\pi,\pi}$	$p_{2\mu\pi(\pi)}$	Event Type tracks	stubs
3.16	.058	100	39	139	3.93	.076	17,55	211	4	0
3.13	.141	50.6	39.4	89.9	3.51	.110	14	104	3	1
3.11	.085	38	44	82	3.53	.287	94	12	3	1
3.19	1.210	85	101	186	3.69	.640	9.7	196	3	0
3.11	.017	48	96	144	3.40	.094	5.3	149	3	0
3.01	.589	39	61	100	3.18	.529	6.52	106	3	0
3.01	2.570	65	64	129	---	---	---	---	2	1
3.08	.218	41	67	108	---	---	---	---	2	1
3.10	.168	46	177	222	---	---	---	---	2	1
3.10	.542	100	80	180	---	---	---	---	2	1
3.21	.049	91	61	152	---	---	---	---	2	1
3.07	.490	91	64	155	---	---	---	---	2	1

$M_{2\mu}$ = mass of dimuon

$p_{\perp}^2 = p_{\perp}^2$ of dimuon

p_1, p_2 = momentum of each muon

p_{12} = momentum of dimuon

$M_{2\mu\pi(\pi)}$ = Mass of 3 or 4 body system

$p_{\perp}^2{}_{2\mu\pi(\pi)} = p_{\perp}^2$ of 3 or 4 body system

$p_{\pi,\pi}$ = momentum of each pion

$p_{2\mu\pi(\pi)}$ = momentum of system